2022

# Identifying the Optimal Combination of Critical Roadside Slope Segments Susceptible to Rainfall-induced Failures for Minimizing Vulnerability of Highway Networks

Anil Baral

# Identifying the Optimal Combination of Critical Roadside Slope Segments Susceptible to Rainfall-induced Failures for Minimizing Vulnerability of Highway Networks

by

ANIL BARAL

DISSERTATION

Submitted in partial fulfillment of the requirements

for the degree of Doctor of Philosophy at

The University of Texas at Arlington

August 2022

Arlington, Texas

Supervising Committee:

Dr. Mohsen Shahandashti, Supervising Professor

Dr. Mohammad Najafi

Dr. Nilo Tsung

Dr. Atefe Makhmalbaf

## Acknowledgments

I would like to thank my academic advisor and mentor, Dr. Mohsen Shahandashti, for his continued support, guidance, and supervision. My completion of PhD would not have been accomplished without his vision, encouragement, and faith in me. He has been an immensely good mentor to me, and I have been fortunate to obtain ample opportunities to improve my understanding of scientific research and life in general. I have been privileged to have him as my supervisor and will always be indebted for the guidance and support he provided me during my PhD program.

I would also like to thank my committee members Dr. Mohammad Najafi, Dr. Nilo Tsung, and Dr. Atefe Makhmalbaf for being part of my PhD program and providing their insightful comments, advice, and contribution to my dissertation.

My sincere thanks also go to my friends and colleagues at UTA. I was blessed with lab mates who are real friends and a constant source of inspiration. I am always thankful for the precious experience at UTA.

My appreciation also goes to my family, especially my mother, my father, and my brother for their unwavering support, prayers, and belief in me. I also want to thank my wife for her unconditional love and for dealing with my frequent absence over the past few years. Without their dedication and love, it would not have been possible for me to accomplish this research work.

Lastly, I am grateful to the Texas Department of Transportation for partially funding my studies at UTA.

## Abstract

Identifying the Optimal Combination of Critical Roadside Slope Segments Susceptible to Rainfall-induced Failures for Minimizing Vulnerability of Highway Networks

Anil Baral, PhD

The University of Texas at Arlington, 2022

Supervising Professor: Mohsen Shahandashti

The stability of roadside slopes is vital for the smooth operation of the highway transportation system. The failure of slopes adjacent to the highway corridors adversely impacts the network users and network operators. The network users are subjected to delays through speed restrictions, stoppage, and diversions due to the blockage of a motorway. The network operators face the burden of implementation and finance of emergency slope repairs. Proactive rehabilitation of slopes helps to reduce roadside slope failures and minimize the disruption of transportation networks resulting from rainfall-induced slope failures. However, all the slope segments susceptible to rainfall-induced failures cannot be rehabilitated at once due to the limited availability of rehabilitation resources in federal and state transportation agencies. This research aims to develop an approach to identify the optimal combination of slope segments that should be proactively rehabilitated to reduce the vulnerability of transportation networks when only limited slope segments can be rehabilitated. To achieve the objective, first, a combination of a physically-based slope stability model and a hydrological model was used to determine the location of all slopes that are susceptible to rainfall-induced slope failures. Then, a stochastic combinatorial optimization problem was formulated with an objective function that measured the impact on the road users and transportation agencies (i.e., network operators) for different slope failure scenarios. The combinatorial optimization problem was solved using the genetic algorithm-based approach

to provide the most suitable combination of slope segments that should be proactively rehabilitated for minimizing the impacts on the road user and transportation agencies following rainfall-induced instabilities. The decision-making approach for slope rehabilitation should also ensure low risk associated with the selected rehabilitation strategy. However, current slope-rehabilitation decision models do not consider the risk (i.e., distribution of failure cost) associated with the rehabilitation strategies in the decision-making process. Therefore, a risk-averse stochastic combinatorial optimization problem was further formulated and solved using a simulated annealing technique to facilitate the selection of slope rehabilitation strategies, which leads to the least expected cost and conditional value at risk (CVaR) for extreme rainfall events.

The proposed approach to identify the optimal combination of critical slope segments was implemented in the transportation network of Lamar County, Texas. The proposed metaheuristic-based approaches outperformed the commonly used index-based methods in the literature for identifying the critical roadside slopes susceptible to rainfall-induced failures. The risk-averse simulated annealing approach also provided a range of solutions in the Pareto-efficient frontier enabling the transportation agencies to select the rehabilitation combination with different risk aversion levels.

The primary contribution of this research work to the body of knowledge is the development of metaheuristic optimization approaches to facilitate the identification of the critical combination of slope segments for proactive repair, with consideration of slope failure probabilities, slope failure cost, and risk aversion levels in rehabilitation decision-making. More importantly, the proposed rehabilitation approaches will aid transportation agencies in making an optimal allocation of the limited rehabilitation budget to improve the performance of clayey soil slopes that are susceptible to rainfall-induced shallow failures.

# TABLE OF CONTENTS

# LIST OF FIGURES

# LIST OF TABLES

# CHAPTER 1 INTRODUCTION

Natural disasters occurring due to meteorological events are increasing rapidly with a significant impact on the population and infrastructures, hampering the economic progress and well-being of the countries. Rainfall-induced slope instabilities occur every year, and globally, 14 % of the total economic loss and 0.53 % of total death caused due to natural disasters are attributed to slope instabilities (Hidalgo et al., 2018). The United States is experiencing damages of approximately $3.5 billion and about 50 deaths annually due to slope failures (Highland, 2004). The rainfall-induced shallow slope failures are common in cut slopes and embankments, which are the primary component of transportation networks (Miller et al. 2012). The failure of slopes adjacent to the highway corridors impacts the network users and network operators (Wilks et al., 2015; Mattsson and Jenelius, 2015). The network users are subjected to delays through speed restrictions, stoppage, and diversions due to the blockage of a motorway. The network operators must face the burden of implementation and finance of emergency slope repairs. Highway agencies spend millions of dollars for maintaining the highway embankments and cut slopes (FHWA, 2008). Walkinshaw (1992) estimated the cost of correction to the damages to the U.S. highways due to landslides to be at least $162 million per year. More recently Shahandashti et al. (2019) reported a cost of $ 28.5 million in the 2018 fiscal year for the repair of slopes along the Texas highway corridors. Due to the significant impact on the transportation agency's state and federal budget, the management and maintenance of slopes along highway corridors remain a thorny issue for highway agencies (Anderson et al. 2013).

During prolong and intense rainfall, the shear strength of the soil is reduced due to an increase in pore water pressure resulting from rainfall infiltration. This reduction of shear strength makes some slopes prone to failure (critical) during rainfall. It is, therefore, necessary that the highway

agencies identify the critical segments of the highway slopes and conduct routine maintenance for uninterrupted service. Availability of data on spatially varying slope stability variables, such as slope geometry, precipitation, soil hydraulic parameters, and soil characteristics helps to make a reasonable estimate of the stability of earth slopes along highway corridors and identify the critical slope segments susceptible to rainfall-induced failures. However, the publicly available data on slope stability variables cannot be readily used for the condition assessment of roadside slopes. The publicly available datasets with disparity in the level of detail (granularity), reference (coordinate) system, and representation (vector or raster file) should be made compatible with one another before using the datasets for assessing the stability of roadside slopes in clayey soils. Also, due to agencies' restricted capacity (i.e., budget and manpower), all slope segments that require maintenance cannot be rehabilitated within a short period with limited available resources. The highway network operators should make a difficult decision of selecting limited critical slope segments for remediation works. For example, highway agencies have the budget to repair 200 m of slope segments in a network where more than 1000 m lengths of slopes are susceptible to failures. The maintenance personnel must identify and maintain 200 m of critical slope length so that the serviceability of the network is least compromised in the event (e.g., rainfall, earthquakes) triggering slope failures. Hence, identification and prioritization of critical slope segments for proactive repair under a constraint budget is of significant value to transportation agencies. Further, the roadside slope failures during rainfall are probabilistic. As the failures are probabilistic, the generalized cost (i.e., impact on road users and transportation agencies) associated with the rainfall-induced failures is also probabilistic. Hence, the proactive decision-making on roadside slope rehabilitation should also ensure that the conditional value of risk (CVaR) associated with the maintenance decision is low.

The ultimate goals of this research are (1) To develop a data integration approach for performing slope failure susceptibility analysis to determine the usefulness of publicly available data sources for mapping rainfall-induced shallow slope failure susceptibilities in roadside slopes; (2) To integrate the slope failure susceptibility analysis with the metaheuristic optimization model to determine the most suitable combination of roadside slopes for proactive rehabilitation when agencies can only rehabilitate limited slopes due to budget constraint; (3) To incorporate the risk associated with the slope rehabilitation decisions into the optimization framework to facilitate the selection of rehabilitation strategies at appropriate risk-aversion levels.

Chapter 2 provides a comprehensive review of the literature on slope susceptibility analysis and transportation vulnerability analysis. Chapter 2 also provides the gaps in knowledge and research objective. Chapter 3 discusses the methodology of integrating the publicly available data on slope stability variables for the assessment of roadside slope stability. Chapter 3 also presents the application of the data integration approach along the corridors of the Paris district in Texas. Chapter 4 proposes a methodology to determine slope failure probability and identify the optimal combination of critical slope segments that should be proactively rehabilitated to reduce the vulnerability of transportation networks when transportation agencies' capacity is restricted to rehabilitate limited slope segments due to budget constraints. Chapter 5 presents a risk-averse optimization approach to aid transportation agencies in identifying slope rehabilitation strategies along the Pareto-efficient frontier. Chapter 6 presents the conclusion.

# CHAPTER 2 BACKGROUND

## 2.1. CAUSATIVE FACTOR FOR SLOPE INSTABILITY

A list of major causative factors is determined from the literature that would be relevant for assessing the stability of roadside earth slopes (Bhattarai et al., 2004; Chau et al., 2004; Ramanathan et al., 2012; Mohseni et al., 2018). These causative factors are listed below:

### 2.1.1. Slope Angle

A slope angle is one of the most widely selected factors for slope stability analysis. Slope failure can take place gradually or suddenly when the shear strength of the soil cannot resist the gravimetrical forces, which increases with the increase in slope angle, moving the soil mass down the slope (Hossain et al., 2017). Steeper slopes are more susceptible to failure compared to shallow slopes (Nelson, 2013). However, the slope angle alone should not be used to determine the stability of slopes. Other factors, such as soil properties, vegetation, and drainage system, which influence the stability of slopes, may cause the relatively shallow slope to be prone to failure, while a relatively steep slope to be stable (Mohseni et al., 2018).

### 2.1.2. Soil Type and Properties

The stability of slopes is highly dependent on the geotechnical properties (shear strength, permeability) of the soil. Clayey soils are susceptible to shallow slope failure during intense and prolonged rainfall events (Khan et al., 2017; Baral and Shahandashti, 2022b). The soils with higher friction angle and cohesion are less prone to failure (Stark et al., 2005; Nelson, 2013). Physical geotechnical models take into consideration the soil type and properties for analyzing the stability of slopes. The determination of rainfall intensity and duration that causes the failure of slopes

depends on the hydraulic properties (e.g., saturated conductivity, water holding capacity) of soil (Iverson, 2000; D'Odorico et al., 2005).

### 2.1.3. Precipitation

The shallow slope failures are typically followed by rainfalls (Hossain, 2013). Empirical equations have been formulated to obtain minimum intensity duration relation that can initiate shallow landslide and debris flow (Caine, 1980; Innes, 1983; Crosta et al., 2001; Guzzetti et al., 2008). Highway slopes with clayey soils are prone to desiccation due to wetting and drying weather cycles, which allows greater moisture infiltration into the embankment from precipitation (Jafari et al., 2018). This causes an increase in the moisture content of the soils and a reduction in the soil's shear strength.

### 2.1.4. Vegetation

Vegetation enhances slope stability by modifying the soil water regime, which results in a change in pore water pressure and soil suction, and through root reinforcement (Coppin et al., 1990; Chok et al., 2004). Trees increase the stability of slopes hydrologically by increasing the matric suction of soil which leads to an increase in the shear strength (Ali et al., 2012). The root density within the soil mass and tensile strength of the roots mechanically increase the soil strength (Greenwood et al., 2004). Plant rooting systems in many biotechnical methods provide better reinforcement and drainage characteristics than the earthwork associated with mechanical methods such as slope repair, retaining walls, and sheet piles (Shahandashti et al., 2019). One of the studies in Maryland revealed that 56% of the total number of slope failures occurred in the area with medium to low grass density (Ramanathan et al., 2014). Vegetation also aids in the stability of slopes by reducing the infiltration and providing erosion protection for the top layer of the soil (Zuazo et al., 2009).

### 2.1.5. Drainage System

Water drainage systems are essential to the durability and performance of embankment slopes. Many slope failures are caused due to the absence of a surface and subsurface drainage system (Shahandashti et al., 2019). The surface drainage system must be used to reduce infiltration and a subsurface drainage system must be used to control groundwater. Effective water drainage decreases driving forces for slope instability and increases soil shear strength (Lohnes et al. 2001).

## 2.2. SLOPE SUSCEPTIBILITY ANALYSIS

Many studies have been performed to assess the slope failure susceptibility of hill slopes and to map slope failure hazards (Caine, 1980; Guzzetti et al., 1999; Crosta and Frattini, 2001; Huabin et al., 2005; Carrara et al., 1999; Clerici et al., 2002; Bhattarai et al., 2004; Guzzetti et al., 2008; He and Beighley, 2008; Jaiswal et al., 2010; Ramanathan, 2012; Pellicani et al., 2017; Zhang et al., 2018). Slope failure susceptibility analysis methods have been classified into qualitative and quantitative methods (Mohseni et al., 2018). Qualitative methods include geomorphological mapping (Seeley and West, 1990; Zimmerman et al., 1986; Lee, 2001; Whitworth et al., 2011) landslide inventory mapping (Guzzetti et al., 1999; Chau et al., 2004; Guzzetti et al., 2012), and heuristic or index-based approaches (Singh et al., 2008; Ramanathan, 2012). Geomorphological mapping is used to depict surface topography and features in the landform. Geomorphological maps are widely used tools for land development planning and geological risk management (Otto and Smith, 2013). Landslide inventory maps are the simplest form of slope susceptibility maps that delineate the size and location of past landslides. Heuristic or index-based approaches include methods, such as the analytical hierarchy process (AHP) and weighted overlay methods (Achour et al., 2017; Shano et al., 2020). The AHP method involves determining the relative weight and priority of the causative factors and subfactors for slope susceptibility mapping (Kayastha et al.,

2013). In weighted overlay models, a common measurement scale is applied for different causative factors for performing integrated analysis to assess slope stability (Ramanathan et al., 2015). Heuristic or index-based approaches are subjective as the approach depends on expert opinions and past experiences to estimate the slope failure hazard (Fall et al., 2006).

Quantitative methods can be categorized into statistical models (Carrara, 1983; Baeza and Corominas, 2001; Santacana et al., 2003; Nandi et al., 2010; Shahabi et al., 2013; Shahandashti et al. 2022), Artificial Intelligence (AI) models (Nhu et al., 2020), and physically-based models (Iverson, 2000; Bhattarai et al., 2004; D'Odorico et al., 2005; Berti and Simoni, 2010; Mohseni et al., 2018; Zhang et al., 2018; Hidalgo et al., 2018). Statistical methods, such as bivariate and multivariate analysis tools, are used to establish a relationship between the causative factors and failure at a site (Carrara, 1983; Baeza and Corominas, 2001; Shahabi et al., 2013). AI-based methods are more suitable for slope susceptibility mapping when a direct relationship between causative factors and failure is difficult to establish (Shano et al., 2020). However, both statistical and AI-based methods require large datasets on historical slope failures and factors affecting slope stability over large areas. These methods do not provide reliable results if the information on historical slope failures is sparsely available. Physically-based models (Iverson, 2000; Bhattarai et al., 2004; D'Odorico et al., 2005; Berti and Simoni, 2010; Mohseni et al., 2018; Zhang et al., 2018; Hidalgo et al., 2018) use a combination of geotechnical and hydrological models to determine slope stability. The infinite slope stability theory coupled with the hydrological model is a commonly used approach for the assessment of rainfall-induced slope instability (Montgomery and Dietrich, 1994; Iverson, 2000; D'Odorico et al., 2005). The physically-based models can provide acceptable results only when factors affecting slope stability are available with reasonable accuracy (Van Westen et al., 1997). The main advantage of physically-based models in slope

failure susceptibility mapping is that the models do not require data on past slope failures, and the slope stability can be quantified by a factor of safety (FOS).

Several physically-based models have been used in the slope susceptibility mapping of hillslopes. Shallow landslide stability model (SHALSTAB; Montgomery and Dietrich, 1994), Stability Index Mapping (SINMAP; Pack et al., 1998), and Transient Rainfall Infiltration and Grid-based Regional Slope Stability (TRIGRS; Iverson, 2000 and Baum et al., 2008) are physically-based methods used for predicting rainfall-induced slope instability on a regional scale. The stability of slopes in a regional context was assessed in discrete landscape cells, and values of the parameters used in stability analysis were assigned to each discrete cell. SHALSTAB combines the steady-state hydrological model (Beven and Kirkby,1979; O'Loughlin, 1986) and the infinite slope stability method (Skempton and DeLory, 1957) to determine the minimum amount of steady-state rainfall required to trigger the shallow slope instabilities. SINMAP is a model similar to SHALSTAB but classifies the slope stability based on stability index (SI). Unlike SHALSTAB, SINMAP does not use zero value for soil cohesion. Instead, SINMAP incorporates uncertain parameters (e.g., cohesion, friction angle) using lower and upper bounds assuming a uniform probability distribution. These methods assume that slope instability due to rainfall results from the change in steady or quasi-steady water table height and groundwater flow parallel to the slope surface. These methods do not account for the change in slope-normal redistributions of groundwater pressures in response to rainfall infiltration. Iverson (2000) developed a model that considers the slope-normal redistribution of groundwater pressure associated with the transient infiltration of rain. TRIGRS is based on the method outlined by Iverson (2000) for computing pore pressure change and an attendant change in a factor of safety due to rainfall infiltration. The TRIGRS model applies to areas that are prone to shallow slope failures and satisfy the model assumptions reasonably well

(Baum et al., 2002). The assumptions include relative isotropic and homogeneous soil properties, steady background flux, and a well-documented water table. Miller et al. (2012) developed a data integration approach for deriving slope stability variables using remotely sensed data to parameterize the physically-based model for mapping the slope failure hazard along the corridor. Raia et al. (2014) modified the TRIGRS model and presented a probabilistic approach to assess the change in the factor of safety of slope due to rainfall infiltration. Zhang et al. (2018) argued that landslide forecasting based on the factor of safety calculated using a physically-based model is highly uncertain due to the use of cohesion and internal angle of friction, which has a high degree of uncertainty on a regional scale. They considered the uncertainties in soil mechanical parameters in a physically-based model for forecasting rainfall-induced shallow slope instabilities. Strauch et al. (2019) proposed a new approach for mapping shallow land sliding by combining probabilities of landslide impact derived from a physically-based model and statistical approach.

The use of the physically-based models for slope failure susceptibility analysis can provide unreliable results due to improper quantification of cohesion and shear strength in clayey soils. The clayey soils are predominantly used in the construction of roadside embankment slopes in areas that are primarily plain landforms as in Texas. The development of fissures and repeated cycles of drying and weathering lead to the softening of clayey soils (Skempton, 1970; Kayyal and Wright, 1991; Saleh and Wright, 1997; Castellanos et al., 2016). Softening of overconsolidated clayey soils reduces the cohesion component of the Mohr-Column shear strength parameters, and the shear strength is reduced to fully softened strength (Skempton, 1977; Stark and Eid, 1997; Mesri and Shahien, 2003; USACE, 2003; Wright et al., 2007; Gamez and Stark, 2014). The shear strength is further reduced due to the infiltration of rainwater. The moisture variation due to rainfall infiltration in clayey slopes usually occurs up to the depth of 2 m from the ground surface (Hossain,

2013; Castellanos et al., 2016). The infiltration of water decreases the intergranular or effective stress in the soil. The increase in moisture content will also cause the Diffuse Double Layer (DDL) of clay particles to expand contributing to the softening of the soil (Khan et al., 2017). While the addition of rainfall infiltration increases the driving force, the shear stress of soil decreases due to an increase in pore water pressure. This leads to the failure of clayey slopes at shallow depths. The failure surface of these shallow slope failures is usually restricted to the slope face and has been recorded even in the small embankment with a height of 10 feet (Stauffer and Wright, 1984). Kayyal and Wright (1991) examined two failed embankments constructed of clays in the Texas Paris and Beaumont districts. The examination of the failed slopes showed that the strength mobilized during the failure was equal to the fully softened strength. Kayyal and Wright (1991) also back-calculated the pore water pressure for 34 slope failures in clayey soils of Texas. Sixteen slope failures occurred in embankments constructed of Paris clay; eighteen slope failures occurred in slopes constructed of Beaumont clay. They noticed that mobilization of fully softened strength alone was not enough to explain the failure of these slopes. They concluded that significant pore water pressure due to rainfall infiltration and softening of the soil caused the failure of roadside embankment slopes constructed of Paris and Beaumont clays. Therefore, it is necessary to consider both the reduced soil strength and pore water pressure distribution due to rainfall infiltration in mapping the shallow slope instability of the roadside slopes in clayey soils. However, significant information on spatially varying slope stability variables, such as specific gravity of soil, soil classification, hydraulic conductivity, slope geometry, and rainfall intensity-distribution-frequency are required to assess the effect of rainfall infiltration and fully softened strength on slope stability.

Publicly available spatially varying data on slope stability variables and increasing ability to collect data from different sensing and field data collection technologies provide an unprecedented opportunity in assessing the stability of roadside slopes (Taneja et al. 2011; Shahandashti et al. 2021; Zamanian et al. 2022). However, these publicly available data cannot be readily used for the condition assessment of highway slopes. The data on slope stability variables available in various sources have different levels of detail (granularity), representations (vector or raster data), and reference (coordinate) systems (Shahandashti et al., 2011). The level of detail of a data source can be described in terms of geometric or temporal granularities. For example, the data on precipitation intensity obtained from the US National Oceanic and Atmospheric Administration (NOAA) are available in the geometric granularity of nearly 900 m, whereas 50 cm point cloud LiDAR is available for determining ground elevation. Also, data on spatially variable soil properties are stored as a polygon layer of different sizes with no defined granularity. The data sources with different representations and reference systems pose additional difficulty in slope stability assessment. The representation is the way data is stored in a data source. The reference system can be defined as a coordinate system or projection system of data in a data source (Pradhan et al., 2011). The publicly available dataset with different levels of detail, representation, and reference system should be made compatible with each other before they can be used for slope failure susceptibility analysis of roadside slopes.

### 2.3. TRANSPORTATION VULNERABILITY ANALYSIS

Transportation vulnerability analysis considers the network topology, and in some cases disaster as well as traffic flow to identify critical links and nodes of a transportation network (Myung and Kim, 2004; Matisziw et al., 2007; Taylor and D'Este, 2007; Wilson, 2007). The transportation vulnerability analysis is categorized into four main groups: inventory-based risk assessment,

topologically based methods, serviceability-based methods, and accessibility-based methods (Taylor, 2017). In inventory-based risk assessment, first, the vulnerable assets in the networks are identified, following which, the likelihood of a disruptive event that renders the asset vulnerable and potential consequences are determined. If there is a higher likelihood of the disruptive event and severe consequences on network performance due to damage to assets, those assets should be prioritized for rehabilitation works. Scott and Dunn (2015) defined a vulnerability ($V_a$) of network link 'a' as a product of exposure index ($E_a$), which accounts for potential hazard in a link, and consequence index ($D_a$), which accounts for consequences resulting from rerouting of link closure. Topological vulnerability analysis has its roots in graph theory. In the topologically based method, the network structure and topographic properties, especially the connection between nodes, are considered in the vulnerability analysis of networks (Demšar et al., 2008; Duan and Lu, 2014). The topologically based method is concerned with the identification of the most vulnerable location (typically nodes), the disruption of which will severely impact the functioning of the network. Demšar et al. (2008) used a graph theory and network topology to determine the most critical link in a street network in the Helsinki Metropolitan Area of Finland. The authors reported two graph theoretical measures, betweenness and cut vertices, to be crucial in the determination of critical location in a network. Betweenness measures how the shortest routes in the network are affected due to the closure of the links (Demšar et al., 2008). Cut vertices, when removed, can separate the network into two independent parts (Sullivan et al., 2009; Ray, 2013). The topologically based method helps to understand and assess the importance of each node and link in the connectivity of the network; however, it largely ignores the physical nature of the network and the susceptibility of different network components to various disruptive events (e.g., natural or manmade hazards) (Taylor, 2017). The accessibility-based methods consider the accessibility

between different locations in a network for the vulnerability analysis of a transportation network. Accessibility is the ease with which a location of service is reached from a different location using the transport system (Taylor and D'Este, 2007). The Hansen integral index (Hansen, 1959) is a commonly used accessibility index to measure the accessibility of one location point to a set of other destinations in a network (Taylor and D'Este, 2003; Murray and Grubesic, 2007). Serviceability-based methods assess the ability of the network to fulfill its intended function during a disruptive event that leads to the degradation of some components in the transportation system (Mattsson and Jenelius, 2015). The serviceability-based methods for vulnerability analysis use sophisticated models to represent the demand and supply of transportation systems and travelers' responses to disruptive events (Cascetta, 2009). This approach requires extensive data on the demand and supply aspects of the transportation network for simulating the effect of disruptive events. A simple form of serviceability approach is the determination of an increase in travel cost (e.g., travel time or travel distance) due to the blockage of the road from a disruptive event (D'Este and Taylor, 2003 All the methods of vulnerability analysis help in the identification of critical links and nodes due to any disruptive event like slope failure, routine lane closure, or accidents.

## 2.4. PROBLEM STATEMENT

Transportation planners or maintenance workers may not always want to identify the critical links as identified from the transportation vulnerability assessment, instead, they may need to identify the segments of slope or a combination of critical slope segments that could be rehabilitated with limited resources to minimize the overall vulnerability of transportation network. For example, the network in Figure 2.1 has three critical slope segments [$S_1$, $S_2$, $S_3$] that are susceptible to rainfall-induced failure and the slope failure probability of these roadside slope segments is [0.7,0.3, 0.9]. If the link $L_{BC}$ is identified as the most critical link from the transportation vulnerability analysis,

then the direct message to the network operator is to repair all the slope segments in the $L_{BC}$, irrespective of the slope segment's failure probability. Repairing all the slope segments in a link $L_{BC}$, even the slope segments ($S_2$) with a failure probability lower than the slope segment ($S_1$), may not be an economic decision when there is a constraint on the annual maintenance budget or limited human resources. Therefore, an approach for determining the optimal slope rehabilitation strategy with limited resources should consider the failure probability of slopes and its impact on the network's users and transportation agency during different slope failure scenarios.

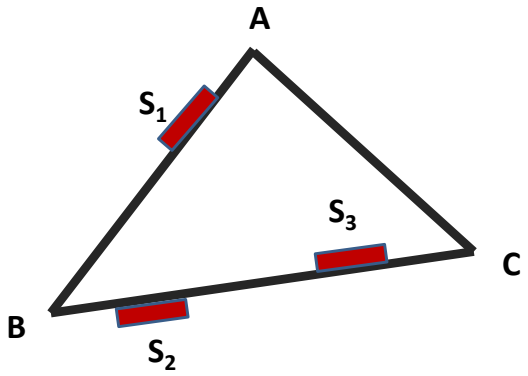


**Figure 2.1** A simplified network showing three critical slope segments.

Further, the generalized cost (i.e., the combined cost of users and transportation agencies) associated with any rehabilitation strategy is probabilistic due to the probabilistic nature of the rainfall-induced slope failures. Hence, the proactive decision-making on roadside slope rehabilitation should also ensure that the conditional value of risk (CVaR) associated with the proactive rehabilitation decision is low (Baral and Shahandashti, 2022c).

## 2.5. GAPS IN KNOWLEDGE

Although the existing studies provide valuable insight for the assessment of slope stability, the proactive rehabilitation decision-making for roadside slopes under a limited budget has been highly elusive. Following gaps were identified from the literature.

(1) Existing literature lack studies assessing the usefulness of the publicly available heterogeneous data on slope stability variables for determining the stability of roadside slopes in clayey soils.

(2) Existing literature does not integrate the slope failure susceptibility analysis with the meta-heuristic optimization model to support proactive rehabilitation decisions of roadside slopes that are susceptible to rainfall-induced geohazards.

(3) Existing literature lacks studies evaluating the risk associated with the proactive slope rehabilitation decisions arising due to the probabilistic nature of slope failures.

## 2.6. RESEARCH OBJECTIVE

The objectives of this research are:

(1) To develop a data integration approach for performing slope failure susceptibility analysis to determine the usefulness of publicly available data sources for mapping rainfall-induced shallow slope failure susceptibilities in roadside slopes;

(2) To integrate the slope failure susceptibility analysis with the metaheuristic optimization model to determine the most suitable combination of roadside slopes for proactive rehabilitation when agencies can only rehabilitate limited slopes due to budget constraints;

(3) To incorporate the risk associated with the slope rehabilitation decisions into the optimization framework to facilitate the selection of rehabilitation strategies at appropriate risk-aversion levels.

The works performed to achieve the goals of the research are outlined in the following chapters.

# CHAPTER 3 SLOPE FAILURE SUSCEPTIBILITY ANALYSIS USING PUBLICLY AVAILABLE DATA SOURCE

The data on slope stability variables available in publicly available sources have different levels of detail (granularity), representations (vector or raster data), and reference (coordinate) systems. The data on slope stability variables obtained from multiple sources should be made compatible with each other before the data can be fused to obtain meaningful information on the stability of roadside slopes. The objective of this chapter is to develop a data integration approach for performing slope failure susceptibility analysis using publicly available data and investigate the usefulness of publicly available data for mapping rainfall-induced shallow slope failure susceptibilities in roadside slopes.

## 3.1. METHODOLOGY

The methodology is comprised of two stages:

(1) Extracting the publicly available data on slope stability variables and transforming the heterogeneous data to a similar level of detail (granularity), representation (vector or raster data), and reference (coordinate) system to create a geo-referenced dataset,

(2) integrating the geo-referenced dataset with a combination of an infinite slope stability model and a hydrological model considering the mobilization of fully softened shear strength to determine the minimum duration of rainfall that triggers slope instability in clayey slopes.

### 3.1.1. *Data Extraction and Transformation*

Soil Survey Geographic (SSURGO) database provides data on the distribution of soil properties on the landscape. The SSURGO database is developed by the National Cooperative soil survey,

an agency of the United States Department of Agriculture (USDA). This database is the most detailed level of soil geographic data. Web Soil Survey (WSS) operated by the Natural Resource conservation system makes the SSURGO dataset publicly available. These data provide an approximation of soil type and properties. The data are geo-referenced and can be obtained as a polygon feature layer. The soil classification is provided based on the unified soil classification system (USCS). The soil properties, such as bulk-specific weight, water content (at one-third bar), liquid limit, clay fraction, hydraulic conductivity, and soil type can be displayed on a table or as a map for most of the United States. The SSURGO dataset provides the soil properties up to a depth of 7 feet from the surface. Soil properties for seven different soil depths, each at an interval of 1 foot along the highway corridor were extracted from the SSURGO datasets. Each soil properties polygon feature at seven different soil depths was converted to a raster file and stored in a geo-referenced integrated database with the granularity and projection system predetermined for slope susceptibility mapping. Figure 3.1 shows the IDEF0 diagram showing the steps to transform the soil properties obtained from the SSURGO database to rasterized soil properties layers.

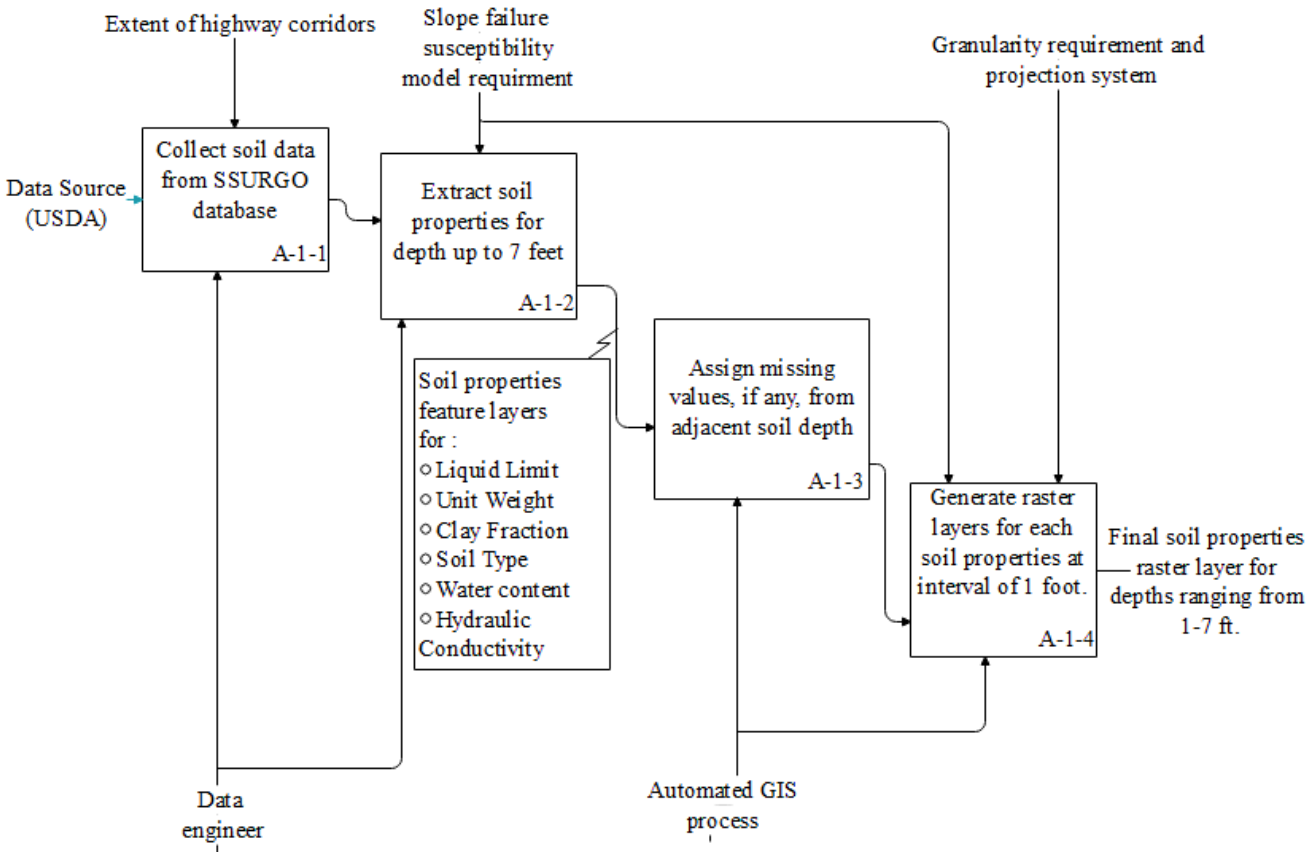


**Figure 3.1** IDEF0 diagram for transforming soil properties feature layers to raster layers

The slope angle is the major causative factor used in slope stability analysis. The publicly available Light Detection and Ranging (LiDAR) dataset was used to obtain slope angles of discrete landscape cells. The IDEF0 diagram (Figure 3.2) shows the process for transforming the LiDAR dataset into a slope raster. The LiDAR data was first converted to an elevation raster, which was further processed to obtain a slope angle raster of the desired granularity and projection system.

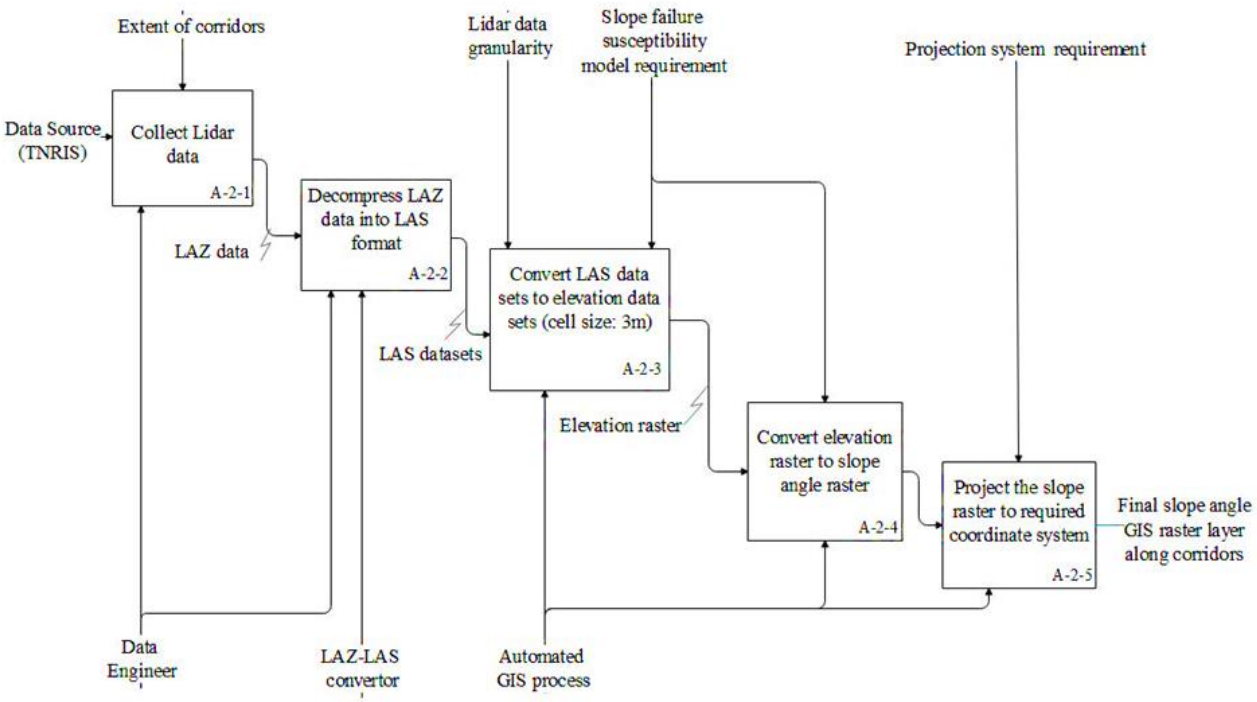


**Figure 3.2** IDEF0 diagram for transforming LiDAR to slope raster layers

The NOAA's National Weather Service (NWS) operates the Precipitation Frequency Data Server (PFDS). The PDFS provides access to point precipitation frequency estimates. Data consist of the depth of precipitation for different durations and varying return periods. NOAA Atlas 14 provides precipitation depth (inches) for ten different frequencies (1, 2, 5, 10, 25, 50, 100, 200, 500, 1000 years) and 19 different durations (5 minutes, 10 minutes, 15 minutes, 20 minutes, 30 minutes, 45 minutes, 60 minutes, 2 hours, 3 hours, 6 hours, 12 hours, 24 hours, 48 hours, 3 days, 4 days, 7 days, 10 days, 20 days, 30 days, 45 days, and 60 days). Raw precipitation data collected from NOAA's Precipitation Frequency Data Server (PFDS) is available in the resolution of approximately 900 m. The precipitation data were obtained as ASCII files and were rasterized using an automated process shown in Figure 3.3. One hundred ninety precipitation intensity raster files (19 durations × 10 frequencies) of different duration and return periods were generated for slope failure susceptibility analysis.

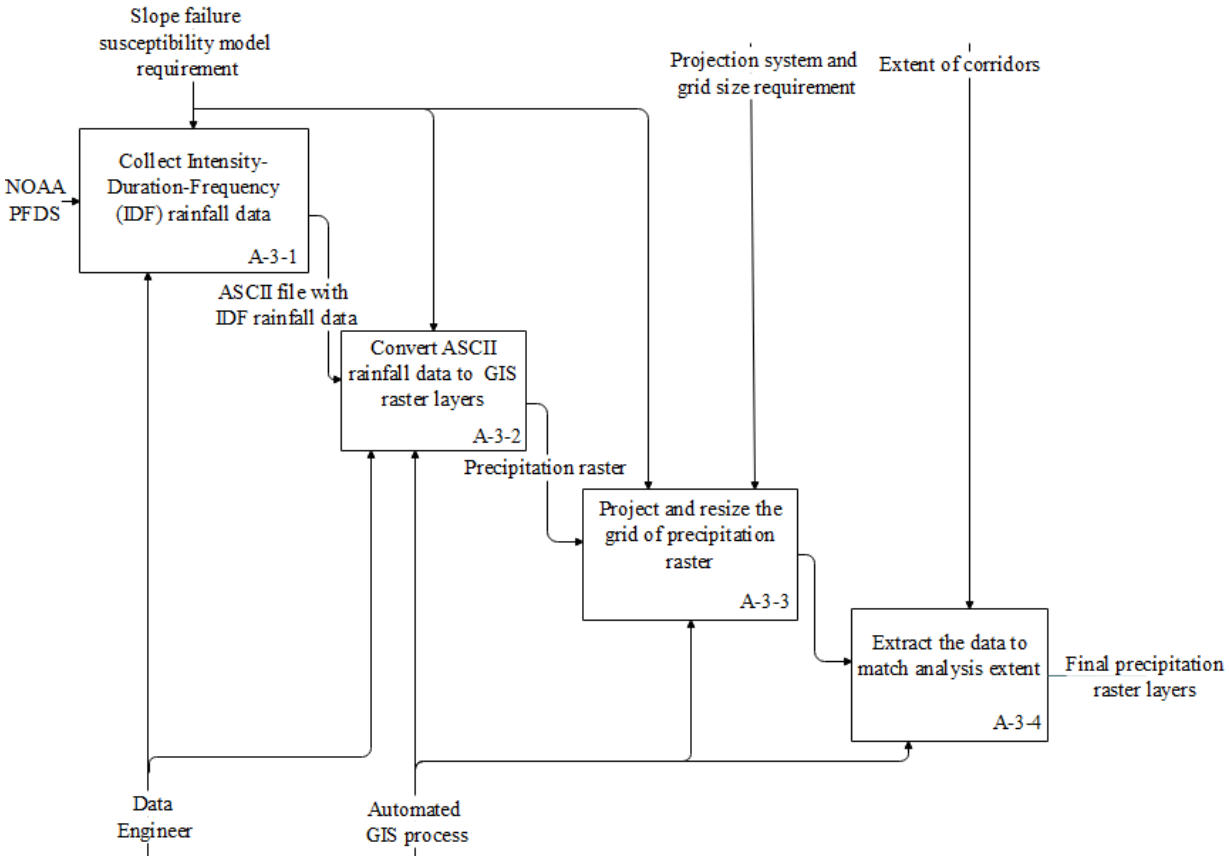


**Figure 3.3** IDEF0 diagram for conversion of point precipitation frequency estimates to raster layers

### 3.1.2. *Slope Failure Susceptibility Analysis*

A combination of an infinite slope stability model and pore pressure response model was integrated with the geo-referenced database to determine the minimum duration of rainfall that triggers slope instability in slopes along the highway corridors. Infinite slope failure refers to the movement of a soil mass approximately parallel to a slope face (Das, 2010). A slope fails when the downslope component due to gravitational force on a soil mass exceeds the resisting force due to column friction. The factor of safety (FOS) for slope at depth z **(**Figure 3.4**)** is given by Equation (3.1).

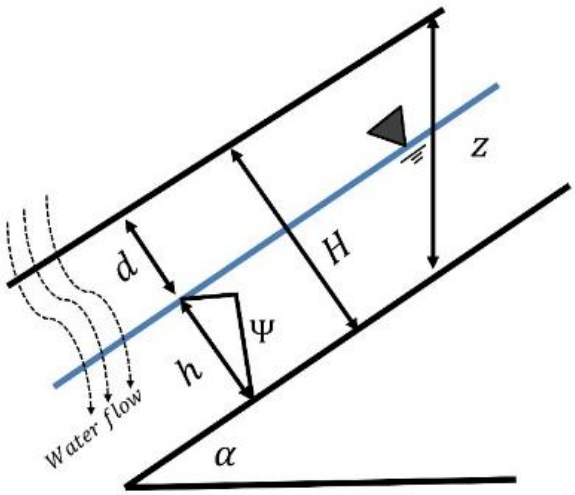


**Figure 3.4** Slope failure parallel to surface showing the model parameters

$$\boldsymbol{FOS} = \frac{\tan\phi}{\tan\alpha} + \frac{C}{\gamma_s z \sin\alpha.\cos\alpha} + - \frac{\Psi(\gamma_w)\tan\phi}{\gamma_s z \sin\alpha.\cos\alpha} \quad (3.1)$$

$$\Psi = (z - d_z)\cos^2 \alpha \quad (3.2)$$

where c is the cohesion of soil, z is the depth of failure, $\gamma_s$ is the unit weight of soil, $\gamma_w$ is the unit weight of water, $\phi$ is drained fully softened internal angle of friction, $\alpha$ is the slope angle, $\Psi$ is the soil water pressure at depth z.

Maximum plausible depth of thickness must be specified in the analysis of slopes using an infinite slope stability model. Without the specification, no bound exists for landslide thickness (Iverson, 2000). The constant soil thickness to develop a slope susceptibility map has been previously used by Montgomery and Dietrich (1994) and Mohseni et al. (2018). Therefore, the depth of failure that renders most slopes unstable along the highway corridors was determined to develop a shallow slope failure susceptibility map of spatially constant soil thickness. Figure 3.5 shows the method for determining the failure depth that triggers most rainfall-induced slope stability in clayey slopes

along the highway corridors. Shallow slope failures in clayey soils do not exceed 10 feet and can be considered infinite slope failures (Day and Axten 1989; Lohnes et al., 2001; Hossain, 2013; Castellanos et al., 2015). The SSURGO database provides the information for the depth up to 7 feet from the surface. The value of FOS is calculated for different soil depths(z), each at an interval of 1 foot, using an infinite slope stability model. The water table was assumed to coincide with the slope surface (i.e., $\Psi = z\cos^2\theta$). The varying fully softened frictional angle, which changes with change in normal stress, was considered in the FOS calculation at various depths. The value of the fully softened frictional angle was determined at each depth based on the empirical correlations defined by Stark et al. (2013) and Gamez and Stark (2014). The empirical correlations used the value of liquid limit, clay-size fraction, and effective stress at each depth to obtain fully softened frictional angles. The cohesion was assigned a value of zero for clayey soils with high swelling and shrinkage potential following the recommendation of Stark et al. (2005). Based on FOS obtained at different depths, the soil thickness that causes most slope failure along highway corridors was selected for developing a slope susceptibility map. The slopes with FOS > 1 are considered unconditionally stable (i.e., rainfall cannot trigger instability in these slopes). Slopes having FOS<1 are unstable and are further analyzed to determine the duration of rainfall that triggers the slope instability.

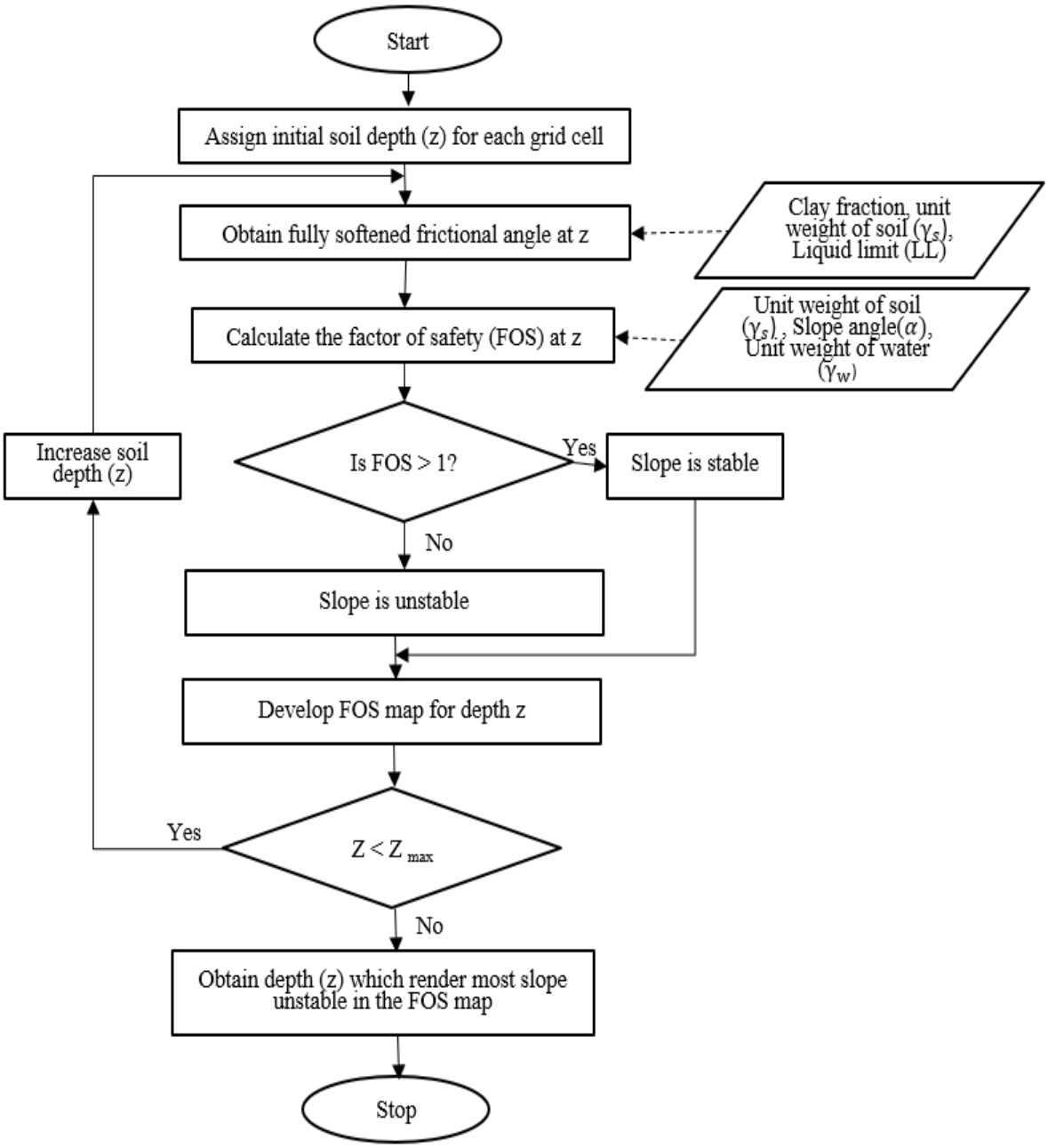


**Figure 3.5** Identification of unstable slopes and soil depth that triggers most slope instability in highway embankments

For the unstable slopes with the factor of safety (FOS) < 1, the ratio of soil water pressure ($\Psi$) to the depth of failure (z), $\Psi^*_{crit}$, which would initiate the failure (i.e., FOS =1), should be obtained. $\Psi^*_{crit}$, also termed dimensionless critical soil water pressure, was found using Equation (3.3):

$$\boldsymbol{\psi}^{*}_{\mathbf{crit}} = \frac{\Psi}{z} = \frac{\gamma s}{\gamma w}\left(1 - \frac{tan\alpha}{tan\phi}\right)\cos^2\alpha + \frac{C}{\gamma w\, z tan\phi} \tag{3.3}$$

Iverson's (2000) pore pressure response model was then used to determine the minimum duration of rainfall causing pore water pressure equivalent to $\Psi^*_{crit}$. Iverson (2000) obtained time-varying dimensionless soil water pressure, $\Psi^*(t^*)$, due to rainfall rate, Iz, by solving linearized Richards equation with suitable initial and boundary conditions driving Equation (3.4):

$$\boldsymbol{\Psi^*(t^*) = \frac{\Psi(t^*)}{z} = \left(1 - \frac{d_w}{z}\right)\cos^2\alpha + \frac{I_z[R(t^*)]}{k_z} \qquad 0 \le t^* \le T^*} \tag{3.4a}$$

$$\boldsymbol{\Psi^*(t^*) = \frac{\Psi(t^*)}{z} = \left(1 - \frac{d_w}{z}\right)\cos^2\alpha + \frac{I_z[R(t^*) - R(t^* - T^*)]}{k_z} \qquad t^* \ge T^*} \tag{3.4b}$$

$\Psi(t^*)$ is the pore water pressure at time t*, $d_w$ is the depth of the initial groundwater table (Figure 3.4), and $k_z$ is the hydraulic conductivity. T* is non-dimensional rainfall duration, and t* is nondimensional time given by:

$$\boldsymbol{T^* = \frac{4D_0\cos^2\alpha}{z^2}T \qquad t^* = \frac{4D_0\cos^2\alpha}{z^2}t} \tag{3.5}$$

In Equation (5), T is the rainfall duration, and t is the time at which soil water pressure should be determined where $Do = k_{sat} / C_0$. $C_0$ is the minimum value of $C(\Psi)$. $C(\psi) = d\theta / d\psi$ presents the change in volumetric water content per unit change in pressure head. The value of $C_0$ is assigned based on soil type (Mohseni et al., 2018). R(t*) is a response function given by:

$$\mathbf{R(t^*) = \sqrt{\frac{t^*}{\Pi}}\exp\left(-\frac{1}{t^*}\right) - erfc\left(\sqrt{\frac{1}{t^*}}\right)} \tag{3.6}$$

Where erfc is the complementary error function.

To determine the rainfall duration triggering shallow slope failure, it is necessary to determine the peak value of the pressure head due to rainfall infiltration. The peak value of the pressure head can

occur during or after the rainfall. Therefore, it is crucial to determine the time, $t_p$*, at which the peak value of pressure head occurs for the rainfall duration of T*. The peak time, $t_p$*, was determined by solving the condition $d\psi^*(t^*)/d(t^*) = 0$ for Equation (4) (D'Odorico et al., 2005):

$$\frac{I_z}{k_z}\frac{dR(t^*)}{dt^*} = \frac{I_z}{k_z} r(t^*) = 0 \qquad 0 \le t^* \le T^* \qquad (3.7a)$$

$$\frac{I_z}{k_z}\frac{dR(t^*)}{dt^*} = \frac{I_z}{k_z} \left(r(t^*) - r(t^* - T^*)\right) = 0 \qquad t^* \ge T^* \qquad (3.7b)$$

where,

$$r(t^*) = \frac{dR(t^*)}{d(t^*)} = \frac{1}{2\sqrt{\pi t^*}} exp\left(-\frac{1}{t^*}\right) \qquad (3.7c)$$

Equation (7) can be solved, providing the estimate of $t_p$* for different rainfall duration, T*. Figure 6 [modified from Iverson (2000)] shows the plot of $t_p$* for the rainfall duration of T*. For the duration of rainfall T*≤ 1, the time to peak is almost constant, $t_p$*~2, and linearly increases with T* when T*>1. For longer rainfall durations, peak soil water pressure occurs at the end of rainfall duration; $t_p$*~T*.

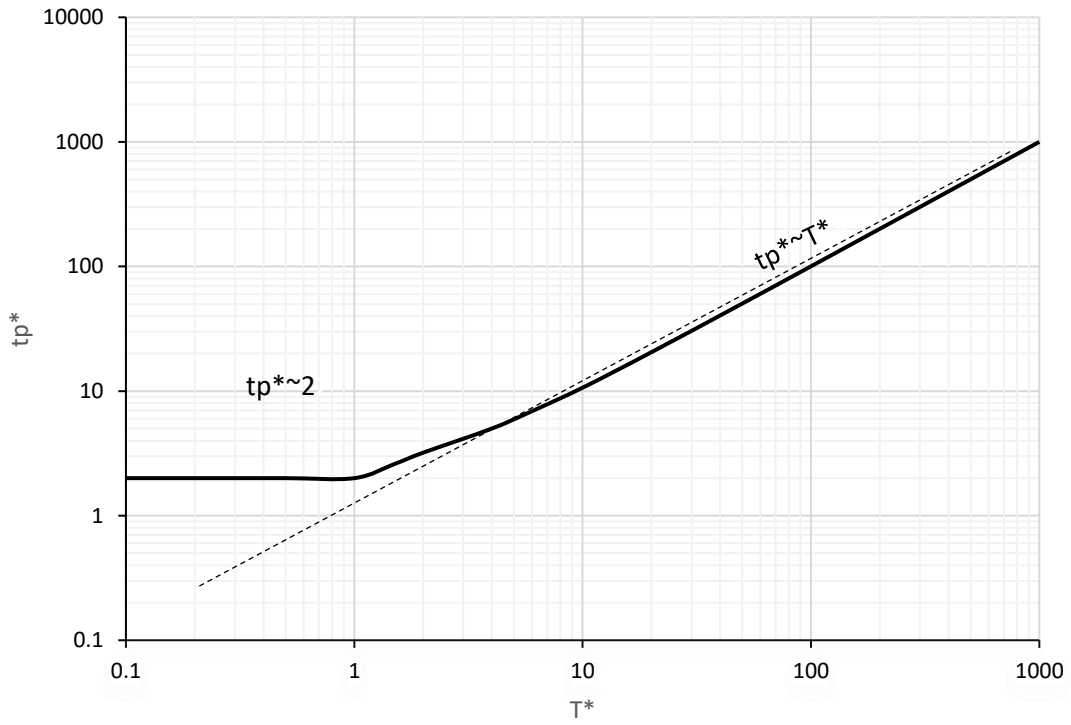


**Figure 3.6** Graph of peak response duration, tp*, for a wide range of normalized rainfall duration T*

The US National Oceanic and Atmospheric Administration (NOAA) provides the intensity for 19 different durations and 10 different return periods. The rainfall intensity (depth) for different durations and return periods was converted to a steady-state rainfall rate ( $I_z$ ) for use in Equation (4). For all the 19 rainfall durations corresponding to 10 different return periods, the time $t_p$* that causes the peak soil water pressure was determined using Equation (3.7). Then, peak soil water pressure $\Psi p^*(t^*)$ at time $t_p$* was determined using Equation (3.4). Figure 3.7 shows the plot of dimensionless peak soil water pressure, $\Psi p^*(t^*)$, due to rainfalls with 19 different durations and 10 different return periods for a single landscape cell of a roadside slope in clayey soils. The critical rainfall duration that triggers slope failure is of duration $T^*$+ (Figure 3.7), which develops a dimensionless peak soil water pressure $\Psi p^*(t^*)$ equivalent to the dimensionless critical soil water

pressure ($\Psi^{*}crit$) required to initiate failure in clayey soil slopes. Figure 3.7 shows that the rainfall durations of different return periods produce the same peak soil water response for smaller values of T*. This is because the maximum value for the ratio of rainfall rate ($I_z$) to the infiltration rate ($k_z$) is limited to 1 in Equation (3.4). If the rainfall rate is higher than the infiltration rate ($I_z/k_z >$ 1), the surplus rainfall, which is higher than the infiltration rate runs off as Horton overland flow. Hence, if the steady-state rainfall rates across different rainfall durations and return periods are higher than the rainfall infiltration rate, the curve (Figure 3.7) showing the increase in peak soil water pressure with rainfall duration will overlap for different return periods. This is supported by a stability analysis of clayey slopes in Texas, where FOS was found to decrease with increasing rainfall duration, but the decrease in FOS was similar for rainfall of different return periods (Hossain, 2013). In clayey soils, the infiltration capacity is usually lower compared to the rainfall rate ($i.e., I_z/k_z > 1$) due to which the rainfall greater than the infiltration rate will overflow over the slope surface. Hence, for slopes constructed of clayey soils, it is more convenient and practical to categorize the slope failure susceptibility based on the rainfall duration. Figure 3.8 shows the overall process to determine the minimum duration of rainfall, triggering shallow slope instability for the clayey slopes.

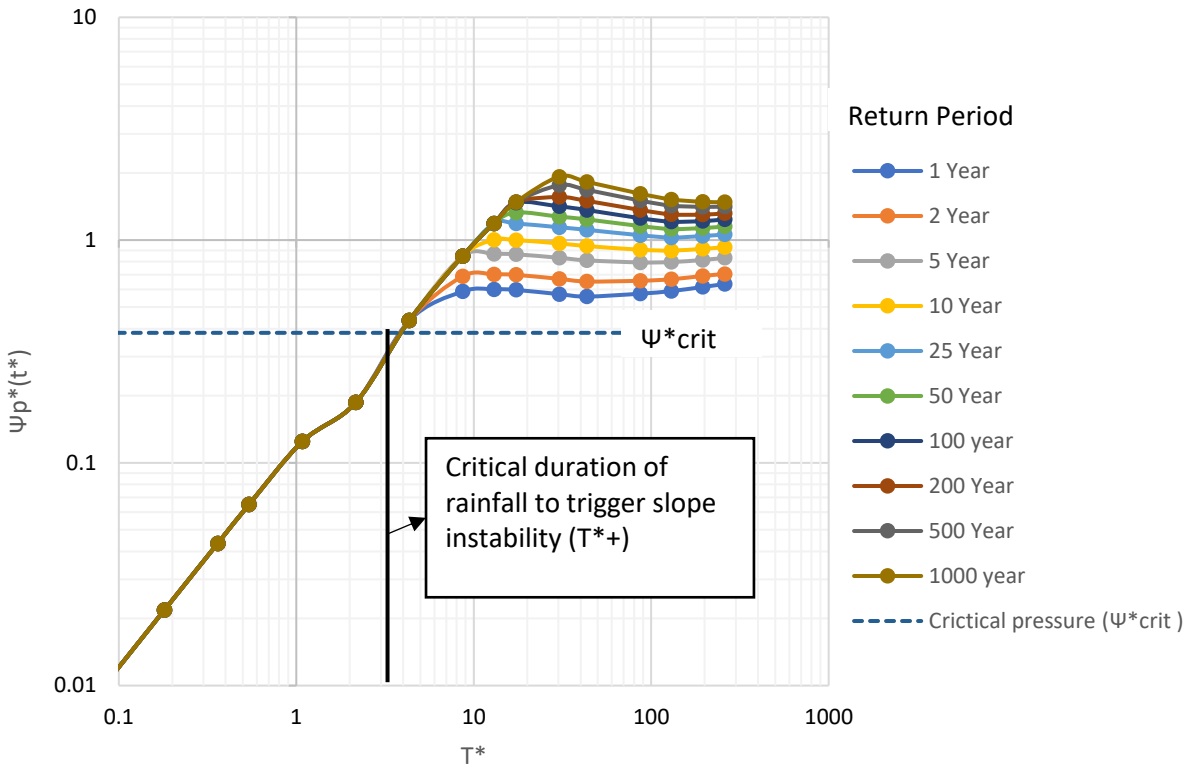


**Figure 3.7** Graphs of pressure head Ψp*(t*) versus normalized rainfall duration T* for different return periods

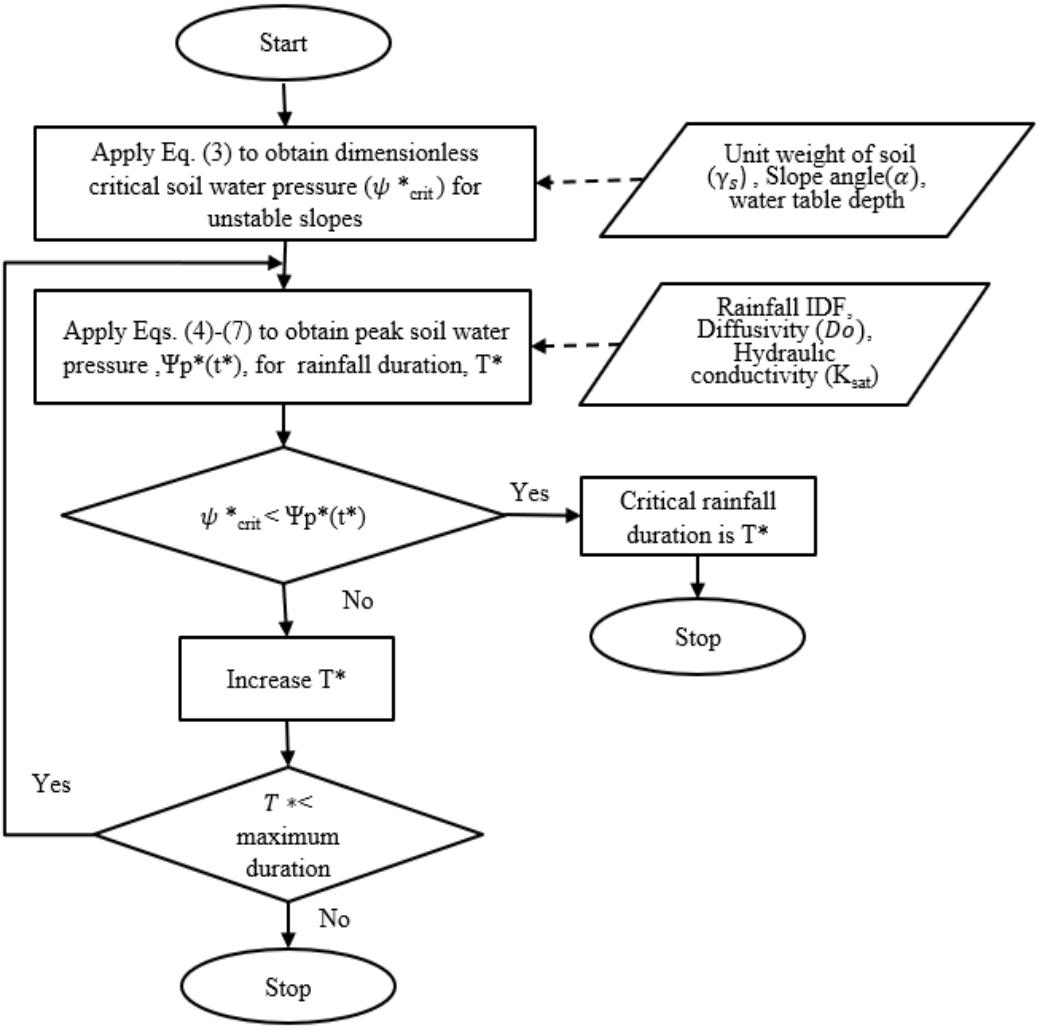


**Figure 3.8** Determination of critical rainfall duration for unstable slopes

## 3.2. APPLICATION

The proposed geo-referenced data integration approach was applied to a total of 498 kilometers (309.433 miles) of highway corridors in the TxDOT Paris district. These include sections of US0082, US0075 US0069, IH0030, and US0380 highways. The embankments in these corridors were determined by the district engineers as being prone to shallow slope failures. Slope failure susceptibility analysis was performed to cover 300 ft width on either side from the centerline of the corridor. LiDAR data obtained from the Texas Natural Resource Information System (TNRIS)

are available for this length of corridors (Figure 3.9). The district has a warm, moist, humid, and subtropical climate characterized by heavy rains (Ressel, 1979). The mean annual average precipitation in Paris is 45.32 inches. The vegetation of the TxDOT Paris district is representative of those found around Northern Texas (McMahan et al., 1984; Ludeke et al., 2009); grass, shrubs, and small trees act as the primary cover for the embankments.

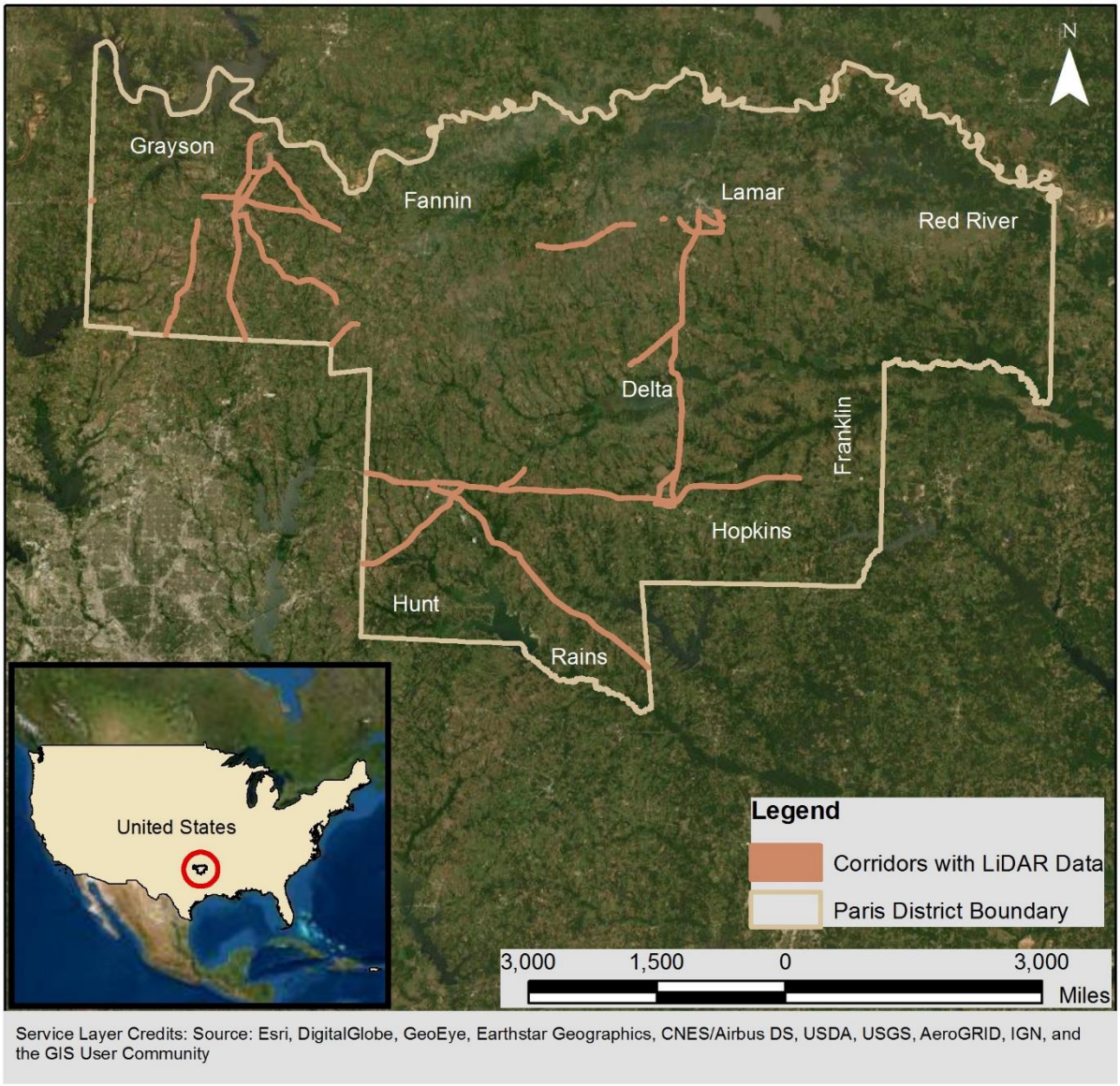


**Figure 3.9** Corridors selected for slope susceptibility analysis

Clayey soils are predominant along the corridors selected for slope susceptibility analysis (Zamanian and Shahandashti, 2021). Table 3.1 shows the distribution of the soil types based on the unified soil classification system (USCS) for the corridor embankments. More than 70% of the embankment slopes are constructed in clayey soils with high swelling and shrinkage potential. Data on soil type, liquid limit, clay size fraction, saturated hydraulic conductivity, water content at field capacity, and unit weight up to a depth of 7 feet were obtained from the Soil Survey Geographic (SSURGO) database. The accuracy of the SSURGO database was investigated by comparing the soil properties obtained from the SSURGO database with the laboratory-measured soil properties at the most recent slope failure locations. Table 3.2 shows the soil properties obtained from the SSURGO database and a recent geotechnical study (Jafari and Puppala 2018) for three past slope failures in the TxDOT Paris district highway embankments. The comparison of the data shows that the SSURGO database provides a reasonable approximation of soil properties at recent slope failure sites. The data on rainfall intensity, duration, and return period were acquired from NOAA's National Weather Service (NWS). The publicly available data extracted from the various heterogeneous sources were transformed to a similar level of detail (granularity), representation (raster layer), and reference (coordinate) system to create an integrated geo-referenced dataset for slope susceptibility analysis. The geo-referenced dataset contains data on soil properties, slope angle, and rainfall intensities of different duration and return periods for each landscape cell with a granularity of 3 m. Figure 3.10 shows slope angles, soil type, unit weight, liquid limit, saturated hydraulic conductivity, and fully softened frictional angle for a 1500 m stretch of the corridor along US0075.

**Table 3.1** Soil types along the corridors

| Unified soil classification system (USCS) | No. of Grid (size: 3 m) | Percentage area (%) |
|---|---|---|
| **CH** | 2773974 | 28.87% |
| **CL** | 3457504 | 35.99% |
| **CL-ML** | 272493 | 2.84% |
| **GC** | 13032 | 0.14% |
| **SC-SM** | 552546 | 5.75% |
| **SM** | 272306 | 2.83% |
| **ML** | 197244 | 2.05% |
| **SC** | 24245 | 0.25% |
| **Others** | 2044540 | 21.28% |

**Table 3.2** Soil properties for three different locations in embankments of the TxDOT Paris district

| Location | Source | Soil type | Liquid Limit | Clay size fraction | Bulk Specific gravity |
|---|---|---|---|---|---|
| **U.S. 75 at Randell Lake Rd Intersection, Grayson Co., Paris district** | USDA | CH | 58 | 48 | 1.42 |
| | Jafari and Puppala, 2019 | CH | 59 | 55 | 1.6 |
| **U.S. 82 at FM 79 Intersection, Lamar Co., Paris district** | USDA | CL | 59 | 43 | 1.46 |
| | Jafari and Puppala, 2019 | CH | 61 | 47 | 1.53 |
| **U.S. 82 nearby N Main Street, Lamar Co., Paris district** | USDA | CL | 59 | 43 | 1.46 |
| | Jafari and Puppala, 2019 | CL | 47 | 33 | 1.64 |

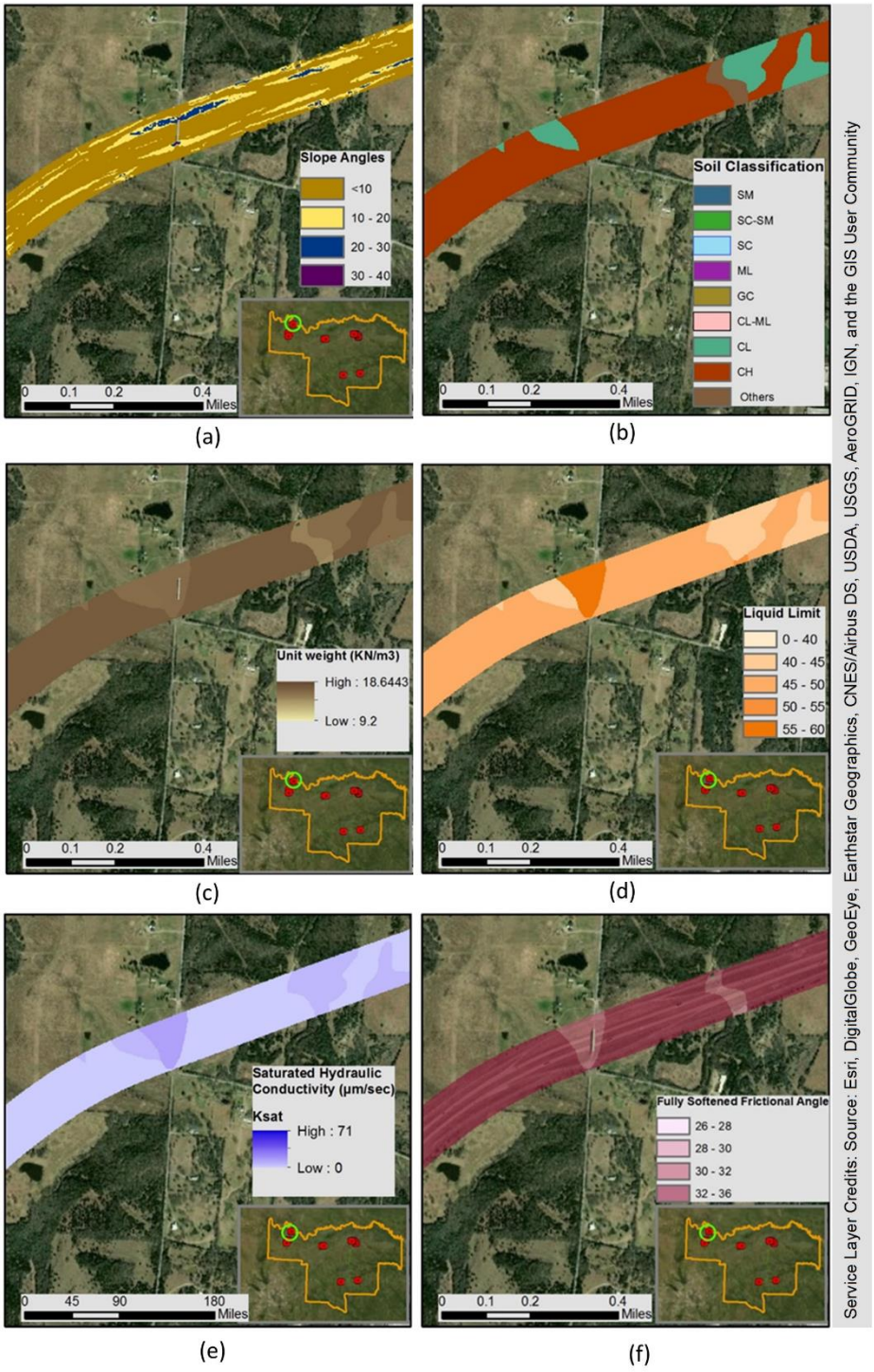


**Figure 3.10** (a) Slope angles in degree (b), Soil classification (USCS), (c) Unit weight of soil ($KN/m^3$), (d) Liquid limit, (e) Saturated hydraulic conductivity, (f) Fully softened frictional angle

After the development of the integrated geo-referenced dataset, the fully softened frictional angles were obtained for the seven different soil layers at one-foot intervals using the empirical correlation developed by Stark et al. (2013) and Gamez and Stark (2014). This empirical correlation was validated for obtaining the fully softened frictional angle for clayey soil in Texas (Jafari and Pappula, 2019). Infinite slope analysis was used to determine the FOS at each landscape cell at various soil layers assuming the water table to coincide with the slope surface. Table 3.3 shows the number of unstable and stable landscape cells (3 m dimensions) for 498 kilometers (309.433 miles) of highway corridors in the TxDOT Paris district. 3.8% of the landscape cells were found to be unstable due to rainfall infiltration. The critical dimensionless soil water pressure ($\Psi^*_{crit}$) (Equation 3.4) that initiates the slope instability was determined for all the unstable slopes. The time-varying peak dimensionless soil water pressure ($\Psi p^*(t^*)$) due to the rainfall of varying duration was determined and compared with critical dimensional soil water pressure ($\Psi^*_{crit}$) to obtain the minimum rainfall duration required to trigger the slope instability. The slopes along highway corridors were classified in accordance with the rainfall duration that triggers the slope instability:

***Highly Critical***: slopes that are susceptible to failure due to the rainfall duration of fewer than 3 days.

***Critical***: slopes that are susceptible to failure due to the rainfall duration between 3- 10 days.

***Moderately Critical***: slopes that are susceptible to failure due to the rainfall duration between 10 -45 days.

***Non-Critical***: slopes that are susceptible to failure due to the rainfall duration of more than 45 days.

Color-coded maps were created to display the rainfall-induced slope failure susceptibilities along the highway corridors. Figure 3.11 shows the slope susceptibility map for a 1500 m stretch of highway corridor at US 75 and Randall Lake Rd intersection in the TxDOT Paris district. The rainfall durations triggering the slope instability in unstable landscape cells are shown in Table 3.4. The result of the slope susceptibility mapping shows that 17.71%, 27.33 %, and 11.24 % of unstable slopes are susceptible to failure due to rainfall duration of fewer than 3 days, 10 days, and 45 days, respectively.

**Table 3.3** Number of stable and unstable slopes along highway corridors

| Slope classification based on stability | Number of cells | Area (%) |
|---|---|---|
| **Unstable slopes** | 365665 | 3.8% |
| **Unconditionally stable slopes** | 9242219 | 96.2% |

**Table 3.4** Duration of rainfall that triggers slope failure in unstable slopes

| Susceptibility indicator scheme | Rainfall Duration for slope instability | Number of cells | Area (%) |
|---|---|---|---|
| **Highly Critical** | < 3 days | 64750 | 17.71% |
| **Critical** | 3-10 days | 99938 | 27.33% |
| **Moderately critical** | 10-45 days | 41114 | 11.24% |
| **Non-critical** | >45 days | 159863 | 43.72% |

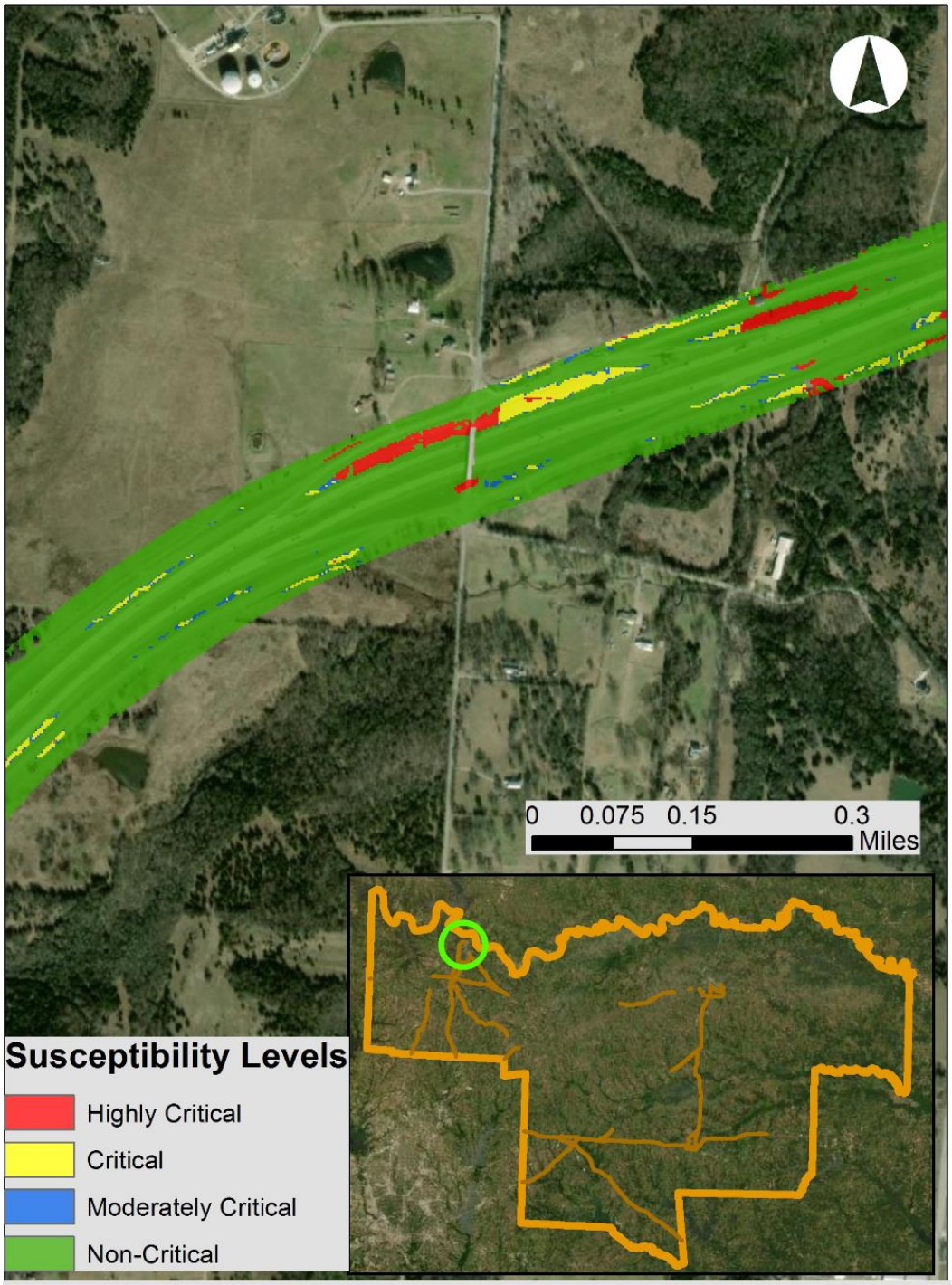


**Figure 3.11** Slope failure susceptibility map at US 75 and Randall Lake Rd intersection in TxDOT Paris District

## 3.3. VALIDATION

The slope failure susceptibility maps generated for the TxDOT Paris district slopes were validated using recent slope failures along highway corridors. Data on recent slope failures in the study area were obtained from the Texas Department of Transportation (TxDOT). Ten recent slope failures were reported by TxDOT, where slope failure susceptibility analysis was performed. Figure 12 shows the critical segments of highway embankments identified using the geo-referenced data integration approach and the slope failure locations in the TxDOT Paris district. Nine slope failures lie in highly critical regions, which require a rainfall duration of fewer than 3 days to trigger slope instability, and one slope failure lies in the critical region, which requires less than 7 days of rainfall to trigger slope instability. The results demonstrate that the publicly available data with the proposed approach are capable of identifying the critical slope segments along the highway corridors.

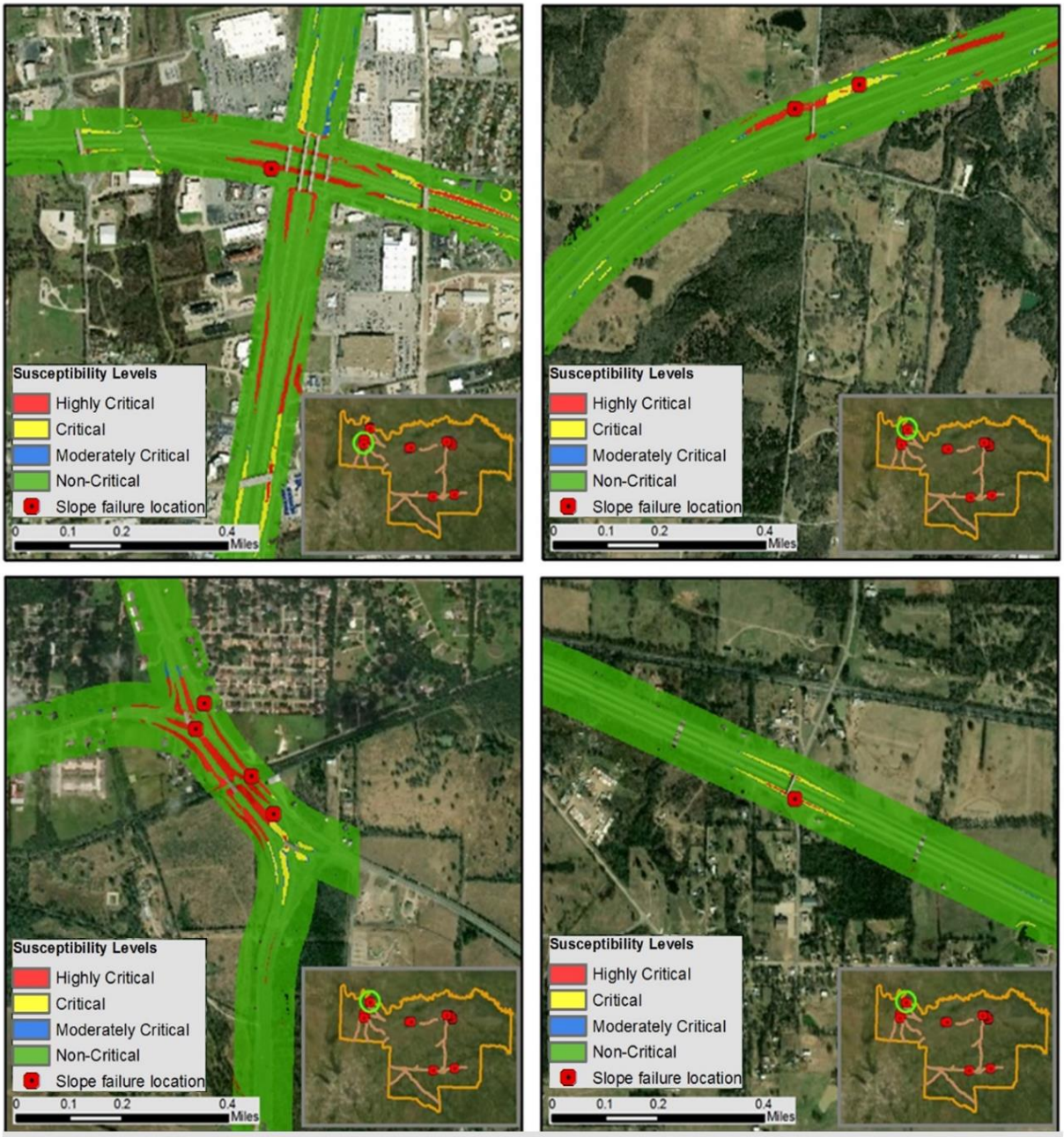


**Figure 3.12** Critical slope identified by the geo-referenced data integration approach and past slope failures along the corridors of the TxDOT Paris district

# CHAPTER 4 IDENTIFYING THE OPTIMAL COMBINATION OF CRITICAL SLOPE SEGMENTS FOR PROACTIVE REHABILITATION

Proactive rehabilitation of slopes can help to reduce roadside slope failures and minimize the disruption of transportation networks resulting from rainfall-induced slope failures. However, all the slope segments that are susceptible to rainfall-induced failures cannot be rehabilitated within a small timeframe due to the limited availability of maintenance budget and manpower in federal and state transportation agencies. This chapter proposes an approach to identify the optimal combination of critical slope segments that should be proactively rehabilitated to reduce the vulnerability of transportation networks when transportation agencies' capacity is restricted to rehabilitate a limited length of slope segments.

## 4.1. METHODOLOGY

The methodology of this research is divided into the following steps:

- A stochastic combinatorial optimization problem is formulated to determine a rehabilitation strategy that minimizes the combined user and agency cost aftermath of rainfall-induced failures in a network for which a constraint imposed on highway agencies is to rehabilitate a limited number of slope segments due to budget restrictions.
- The stochastic combinatorial optimization is solved by integrating a genetic algorithm with a generalized cost estimation model, which provides combined user and agency costs associated with slope failures, to determine the optimal combination of slope segments for proactive rehabilitation.

### 4.1.1. Formulating Optimization Problem

The problem is defined as the minimization of the generalized cost, which is the cost of travel (user cost) and slope restoration (agency cost) following rainfall-induced slope failures. Let V be the generalized cost (overall user and agency cost) of the network due to the disruption caused by slope failure. Then, the objective function is given by:

$$\boldsymbol{min_{p\in \mathbf{P}}\ E(V_N^p)}$$

Where P signifies the set of all the rehabilitation policies (p) for maintenance of critical slope segments. The rehabilitation policy p is generated by considering two possible outcomes: "rehabilitation" or "no rehabilitation" for each roadside slope segment that is identified as critical from slope failure susceptibility analysis. For example, consider a road network as shown in Figure 4.1 where only three slope segments are susceptible to slope failures. The rehabilitation policy can be represented by $\{r_1, r_2, r_3\}$, where $r_k$=1 represents $k^{th}$ slope segment is rehabilitated and $r_k$= 0 means $k^{th}$ slope segment is not rehabilitated. Based on this, for network in Figure 4.1, all the possible slope rehabilitation policy would be P = {{0,0,0}, {0,1,0}, {1,0,0}, {1,1,0}, {0,0,1}, {0,1,1}, {1,0,1}, {1,1,1}}. Without feasible constraint, $P \in X^{2^{N_s}\times N_s}$ is the total combinatorial decisions space for a network with $N_s$ number of critical slopes. However, the size of P is limited by the constraint that any rehabilitation policy (p∈P) cannot recommend rehabilitation of slope segments whose sum exceeds the available budget ($B_{rehab}$). For demonstrating the application of the proposed approach, the rehabilitation budget was used as the feasibility constraint.

The calculation of the increase in generalized cost (V) requires (a) solving physically-based equations and knowledge of soil mechanical properties to evaluate the failure probability of roadside slopes; (b) data on traffic flow in the networks; and (c) cost estimates of slope repair.

Considering the uncertainty in the cohesion and internal angle of friction of soil, the result of the stability assessment can be presented as slope failure probability (Zhang et al., 2018). As the rainfall-induced slope failures are probabilistic, the generalized cost (V) resulting from rainfall-induced damages in the network is also probabilistic. Thus, identifying the rehabilitation policy with minimum generalized cost (V) from a set of all possible rehabilitation policies, considering the probabilistic rainfall-induced slope failure, leads to the formulation of stochastic combinatorial optimization.

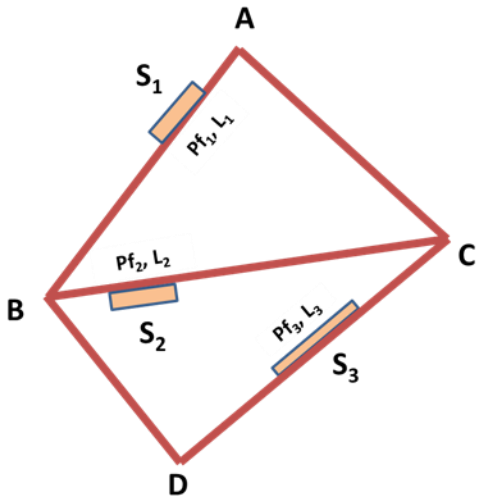


**Figure 4.1** A simplified network showing three critical slope segments.

### 4.1.2. Solving stochastic combinatorial optimization

Combinatorial optimization is difficult to solve using conventional algorithms due to the nonconvex and noncontinuous nature of the objective function, which lacks closed-loop representation (Pudasaini and Shahandashti, 2018). Hence, a genetic algorithm with tournament selection (Pudasaini et al. 2017) was combined with the generalized cost estimation model to identify the optimal combination of critical slope segments, which should be rehabilitated to minimize the generalized cost in events of network disruption caused by rainfall-induced slope

failures. The minimization is constrained by highway agencies' inability to proactively maintain all the slope segments in a network. Figure 4.2 shows the integration of the genetic algorithm and the generalized cost estimation model to identify the optimal combination of slopes for proactive rehabilitation.

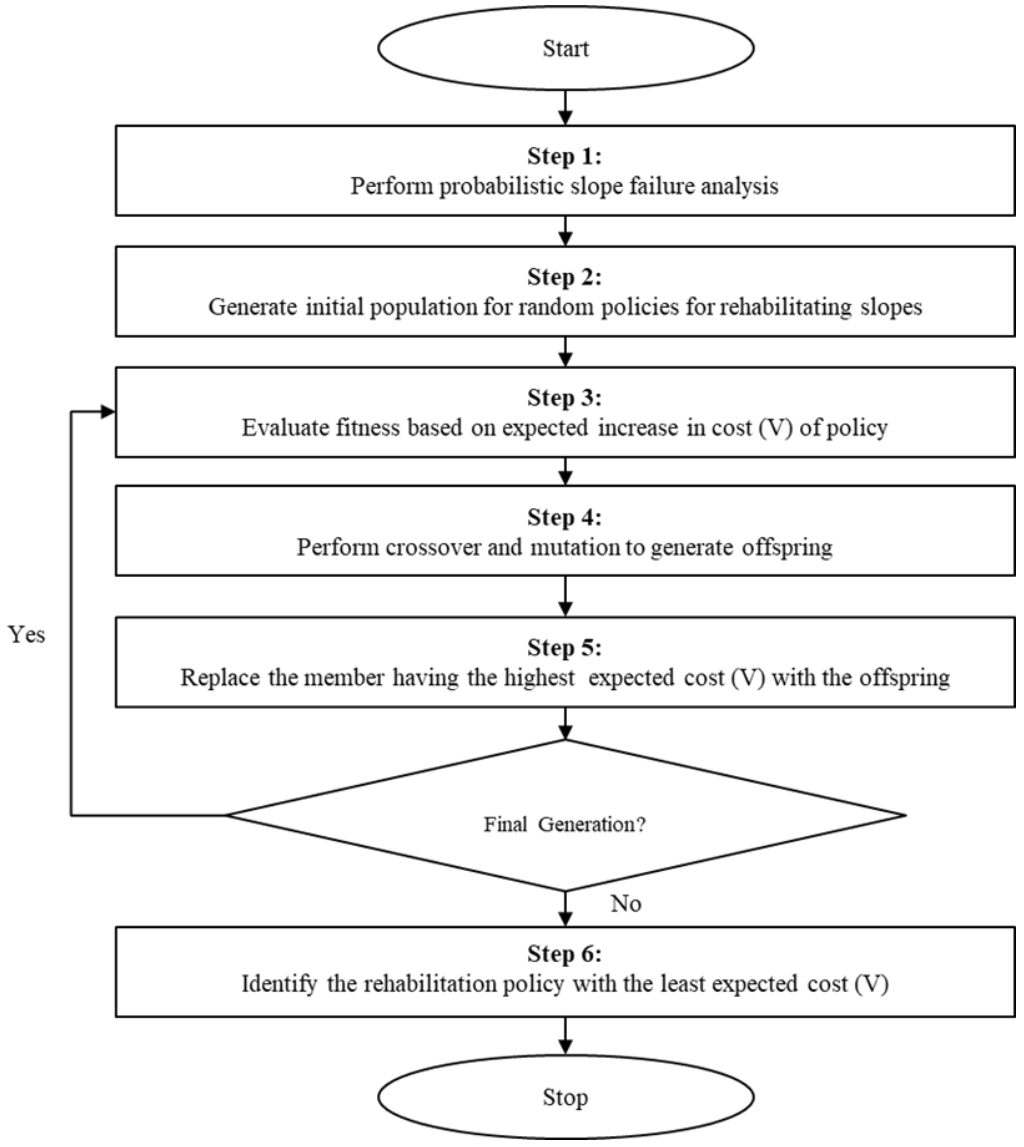


**Figure 4.2** Genetic algorithm integration with vulnerability assessment of transportation network.

For the generation of random rehabilitation policies for slope maintenance, first, all the critical segments along the highway corridors will be identified. A probabilistic slope failure susceptibility map of roadside slopes shall be developed using a combination of the pore pressure response model (Iverson, 200) and the infinite slope stability model (Skempton and DeLory, 1957). A rainfall event of a 10-year return period will be considered for developing a rainfall-induced probabilistic slope failure susceptibility map (GEO, 1984). Iverson's (2000) pore pressure response model will be used to determine the slope-normal redistribution of groundwater pressure associated with rainfall infiltration. Then, the infinite slope stability model will be used to determine the FOS of each pixel in the landscape. The FOS shall be obtained using Equation 4.1.

$$FOS = \frac{\tan\phi}{\tan\alpha} + \frac{C}{\gamma_s z \sin\alpha.\cos\alpha} - \frac{\Psi(\gamma_w)\tan\phi}{\gamma_s z \sin\alpha.\cos\alpha} \quad (4.1)$$

where c is the cohesion of soil, z is the depth of failure, $\gamma_s$ is the unit weight of soil, $\gamma_w$ is the unit weight of water, $\phi$ is drained fully softened internal angle of friction, $\alpha$ is the slope angle, $\Psi$ is the soil water pressure at depth z.

The cohesion and internal angle of friction for the soils at each pixel in a landscape cannot be determined with certainty. The accuracy of the soil mechanical parameter, such as cohesion and internal angle of friction of soil has a significant effect on the value of FOS of the pixels in the landscape (Raia et al., 2014; Zhang et al., 2018). In the calculation of FOS at the pixel level for a large area, the seemingly deterministic soil mechanical parameters have a different amount of uncertainty, which in turn leads to an uncertain forecast of slope stability (Zhang et al., 2018). The uncertainty of soil mechanical parameters will be described using probability density function, e.g., uniform distribution and normal distribution (Zhang et al., 2018). For describing the soil mechanical parameter with a normal distribution density function, expressed as $\phi=N(\mu_\phi, \sigma_\phi^2)$ and

$C=N(\mu_c, \sigma_c^2)$, the mean and the standard deviation should be defined for each pixel in the landscape. To determine the value of mean and standard deviation for each pixel, numerous samples must be taken, and experimental works must be carried out. This is unrealistic for a large region. It is, therefore, desirable to use uniform distribution in an area where information on geo-hydrological parameters is limited and the values of soil mechanical parameters are within the appropriate variation range (Raia et al., 2014; Zhang et al., 2018). In this study, the uncertainties in soil cohesion and frictional angle will be defined by uniform probability distributions in the range of:

$$c = U\,(c_{\min}, c_{\max}) \text{ and} \tag{4.2}$$

$$\phi = U\,(\phi_{\min}, \phi_{\max})$$

The Monte Carlo method will then be used to obtain cohesion and internal angle of friction n times for calculating the factor of safety (FOS) at a specified depth of each pixel.

The values of cohesion $c_i$ and internal friction angle $\phi_i$ shall be determined using Equation 4.3.

$$c_i = k_{ic}\,(c_{\max} - c_{\min}) + c_{\min} \tag{4.3}$$

$$\phi_i = k_{i\phi}\,(\phi_{\max} - \phi_{\min}) + \phi_{\min}$$

$k_{ic} = U\,(0,1)$ and $k_{i\phi} = U\,(0,1)$;

Where $c_{max}$ and $\phi_{max}$ represent the maximum value of cohesion and frictional angle of the $i^{th}$ pixel in the landscape, and $c_{min}$ and $\phi_{min}$ are the minimum values. For each pixel in the landscape, a

matrix $L_i$ will be created after random extraction of cohesion and internal angle of friction as shown in Equation 4.4.

$$Li = [c_i \quad \phi_i] = \begin{bmatrix} c_1 & \phi_1 \\ c_2 & \phi_2 \\ c_3 & \phi_3 \\ :: & :: \\ c_n & \phi_n \end{bmatrix} \tag{4.4}$$

For each set of parameters (i.e., cohesion and internal angle of friction) in $L_i$, $FS_i$= [$FS_1$, $FS_2$, $FS_3$…...$FS_n$] will be generated using Equation 4.1. The $FS_i$ states the n different possible stability state for the $i^{th}$ pixel in the landscape under different possible values of internal angle of friction and cohesion. The failure probability $P_f \in [0,1]$ of a pixel shall be quantified by identifying the number of FS < 1 for n possible values of soil mechanical parameters (Equation 4.5).

$$P_i = \frac{\text{No.of } FS_k<1}{n} \text{ , where k= 1 to n} \tag{4.5}$$

The process to develop a probabilistic slope failure map for the roadside slopes along the highway corridors is shown in Figure 4.3.

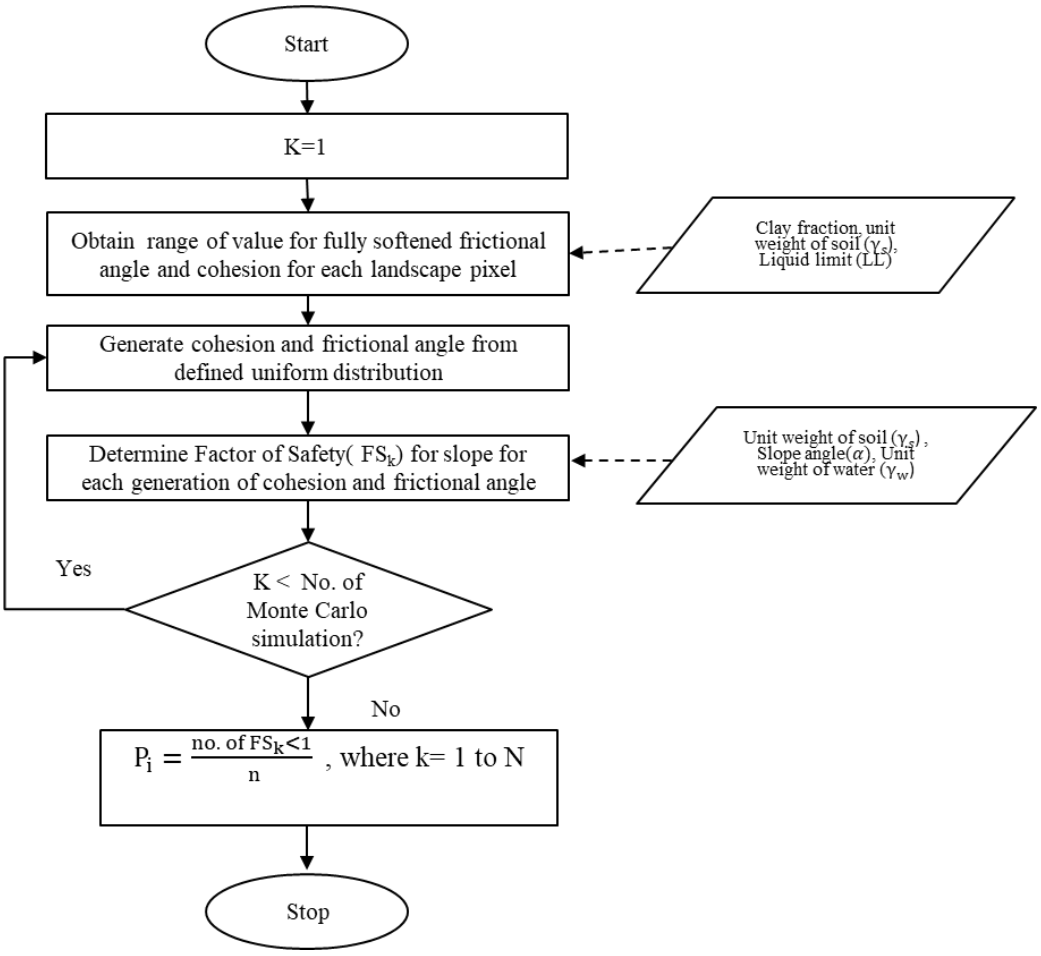


**Figure 4.3** Calculation for obtaining the probability of slope failure

Following the identification of critical slopes that are susceptible to rainfall-induced failures, an initial population of rehabilitation policies was generated. The rehabilitation policies (P) for slope segments were denoted by binary vectors. The binary digit in the vector represents a rehabilitation decision for a slope segment (0 indicates no rehabilitation and 1 indicates slope rehabilitation). The binary digit act as a chromosome for a genetic algorithm. For instance, consider a transportation network with six critical slope segments. A policy of rehabilitating the second and fifth slope segments would then be represented by the binary vector [010010]. These binary vectors are denoted as solution vectors in this paper.

While creating solution vectors (i.e., rehabilitation policies), the following feasibility constraint (Equation 4.6) was employed to reject unreasonable solutions:

$$\sum_{k=1}^{Ns} n_k C_k \leq C_{rehab} \quad (4.6)$$

Where $n_k$ is 1 if the slope segment k is rehabilitated, $n_k$ is 0 if the slope segment is not rehabilitated, $Ns$ is the number of critical slope segments considered in the decision process, $C_k$ is the rehabilitation cost of slope segment k, and $C_{rehab}$ is the total budget available for proactive rehabilitation.

The genetic algorithm to identify the rehabilitation policy with minimum generalized cost begins with the generation of the initial population, which comprises the formation of five arbitrary solution vectors that denote five arbitrary policies for rehabilitating critical slope segments. At the beginning of the genetic algorithm, this initial population of five rehabilitation policies is the current generation. For each rehabilitation policy $p \in P$, the expected generalized cost is obtained using Equation 4.7.

$$\boldsymbol{E(V_N^{p \in P})} = \frac{\sum_{r=1}^{NMCS}(\sum_i \sum_j \boldsymbol{d_{ij}^t}\,[\Delta \boldsymbol{L_{ij}^{p,r}} \boldsymbol{C_{op}} + \Delta \boldsymbol{T_{ij}^{p,r}} \boldsymbol{C_d}] + \boldsymbol{C_{sr}^{p,r}})}{\boldsymbol{NMCR}} \quad (4.7)$$

Where $V_N^{p \in P}$ represents the global measure of the consequence of network disruption (i.e., generalized cost of network) when only slopes segments represented by policy p are rehabilitated; $d_{ij}^t$is the demand of movement from i to j during disruption duration t; $\Delta L_{ij}^{p,r}$ represents the change in travel length from origin i to destination j during r$^{th}$ damage simulation in a network whose rehabilitation policy is represented by p, $\Delta T_{ij}^{p,r}$ represents the change in travel time from origin i to destination j during r$^{th}$ damage simulation in a network whose rehabilitation policy is

represented by p; $C_{op}$ is the per mileage cost associated with the operation and maintenance of vehicles and $C_d$ is the cost associated with delay time; $C_{sr}^{p,r}$ is the cost associated with the slope repair for $r^{th}$ damage simulation in a network whose rehabilitation policy is represented by p. The cost of owning and operating ($C_{op}$) a passenger vehicle is 67 cents per mileage (Bureau of Transportation Statistics 2021) and the cost associated with delay is 30.12 dollars per hour (TxDOT 2022). The user cost is calculated considering 6 hours of traffic disruptions as this should be sufficient to remove the debris from shallow slope failure. The cost of slope restoration ($C_{sr}^{p,r}$) is calculated based on the rebuilding and compaction method incorporating the cost of slope flattening (4H:1V) when applicable (Shahandashti et al. 2022).

Figure 4.4 shows the process to calculate the expected generalized cost for one rehabilitation policy. For a rehabilitation policy $p \in P$, every single run of Monte Carlo simulation starts by generating the slope failures in a transportation network. For each slope segment that is not rehabilitated as per policy p, a random number ($R_n \in [0,1]$) is generated and compared with the failure probability of the slope segments. If the random number exceeds the failure probability, the link adjacent to the slope segment is blocked. After creating the blockages of the link for the current Monte Carlo run, the traffic simulation is performed in the network. The vehicles that were supposed to pass through the blocked lane are rerouted using the next shortest route. Then for all rerouted vehicles in the current Monte Carlo run change in travel cost is calculated. The change in travel cost is noted for a predefined number of Monte Carlo runs (NMCR) for each rehabilitation policy. The expected overall increase in generalized cost is then calculated using Equation 4.7. The process was repeated to determine the expected generalized cost of all the policies in the initial generation (i.e., five initially generated policies) of the genetic algorithm. After acquiring the expected generalized costs (V) of the initial generations, the next generation of policies of the

genetic algorithm is obtained based on the genetic operation proposed in Chen and Shahandashti (2009). First, all initial policies are ranked based on the expected generalized cost (V). Then, a two-point crossover of the two policies with the least expected generalized cost is performed to generate the new offspring policy. The crossover and mutation are performed on the new offspring till the cumulative slope rehabilitation budget of new offspring is less than or equal to the constraint imposed on the rehabilitation budget, i.e., $C_{rehab}$. Calculating the expected generalized cost for new offspring is repeated until a predefined number of generations is reached. The rehabilitation policy with the least expected generalized cost in the last generation is the most critical slope to be rehabilitated for minimizing the network's vulnerability to rainfall-induced failures.

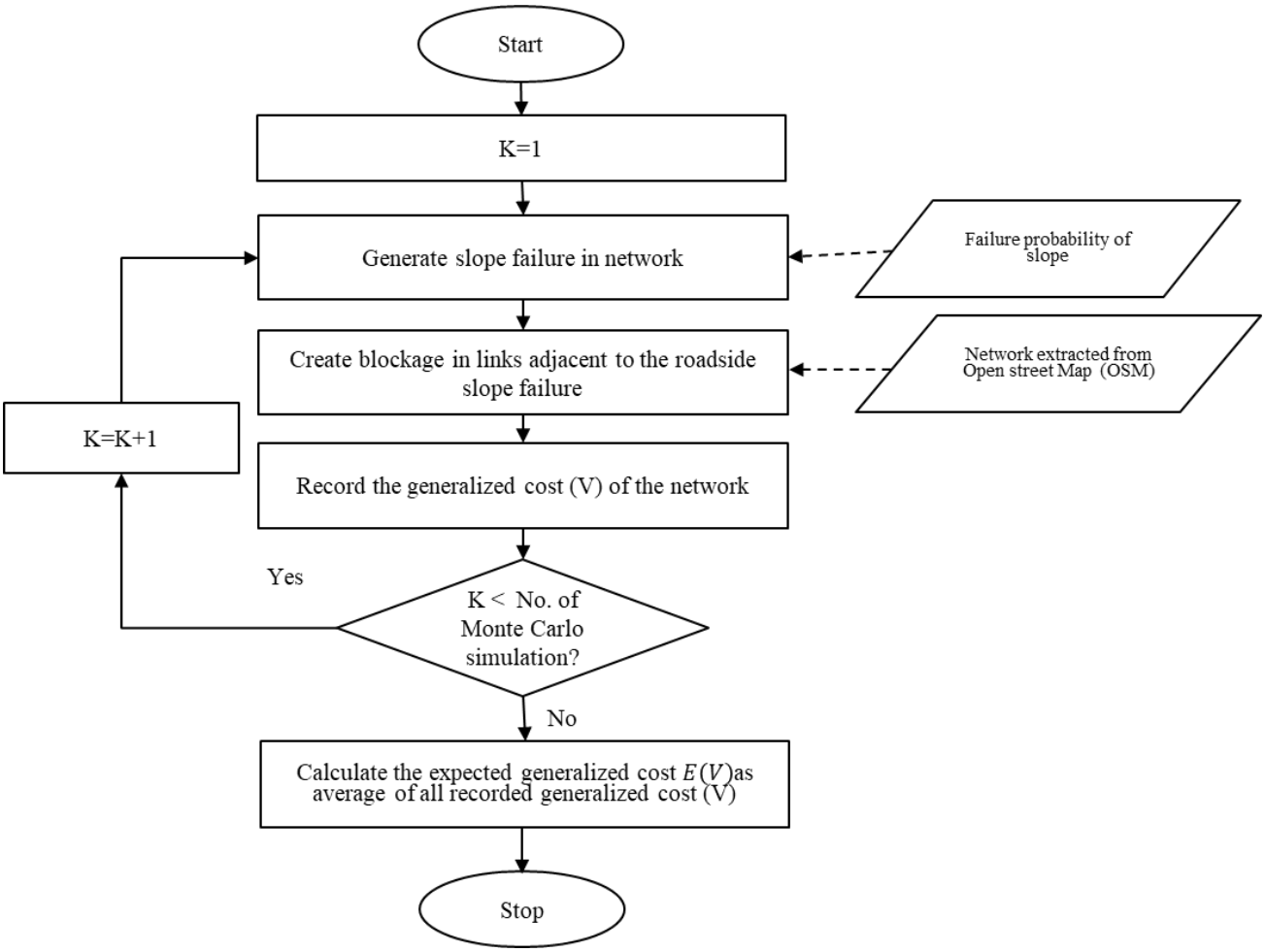


**Figure 4.4** Calculation of generalized cost for a slope rehabilitation policy

## 4.2. APPLICATION

The proposed approach was applied to a road network (Loop 286) in Paris city of Lamar County, Texas. Figure 4.5 shows the network selected for demonstrating the application of the proposed approach.

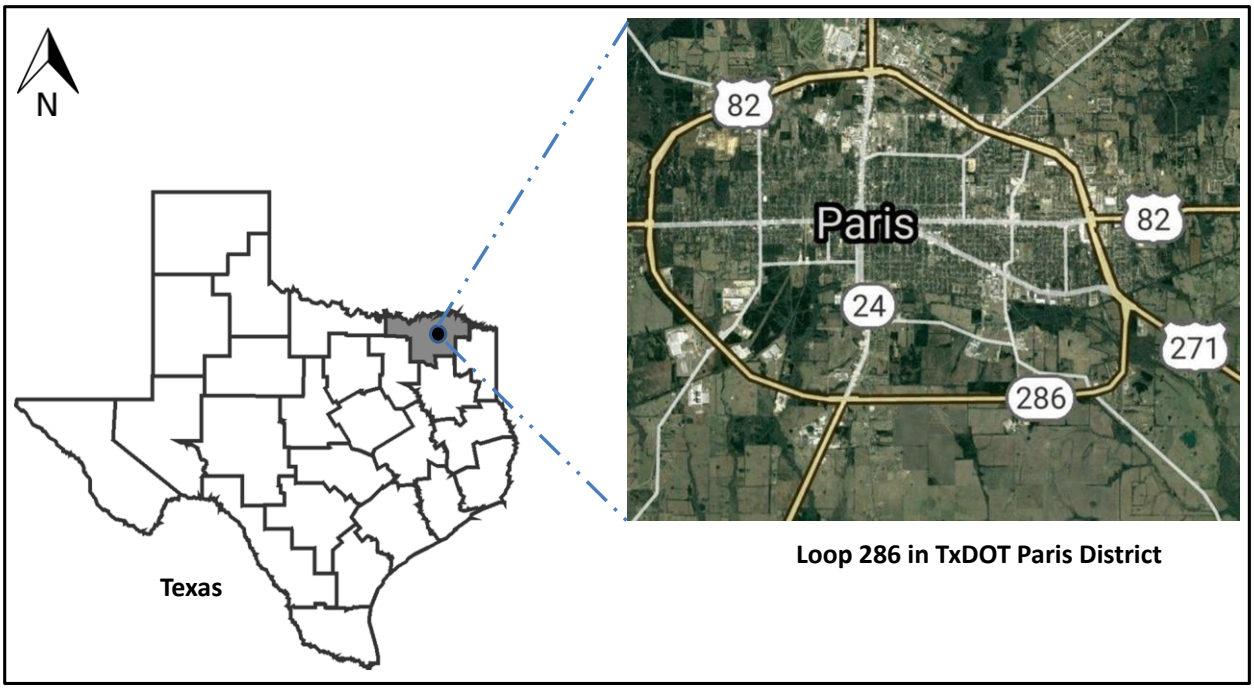


**Figure 4.5** Loop 286 in the Paris district of Texas

First, a probabilistic slope failure susceptibility analysis of the roadside slopes was performed to determine the failure probability of slopes. The rainfall intensity corresponding to a 3-day 10-year return period is considered as a scenario rainfall in assessing the failure probability of roadside slopes (GCO, 1984). A previous study in the Paris district area showed that significant roadside slopes were highly susceptible to failure due to rainfall intensity corresponding to a 10-year return period and 3 days duration (Baral et al. 2021). The data on rainfall was obtained from Precipitation Frequency Data Server (PFDS) operated by NOAA's National Weather Service (NWS). The PDFS provides access to point precipitation frequency estimates (NOAA, 2018). The rainfall distribution function (Equation 4.8) is used to define the rainfall intensity distribution corresponding to 3-day 10-year return period rainfall for the study region. The mean intensity of a 3-day 10-year rainfall event is 7.21 inches with a 90 percent confidence interval in the range of 5.88 to 8.80 inches (NOAA 2021).

$$f(x) = \frac{1}{0.125x\sqrt{2\pi}} \exp\left(-\frac{(lnx - \ln(7.21))^2}{0.03125}\right) \quad (4.8)$$

Data on soil properties were obtained from Soil Survey Geographic (SSURGO) database (Soil Survey Staff, 2019). The Natural Resource Conservation System (NRCS) makes the SSURGO dataset available for public use. The slope angle was obtained using the publicly available Light Detection and Ranging (LiDAR) dataset (TNRIS, 2019). All the data were processed to create a raster of 3 m granularity in ArcGIS. Roadside slopes in the Paris district are mostly clayey soils with high swelling and shrinkage potential. Therefore, a fully softened frictional angle was assumed to be mobilized during slope failures (Castellanos et al., 2015; Khan et al., 2016; Shahandashti et al., 2019; Baral et al. 2021). The mean value of the fully softened frictional angle was assessed in each pixel using the empirical correlations defined by Stark et al. (2005) and Gamez and Stark (2014). The empirical correlations used the value of liquid limit (LL), clay-size fraction (CF), and effective stress at failure depth. The values of spatially distributed soil liquid limit and clay-size fraction are obtained from the SSURGO dataset (Soil Survey Staff, 2019). The effective stress at any soil depth is calculated using the information on the spatial distribution of soil's unit weight from the SSURGO dataset. The SSURGO database provides a reasonable estimate of soil properties in the study area (Baral et al. 2021). Also, the variability in soil texture reported in the SSURGO database is consistent with the variability reported from field-based measurements (Cole 2017). The cohesion of fully softened soil at failure was assigned a value of 50 psf based on the past slope failure studies in Lamar County, Texas (Stauffer and Wright, 1984; Kayyal and Wright, 1991; Jafari and Puppala, 2019). Once the average value of the internal angle of friction and cohesion were determined, the lower and upper bound of fully softened frictional angle and cohesion of each pixel is assumed to be within 50% of the mean value (Equation 4.9).

Similar assumptions were made by Raia et al. (2014) and Zang et al. (2018) to develop probabilistic slope failure susceptibility maps.

$$c_{\text{random}} \in [0.5 \times c_{\text{mean}}, 1.5 \times c_{\text{mean}}] \quad (4.9)$$

$$\phi_{\text{random}} \in [0.5 \times \phi_{\text{mean}}, 1.5 \times \phi_{\text{mean}}]$$

The slope failure susceptibility map was created using the step outlined in Figure 4.3. The probabilistic slope failure susceptibility map was used to identify the location and failure probability of roadside slope segments. The slopes with a failure probability higher than 0.1 were considered susceptible to failure by Park et al (2013). The failure probability of 0.2 was considered as a threshold for unstable slopes by Ko Ko et al. (2004). In this study, we considered roadside slope segments with a failure probability higher than 0.15 for the demonstration of the approach proposed to determine optimal slope rehabilitation policies. Thirty-three critical slope segments were identified in the highway network. The locations of these 33 critical slope segments are shown in Figure 4.6. The area of susceptible slopes and the probability of failure of each segment are shown in Table 4.1. The cost of restoration of slopes after failure is also shown in Table 4.1. From these 33 critical slope segments, an optimal combination of slope segments should be determined for proactive rehabilitation so that generalized cost is minimized during the network disruption caused by rainfall-induced failures.

The restoration costs after slope failures vary based on the type of repair methods, the selection of which in turn depends on the criteria, such as desired service life, availability of special equipment, availability of skilled workers, available emergency funds, etc (Adhikari et al. 2021). Hence, for simplicity, the cost of slope restoration in this study is calculated based on the rebuilding and compaction method incorporating the cost of slope flattening (4H:1V) when required. The

selection of an appropriate slope repair technique however will require a detailed cost-benefit analysis (Zahed et al. 2018). The life cycle costs of slopes should also be incorporated into the cost-benefit analysis (Janbaz et al. 2017; Zahed et al. 2019).

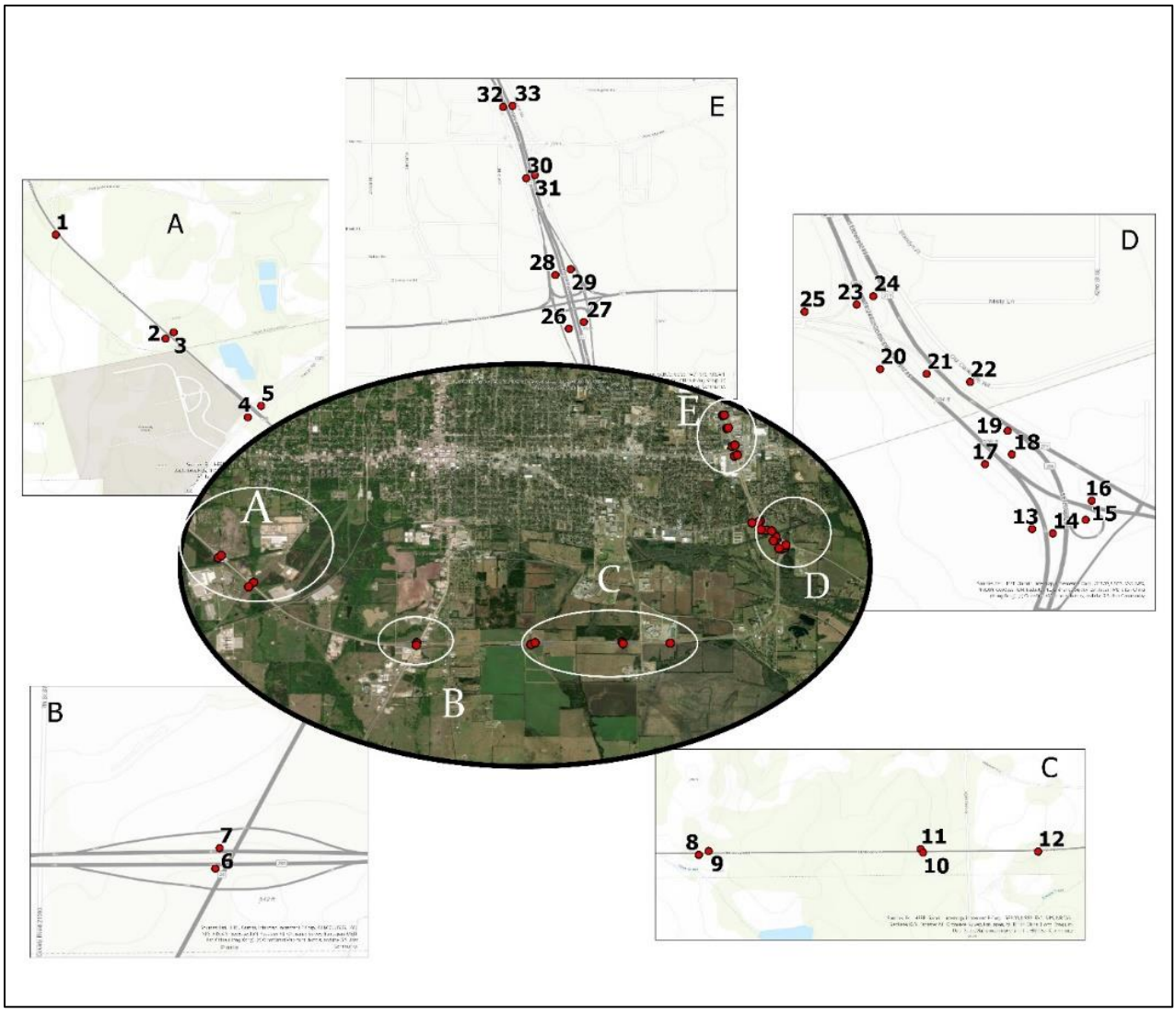


**Figure 4.6** Critical slopes along the highway corridors

**Table 4.1** Failure probability and rehabilitation cost of critical slope segments

| S.N. | Segment | Latitude | Longitude | Failure Probability ($P_f$) | Cost of Rebuilding and Compaction (USD) |
|---|---|---|---|---|---|
| **1** | *S1* | 33.650795 | -95.59738 | 0.16 | 67251 |
| **2** | *S2* | 33.644777 | -95.59103 | 0.15 | 188333 |
| **3** | *S3* | 33.645141 | -95.59056 | 0.16 | 226252 |
| **4** | *S4* | 33.640225 | -95.58627 | 0.19 | 26890 |
| **5** | *S5* | 33.640892 | -95.58549 | 0.17 | 25274 |
| **6** | *S6* | 33.631041 | -95.55988 | 0.42 | 75574 |
| **7** | *S7* | 33.631421 | -95.5598 | 0.33 | 50542 |
| **8** | *S8* | 33.631145 | -95.54185 | 0.19 | 150104 |
| **9** | *S9* | 33.631389 | -95.54122 | 0.16 | 123781 |
| **10** | *S10* | 33.631286 | -95.52739 | 0.16 | 73088 |
| **11** | *S11* | 33.631521 | -95.52754 | 0.17 | 77651 |
| **12** | *S12* | 33.631362 | -95.51996 | 0.16 | 55622 |
| **13** | *S13* | 33.646242 | -95.50286 | 0.28 | 53022 |
| **14** | *S14* | 33.646162 | -95.50248 | 0.31 | 74904 |
| **15** | *S15* | 33.646415 | -95.50187 | 0.33 | 32054 |
| **16** | *S16* | 33.646768 | -95.50176 | 0.41 | 26132 |
| **17** | *S17* | 33.647445 | -95.50374 | 0.16 | 94818 |
| **18** | *S18* | 33.647626 | -95.50324 | 0.32 | 88389 |
| **19** | *S19* | 33.648061 | -95.50331 | 0.34 | 32889 |
| **20** | *S20* | 33.649207 | -95.50568 | 0.33 | 103890 |
| **21** | *S21* | 33.649117 | -95.50482 | 0.47 | 83582 |
| **22** | *S22* | 33.648972 | -95.50401 | 0.35 | 96023 |
| **23** | *S23* | 33.650401 | -95.50611 | 0.27 | 26142 |
| **24** | *S24* | 33.650558 | -95.50581 | 0.24 | 58700 |
| **25** | *S25* | 33.65027 | -95.50708 | 0.21 | 19023 |
| **26** | *S26* | 33.660763 | -95.50983 | 0.16 | 30067 |
| **27** | *S27* | 33.660955 | -95.5094 | 0.14 | 18318 |
| **28** | *S28* | 33.662315 | -95.51022 | 0.21 | 25721 |
| **29** | *S29* | 33.662481 | -95.50978 | 0.17 | 29743 |
| **30** | *S30* | 33.665119 | -95.51106 | 0.79 | 18953 |
| **31** | *S31* | 33.665211 | -95.51082 | 0.68 | 21151 |
| **32** | *S32* | 33.667181 | -95.51173 | 0.81 | 23787 |
| **33** | *S33* | 33.667214 | -95.51146 | 0.84 | 23517 |

The traffic simulation was performed in Simulation of Urban Mobility (SUMO), an open-source traffic simulation package (Lopez et al., 2018). The map of the study area was extracted from OpenStreetMap (OSM). The extracted map was converted to the SUMO network (Figure 4.7) using the NETCONVERT, which imports the digital road network from different sources and generates a road network compatible with SUMO to run the traffic simulation (German Aerospace Center (DLR), 2021a). The network generated using the NETCONVERT needed manual refinement or additional traffic infrastructure. NETEDIT, a visual network editor, was used to edit the network (German Aerospace Center (DLR), 2021b). The detector count from 98 different network locations, obtained from the Texas Department of Transportation (TxDOT) traffic count database system (TxDOT, 2021), was used to generate the traffic flow in the network. The detector count data for traffic flow at peak hours were considered for simulating the network traffic. A 'routeSampler' tool in SUMO was used to heuristically sample the routes so that the resulting routes fulfill the detector count at different locations (German Aerospace Center (DLR), 2021c).

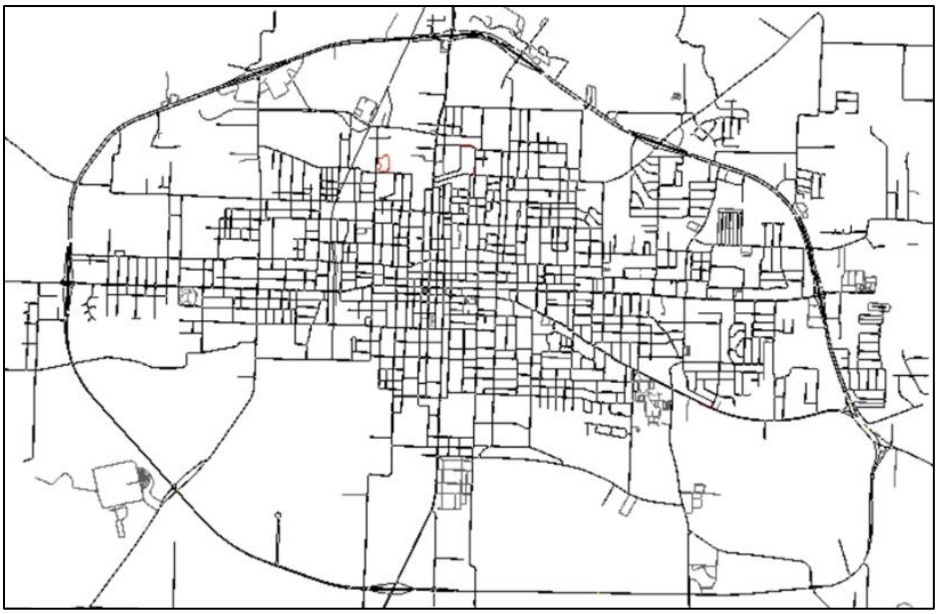

**Figure 4.7** Network generated in Simulation of Urban Mobility (SUMO)

After probabilistic slope failure analysis and generation of the network's traffic, the algorithm detailed in Figure 4.2 was used to determine the best policy for rehabilitating critical slope segments under different budget constraints imposed on slope rehabilitation, i.e., when transportation agencies only have 10 %, 20%, 30%, 40%, and 50% of the total failure restoration budget for the proactive slope rehabilitation. The parameter used for the genetic algorithm is shown in Table 4.2.

**Table 4.2** Parameters of Genetic Algorithm

| Parameter | Value |
|---|---|
| **Initial Population** | 5 |
| **Maximum number of generation** | 30 |
| **Initial mutation rate** | 0.9 |
| **Decrease of mutation rate** | 5% every generation |
| **Cross over type** | 2-point cross over |
| **Mutation of bits** | 20% (7 bits) |
| **Maximum Monte Carlo Runs** | 300 |

A convergence study was carried out to identify the adequate number of Monte Carlo runs for determining the expected generalized cost (Figure 4.8). No rehabilitation of slopes was considered in the convergence study as a network with no rehabilitation policy has the highest uncertainty compared to a network with any rehabilitation policy (Shahandashti and Pudasaini, 2019). The user cost was calculated considering six hours of disruption and the agency cost of slope restoration were calculated based on the compaction and rebuilding method. The number of Monte Carlo runs leading to the convergence of an unrehabilitated network would also be adequate for any rehabilitated network. From the convergence study, it was concluded that 300 Monte Carlo runs

are adequate to measure the performance of the network due to disruptions caused by rainfall-induced failures.

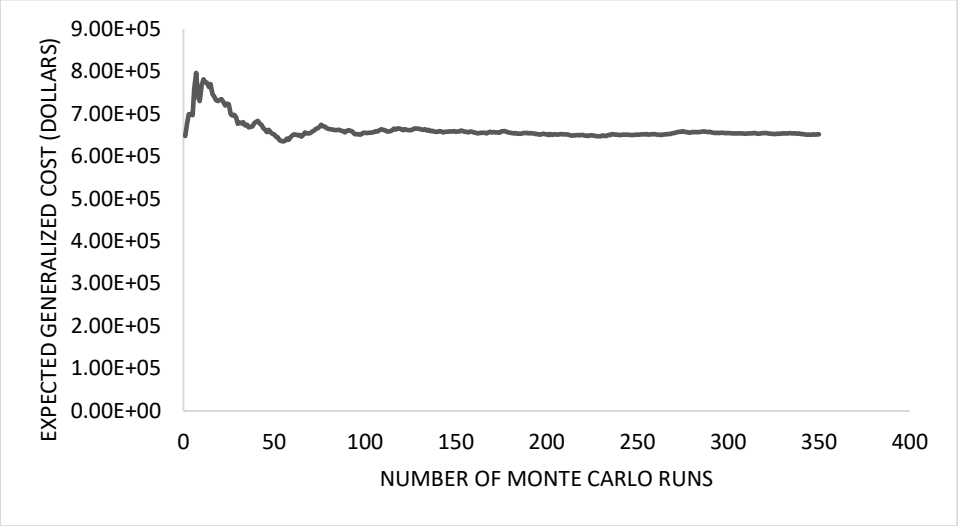


**Figure 4.8** Convergence study to identify the adequate number of Monte Carlo runs

Table 4.3 shows the combination of slopes that should be proactively rehabilitated when transportation agencies are constrained to rehabilitate only a limited slope segment due to the constraint on the rehabilitation budget. The slope segments recommended for repair by the proposed approach are represented by 1, whereas zero otherwise. The expected generalized cost for different rehabilitation constraints is shown in Table 4. The actual rehabilitation percent in Table 4 represents the percentage of total rehabilitation cost that was recommended by the proposed approach for proactive rehabilitation under different budget constraints. The proposed methodology helps in determining proactive slope rehabilitation strategies that will lead to the least generalized cost when agencies are constrained to repair only a certain portion of the total critical slope segment due to budget constraints. The 10%, 20%, 30%, 40%, and 50% policies are shown to demonstrate the proposed approach of finding the rehabilitation policies under different

rehabilitation budget constraints. The slope rehabilitation policies determined under 10%, 20%, 30%, 40%, and 50% are independent of each other.

**Table 4.3** Policies identified for different constraints on rehabilitation budget constraints

| S.N. | Slope Segment | Rehabilitation policy for different repair percentages | | | | |
|---|---|---|---|---|---|---|
| | | 10% | 20% | 30% | 40% | 50% |
| **1** | *S1* | 0 | 0 | 0 | 1 | 0 |
| **2** | *S2* | 0 | 0 | 0 | 0 | 0 |
| **3** | *S3* | 0 | 0 | 0 | 0 | 0 |
| **4** | *S4* | 0 | 0 | 1 | 1 | 1 |
| **5** | *S5* | 1 | 1 | 1 | 1 | 1 |
| **6** | *S6* | 0 | 1 | 1 | 0 | 1 |
| **7** | *S7* | 0 | 1 | 0 | 1 | 1 |
| **8** | *S8* | 0 | 0 | 0 | 0 | 1 |
| **9** | *S9* | 0 | 0 | 0 | 0 | 0 |
| **10** | *S10* | 0 | 0 | 0 | 0 | 0 |
| **11** | *S11* | 0 | 0 | 0 | 0 | 0 |
| **12** | *S12* | 0 | 0 | 0 | 1 | 0 |
| **13** | *S13* | 0 | 1 | 0 | 1 | 1 |
| **14** | *S14* | 0 | 0 | 0 | 0 | 1 |
| **15** | *S15* | 0 | 0 | 1 | 1 | 1 |
| **16** | *S16* | 1 | 1 | 1 | 1 | 1 |
| **17** | *S17* | 0 | 0 | 0 | 0 | 0 |
| **18** | *S18* | 0 | 0 | 0 | 0 | 1 |
| **19** | *S19* | 0 | 0 | 1 | 1 | 1 |
| **20** | *S20* | 0 | 0 | 1 | 1 | 1 |
| **21** | *S21* | 0 | 0 | 1 | 1 | 0 |
| **22** | *S22* | 0 | 0 | 0 | 0 | 1 |
| **23** | *S23* | 1 | 0 | 1 | 1 | 1 |
| **24** | *S24* | 0 | 0 | 0 | 1 | 0 |
| **25** | *S25* | 1 | 1 | 1 | 1 | 1 |
| **26** | *S26* | 0 | 1 | 1 | 1 | 1 |
| **27** | *S27* | 0 | 0 | 0 | 0 | 0 |
| **28** | *S28* | 1 | 1 | 1 | 1 | 1 |
| **29** | *S29* | 0 | 1 | 1 | 1 | 1 |
| **30** | *S30* | 1 | 1 | 1 | 1 | 1 |
| **31** | *S31* | 1 | 1 | 1 | 1 | 1 |
| **32** | *S32* | 1 | 1 | 1 | 1 | 1 |
| **33** | *S33* | 1 | 1 | 1 | 1 | 1 |

**Table 4.4** Results of prioritizing slope rehabilitation based on the proposed approach (considering the flow of traffic)

| Percentage of total rehabilitation budget demand | | Expected Generalized Cost ($) |
|---|---|---|
| Available for rehabilitation (%) | Actual rehabilitation (%) | |
| Not more than 10 | 9.88% | 484186 |
| Not more than 20 | 19.81% | 416657 |
| Not more than 30 | 29.43% | 336995 |
| Not more than 40 | 39.31% | 266973 |
| Not more than 50 | 41.67% | 202393 |

The slope rehabilitation policies under different rehabilitation constraints are not incremental. This is primarily because of the combinatorial nature of the slope rehabilitation decision problem. There are $2^n$ ways (i.e., policies) for rehabilitating n critical slope segments in a network if no constraints are applied for slope rehabilitation. As the range of policy increase exponentially with the number of slope segments, multiple rehabilitation policies can provide similar solutions under any rehabilitation budget constraint. Hence, due to the combinatorial nature of the slope rehabilitation decision problem and large solution space, all the slopes rehabilitated under the 10 percent rehabilitation budget constraint may not be necessarily present in the 20 percent budget constraint.

## 4.3. VALIDATION

The proposed approach to identify the critical combination of slope segments was compared with the commonly used index-based method for identifying critical slope segments in transportation corridors. The index-based approach used by Wachal and Hudak (2000) was followed to determine

the failure index of 33 slope segments that were identified as critical by probabilistic slope failure susceptibility analysis. Based on the failure index, a rehabilitation scheme was developed for different budget constraints imposed on slope rehabilitation: only 10 %, 20 %, 30 %, 40 %, and 50 % of the total required rehabilitation budget are available for slope rehabilitation. The slope with a higher failure index was identified as the most critical slope and was prioritized for rehabilitation. The expected generalized cost for rehabilitation policies obtained from the index-based approach is shown in Table 4.5. The expected generalized cost for policies determined from the index-based method was evaluated using the steps outlined in Figure 4.4.

**Table 4.5** Results of prioritizing slope rehabilitation based on the index-based approach

| **Percentage of total rehabilitation budget demand** | | **Expected Generalized Cost ($)** |
|---|---|---|
| **Available for rehabilitation (%)** | **Actual rehabilitation (%)** | |
| **Not more than 10** | 9.96% | 516589 |
| **Not more than 20** | 19.85% | 445372 |
| **Not more than 30** | 29.55% | 360145 |
| **Not more than 40** | 39.87% | 287044 |
| **Not more than 50** | 49.78% | 217520 |

The expected generalized cost obtained for different budget constraints from the index-based method is higher than the expected generalized cost obtained from the approach proposed in this study (Figure 4.9).

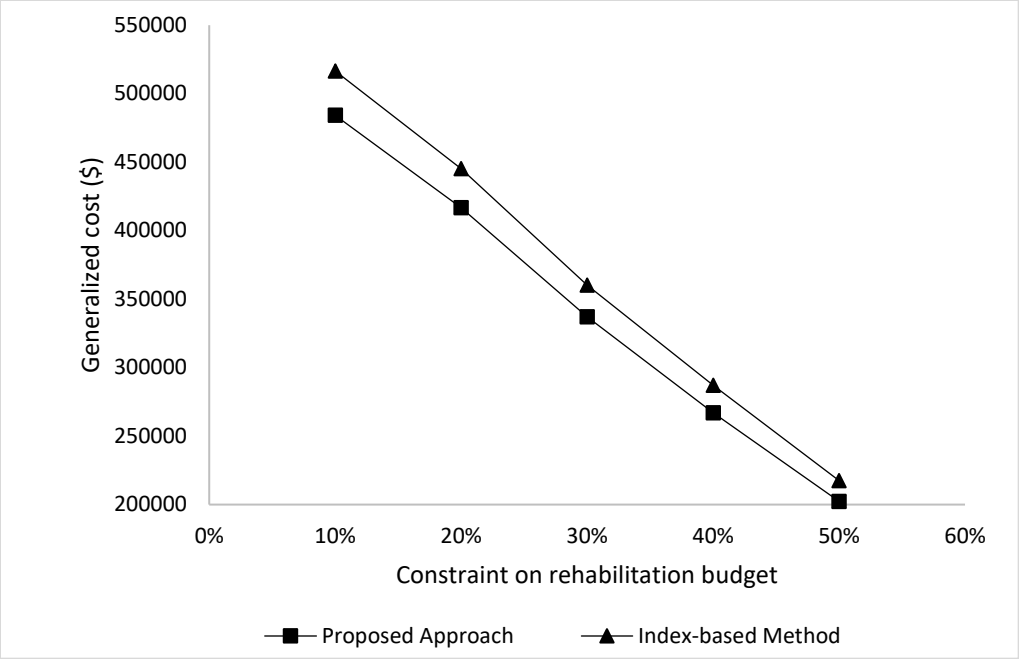


**Figure 4.9** Comparison of generalized cost obtained from proposed approach and index-based method

The proposed approach is effective in identifying the critical combination of slope segments compared to the commonly used index-based method for identifying and prioritizing the critical slope segments. However, the devised approach has some limitations. In this study, the probabilistic slope failure analysis is performed to assess the shallow slope failure susceptibility of roadside slopes, which usually occur at fully softened strength in clayey soils of Texas. The proposed approach is, however, flexible to incorporate other modes of slope failures. Future research should consider various slope failure modes and infiltration mechanisms in slope susceptibility assessment. The optimization constraint applied in this research is a knapsack constraint, which is based on the availability of budgets for the rehabilitation of slope segments. Nonetheless, the proposed approach is flexible to incorporate any other feasibility constraints like prioritizing slope segments for different rehabilitation length constraints.

# CHAPTER 5 RISK-AVERSE REHABILITATION DECISION FRAMEWORK FOR ROADSIDE SLOPES

The decision-making approach for slope rehabilitation should ensure that low risk is associated with the selected rehabilitation policy. Current slope-rehabilitation decision models do not consider the risk associated with the rehabilitation policies in the decision-making process. This chapter discusses a risk-averse stochastic combinatorial optimization to facilitate the selection of slope rehabilitation strategies, which leads to the least expected cost and conditional value at risk (CVaR) for extreme rainfall events. The simulated annealing approach is used to solve the risk-averse combinatorial optimization rehabilitation problem with the objective function that measures the total cost of traffic disruption and slope restoration post-failures. The approach is demonstrated using a transportation network in Lamar County, Texas.

## 5.1. METHODOLOGY

This section outlines the methodology used for risk-averse simulated annealing to determine the critical combination of slopes for proactive rehabilitation. The proposed risk-averse simulated annealing approach incorporates the Conditional Value at Risk (CVaR) associated with rehabilitation policy for determining the most suitable combination of slopes to be proactively rehabilitated under budget constraints. Determining the critical combination of roadside slopes for proactive rehabilitation involves

(1) formulating a risk-averse stochastic combinatorial optimization problem, and

(2) using a simulated annealing-based approach to determine the optimal slope rehabilitation strategy for roadside slopes.

### 5.1.1. Formulation of Risk-averse Combinatorial Optimization Problem

The optimization problem of minimizing expected generalized cost (V) in a transportation network is defined as:

$$min_{p \in P} \; E(V^p) \tag{5.1}$$

Subjected to

$$\sum_{k=1}^{Ns} n_k C_k \leq C_{rehab}$$

$$\mathrm{CVaR}_{\alpha} \leq T_{cost}$$

Where P represents possible combinatorial space of rehabilitation policies (p) for proactive maintenance of roadside slopes. Two possible outcomes can be defined for a slope in the generation of a rehabilitation policy, i.e., either slope can be rehabilitated or left unrehabilitated. For example, consider three slope segments in a road network that are susceptible to rainfall-induced failures. The rehabilitation policy can be represented as $\{rh_1, rh_2, rh_3\}$, where $rh_i=0$ represents no rehabilitation, and $rh_i= 1$ represents the rehabilitation of the $i^{th}$ slope segment. Based on this, the possible rehabilitation strategies for network in with three critical slope segments are are P = {{1,1,1}, {1,0,1}, {0,1,1}, {0,0,1}, {1,1,0}, {1,0,0}, {0,1,0}, {0,0,0}}. In the absence of constraints, the combinatorial decision space for a transportation network with N number of slope segments requiring repair would be $P \in \mathrm{X}^{2^{\mathrm{N}} \times \mathrm{N}}$. However, the combinatorial decision space is reduced by the optimization constraint that no rehabilitation policy ($p \in P$) can result in a rehabilitation cost that exceeds the available rehabilitation budget ($C_{rehab}$). The feasible rehabilitation policy should also have the conditional value at risk less than a specified tolerance cost ($T_{cost}$).

For the generalized cost (V), which can be represented as a continuous distribution function ($F_X(v)$), $CVaR_\alpha(V)$ is the conditional expectation of V subjected to $V \geq VaR_\alpha(V)$ (Sharveen et al. 2022). Figure 5.1 shows the distribution of generalized costs for a rehabilitation policy of roadside slopes.

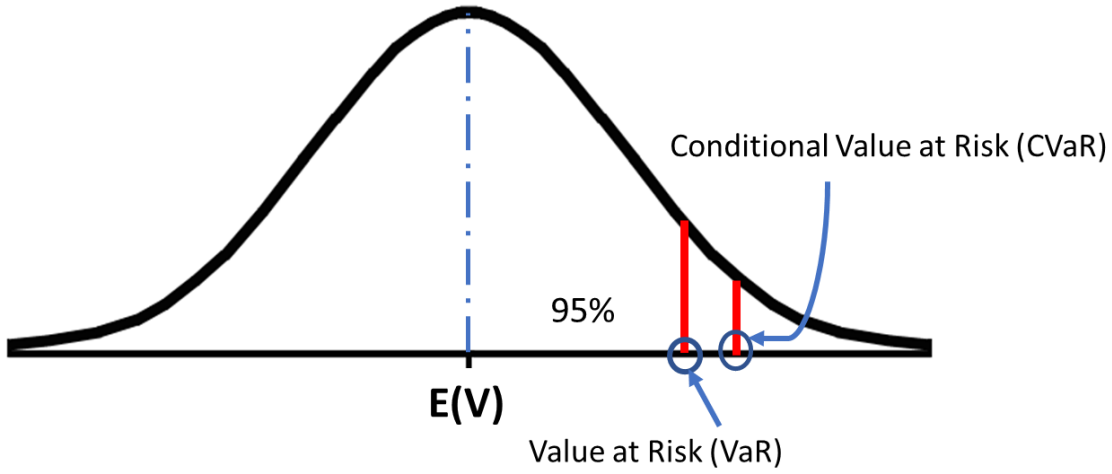


**Figure 5.1** Generalized cost distribution under a rehabilitation strategy

$VaR_\alpha(V)$ represents the value at $\alpha$-percentile of the random variable V. $CVaR_\alpha(V)$ can be determined using Equation 5.2.

$$CVaR_\alpha(V) = \int_{-\infty}^{\infty} v \, dF_X^\alpha(v) \tag{5.2}$$

Where

$$F_x^\alpha(v) = \begin{cases} 0, & when\ v < \ VaR_\alpha(V) \\ \frac{F_X(v)-\alpha}{1-\alpha}, & when\ v > \ VaR_\alpha(V) \end{cases} \tag{5.3}$$

The distribution parameter N ($\mu_v$, $\sigma_v$) of generalized cost (V) for a rehabilitation policy (p) is determined using the Monte Carlo simulations.

### 5.1.2. Solving Optimization Problem

Figure 5.2 outlines the process used for solving the risk-averse optimization problem. Solving the optimization problem starts with determining slope failure probabilities of roadside slopes along the highway corridors. The slope failure probability of roadside slope is assessed using a combination of physics-based hydrological and geotechnical models incorporating the uncertainty associated with soil cohesion, internal angle of friction, and rainfall intensity (Baral and Shahandashti, 2022). First, the increase in soil water pressure due to rainfall infiltration is determined using the pore pressure response model (Iverson, 2000). Then, the decrease in factor of safety (FOS) due to increased soil water pressure is determined using the infinite slope stability model (Skempton and DeLory, 1957). The FOS is determined for n Monte Carlo runs for n different generations of frictional angle, cohesion, and rainfall intensity from a predefined probability distribution function. The probability of slope failure is defined as the ratio of times the FOS is less than 1 to the total number of Monte Carlo runs (Ria et al. 2014).

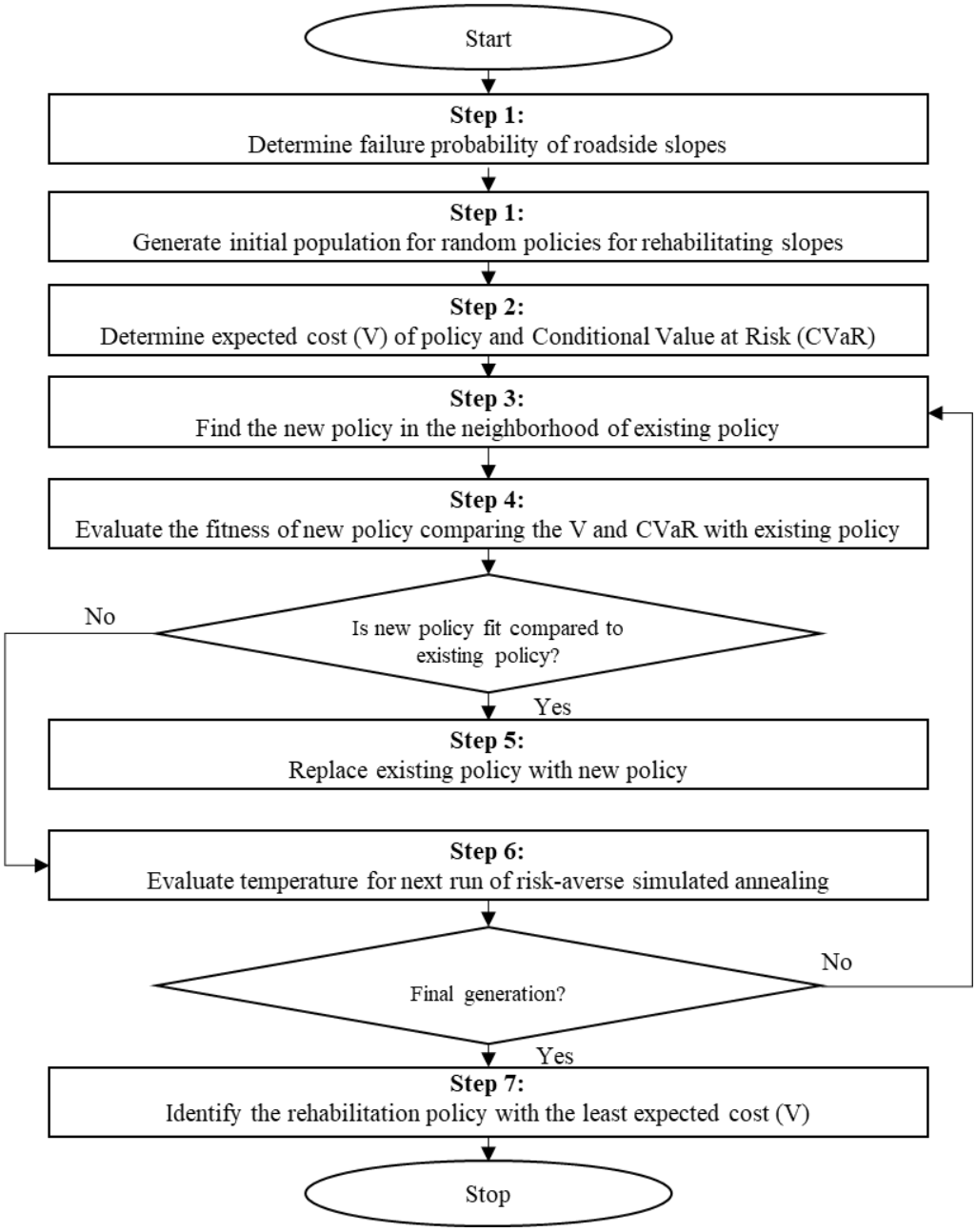


**Figure 5.2** Steps in the risk-averse simulated annealing process

Following the determination of slope failure probabilities of roadside slopes, an initial rehabilitation policy satisfying the cost constraint is generated. For the initial rehabilitation policy, expected cost and conditional value at risk are determined using the process outlined in Figure 5.3.

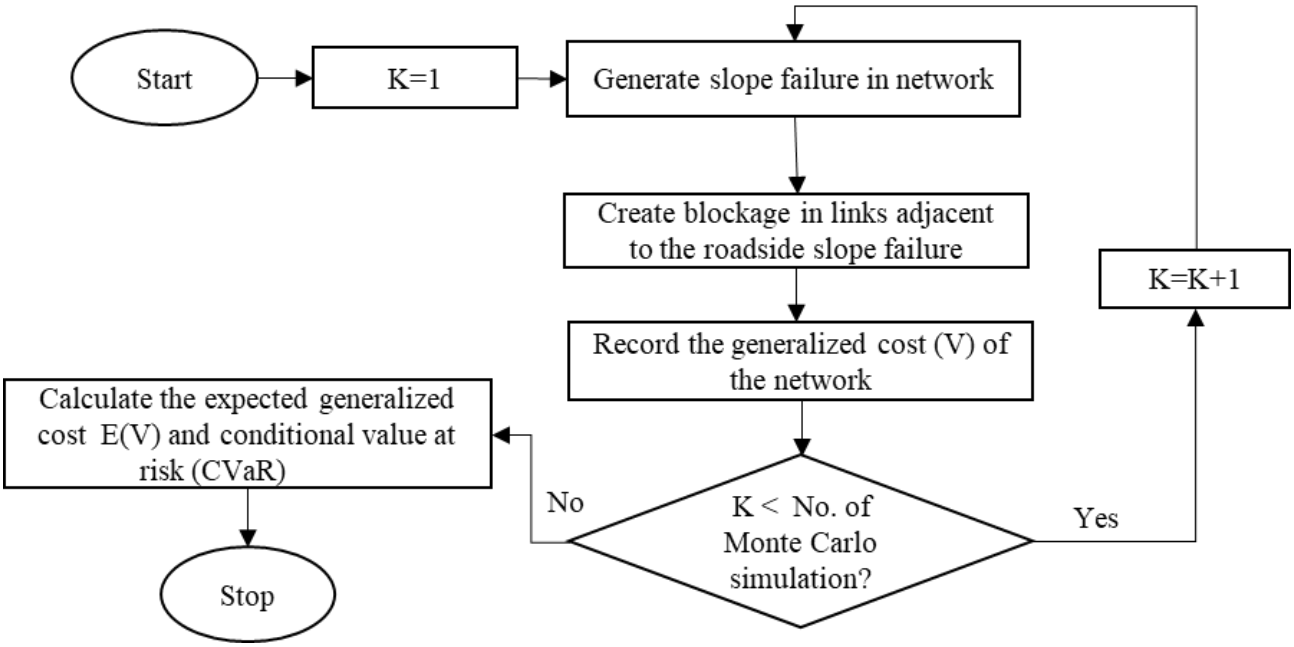


**Figure 5.3** Calculation of expected cost and conditional value at risk

First, a random number is generated ($R_n \in [0,1]$) and compared with the slope failure probability in a transportation network. If the slope is not repaired based on the current rehabilitation policy and the failure probability is less than the randomly generated number, disruption is created in the network by blocking the adjacent link. Then, a traffic simulation is performed for the disrupted network, and an increase in user cost due to rerouting is calculated. The user cost includes both the cost associated with delays and additional costs for the operation of vehicles. The agency cost for restoring the failed slopes is also calculated. The generalized cost (i.e., combined user and agency cost) for a rehabilitation strategy $p \in P$, is obtained using Equation 5.4.

$$V = \sum_i \sum_j d_{ij}^t \left[\Delta T_{ij}^p C_d + \Delta L_{ij}^p C_{op}\right] + C_{sr}^p) \quad (5.4)$$

where V represents combined user and agency cost for a single run of Monte Carlo simulation when slopes are rehabilitated using a policy p, $d_{ij}^t$is the travel demand from node i to node j for

the duration of disruption (t), $\Delta T_{ij}^{r}$ is the increase in time traveling from node i to node j and $\Delta L_{ij}^{r}$ is the increase in travel distance from node i to node j, $C_d$ is the cost due to delay and $C_{op}$ is the per mileage cost of maintaining and operating a motor vehicle, and $C_{sr}^{p}$ is the cost of restoring failed slopes after an extreme rainfall event. The delay cost ($C_d$) due to traffic disruption is assumed at 30.12 dollars per hour (TxDOT, 2022), and the cost of operating ($C_{op}$) a passenger vehicle per mileage is assumed at 67 cents (BTS, 2021). The traffic disruption is considered one-quarter of a day as this duration was assumed to be adequate to remove the debris caused by shallow slides triggered by rainfalls. The slope restoration cost ($C_{sr}^{p}$) is estimated based on the rebuilding and compaction method (Shahandashti et al., 2022a).

After completing N Monte Carlo runs for a rehabilitation strategy r, the list of generalized costs is obtained: $V_i$ = [ $V_1$, $V_2$, $V_3$,……..$V_N$]. The $V_i$ represents N different possible values of generalized cost under a rehabilitation strategy. This distribution of $V_i$ is used to determine the expected value of generalized cost (E(Vp)) and the conditional value of risk $CVaR_{\alpha}(V_p)$ for the rehabilitation strategy p.

The approach outlined in Figure 5.2 for calculating expected generalized cost and conditional value at risk is integrated into a risk-averse simulated annealing algorithm to determine the rehabilitation strategy that would lead to the least expected cost while also reducing the conditional value at risk. Due to the lack of a closed form solution to the objective function represented by Equation 5.1 and the stochastic combinatorial nature of the problem, risk-averse simulated annealing has been used to determine the rehabilitation strategy that would lead to the least expected cost while also reducing the conditional value at risk (CVaR) associated with the rehabilitation strategy. The simulated annealing mimics a solid annealing process, where the state

of the solid resembles the possible solutions, energy resembles the objective function of an optimization problem, and the cooling rate of the solid is analogous to a finite sequence of temperature in simulated annealing (Kirkpatrick et al. 1983). The metropolis criterion is used to determine the acceptance or rejection of a new solution at different temperatures during the progression of simulated annealing (Metropolis et al. 1953). At each temperature, mutation of the existing rehabilitation strategy is performed to generate new solutions. At the initial stage of the simulated annealing process, the temperature is set high, thereby increasing the probability of accepting the inferior solutions (Chen and Shahandashti, 2007). With the decrease in temperature, the probability of accepting an inferior solution is decreased and fine-tuning of the optimal solution takes place in the most promising decision space. The time required for converging to an optimal solution is dependent upon the cooling rate and initial temperature. Typically, the initial temperature, cooling rate, and stopping criteria is determined using sensitivity analysis (Pudasaini and Shahandashti, 2019).

Following the determination of expected cost (E(Vp)) and conditional value of risk ($CVaR_{\alpha}(V_p)$) of a randomly generated initial rehabilitation policy (Figure 5.2), a new rehabilitation policy is generated by randomly mutating the twenty-five percent of the binary strings of the old rehabilitation policy. The initial temperature is set to the generalized cost of failure when no rehabilitation is performed in a network. The fitness of the new rehabilitation policy is evaluated based on E(Vp) and $CVaR_{\alpha}(V_p)$ of new and existing rehabilitation policies in each generation of simulated annealing, until the final temperature is reached. The decision of adopting a new rehabilitation strategy compared to the existing rehabilitation strategy (i.e., the old strategy) is based on the following conditions:

**Case 1:** $\boldsymbol{E(V)_{new} \leq E(V)_{old}}$

**Subcase 1a:** If the CVaR of the new rehabilitation policy is less than the old policy, and the CVaR of the new policy is also less than the tolerance cost, then the new policy replaces the old policy in the next generation of simulated annealing.

**Subcase 1b:** If the CVaR of the new policy is more than the previous policy, then the metropolis function is used to select the rehabilitation policy for the next generation. A random number ( $\lambda \in [0,1]$) is generated and compared with the state of energy $\Delta$ given by Equation 5.5.

$$\Delta = \exp\left(\frac{-(\mathrm{CvaR}_{95}(\mathrm{old}))-(\mathrm{CvaR}_{95}(\mathrm{new}))}{\mathrm{Temp}}\right) \tag{5.5}$$

Where 'Temp' is the temperature at the current simulated annealing run. The old strategy is replaced by the new when $\lambda < \Delta$. Otherwise, the old rehabilitation strategy is carried to the next generation.

**Case 2:** $\boldsymbol{E(V)_{new} > E(V)_{old}}$

**Subcase 2a:** If the generalized cost of the new policy is greater than the old policy, but the CVaR of the new strategy is less than the tolerance cost, the state of energy (D) given by Equation 6 is checked with the randomly generated number ( $\beta \in [0,1]$).

$$D = \exp\left(\frac{-(\mathrm{E}(V_{old}))-(\mathrm{E}(V_{new}))}{\mathrm{Temp}}\right) \tag{5.6}$$

Where 'Temp' is the temperature at the current simulated annealing run. The old policy is replaced by new when $\beta < D$, otherwise old policy is carried to the next generation.

**Subcase 2b:** If the generalized cost of the new policy is greater than the old policy and the CVaR of the new policy is also greater than the previous policy, the state of energy $\Delta$ and D are determined as per Equations 5 and 6. The old policy is replaced by new when $\lambda < \Delta$ and $\beta < D$, otherwise the old policy is carried to the next generation.

## 5.2. APPLICATION

The proposed risk-averse optimization approach is used to identify the most suitable slope combination for proactive repair in Loop 286 in Lamar County, Texas. The Loop 286 selected to demonstrate the proposed risk-averse optimization approach is shown in Figure 5.4.

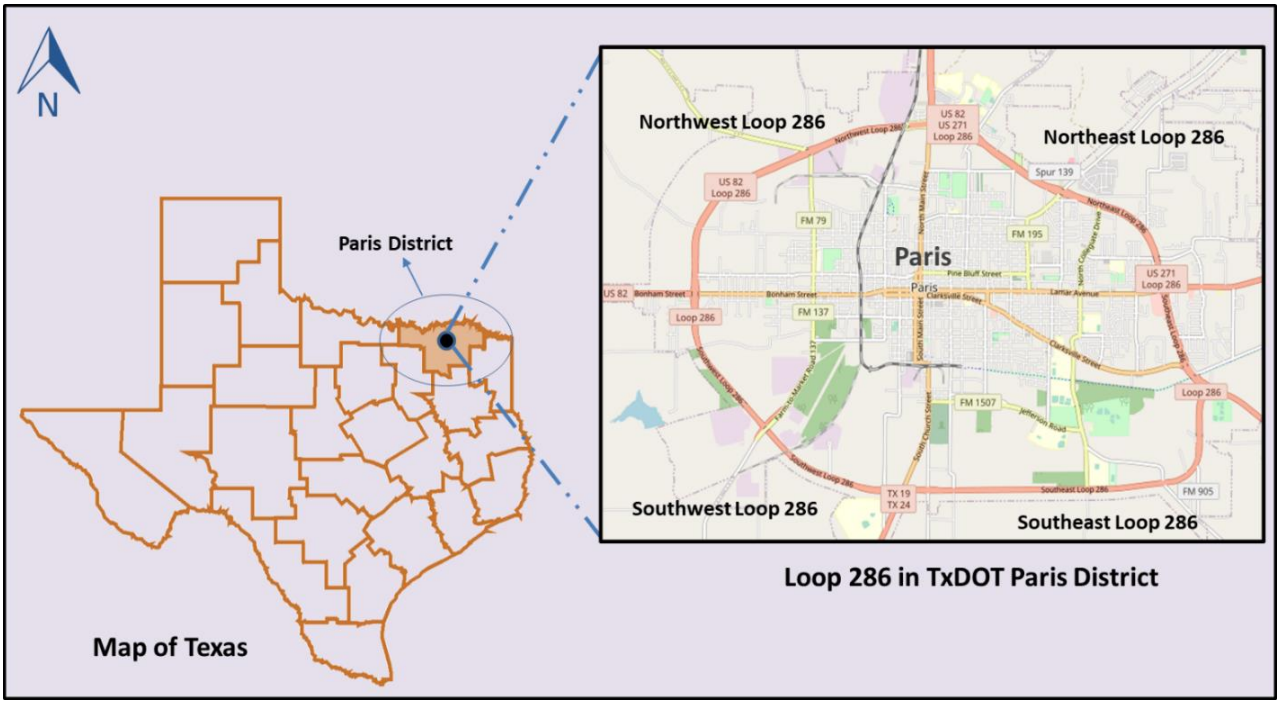


**Figure 5.4** Loop 286 in the TxDOT Paris district

First, the slope failure probabilities of slopes along the highway corridors were determined using a combination of the infinite slope stability model (Skempton and DeLory, 1957) and the rainfall infiltration model (Iverson, 2000). This study considered a rainfall of 3-day and a 10-year return

period to assess the failure probability of the roadside slopes along the highway corridors (GCO, 1984). The data on rainfall for the study area is obtained from the Precipitation Frequency Data Server (PDFS), which is operated and maintained National Weather Service (NWS) (NOAA, 2018). A rainfall distribution function for a 3-day duration and 10-year return period in the study region is given by Equation 5.7, where g(r) represents the probability of rainfall intensity r. The mean rainfall intensity in the study area is 7.21 inches.

$$g(r) = \frac{1}{0.125x\sqrt{2\pi}} \exp\left(-\frac{(\ln(r/7.21))^2}{0.03125}\right) \quad (5.7)$$

The infinite slope stability and rainfall infiltration models require slope angles and soil properties to determine the slope failure probabilities along the highway corridors. The LiDAR (Light Detection and Ranging) data was used to determine the slope angles of the landscape. The LiDAR dataset is publicly available by Texas Natural Resource Information System (TNRIS, 2019). The LiDAR data was processed in GIS to obtain a slope angle raster with a cell size of 3m. The soil properties for slopes were obtained from the Soil Survey Geographic (SSURGO) database (Soil Survey Staff, 2020). The SSURGO database is publicly available by Natural Resource Conservation System (NRCS). Slopes in Lamar County are primarily clayey soils with high shrinkage and swelling potential (Shahandashti et al. 2021), and slope failures usually occur at fully softened strength (Kayyal and Wright, 1991; Castellanos, 2014). At fully softened strength, the shear strength of soil is considerably reduced, and the cohesion of soil is negligible (Jafari and Puppala, 2019). Hence, based on past slope failure literature, the cohesion of 50 psf was assumed for calculating slope failure probability (Stauffer and Wright, 1984; Kayyal and Wright, 1991; Wright et al., 2007). The mean frictional angle for each landscape cell was obtained using the empirical correlation that establishes the relation of frictional angle with Liquid Limit (LL) for

different clay fractions and effective stress (Stark et al., 2005; Gamez and Stark, 2014). After defining the mean cohesion and fully softened frictional angle for each landscape cell, the lower and upper limit of cohesion and friction angle were assumed to lie within 50% of the mean value for developing a probabilistic slope failure map (Ria et al., 2014; Baral and Shahandashti, 2022b). The cohesion for each pixel was assumed to be in the range of $[0.5\times c_{\text{mean}}, 1.5\times c_{\text{mean}}]$, and the internal angle of friction was assumed to be in the range of $[0.5\times \phi_{\text{mean}}, 1.5\times \phi_{\text{mean}}]$. After determining the range of values for frictional angle and cohesion, the slope failure probability was determined using a combination of the infinite slope stability model and hydrological model (Baral and Shahandashti, 2022b). From the probabilistic slope failure analysis, twenty-one slope segments along the highway corridors were found to have a failure probability greater than 0.2. Park et al. (2013) and Ko et al. (2004) considered slope failure probability greater than 0.1 and 0.2, respectively, susceptible to slope failures. This study used a failure probability of 0.2 as a cut-off value for narrowing the number of slope segments to be incorporated into the rehabilitation decision framework. Figure 5.5 shows the twenty-one slope segments considered in the proactive slope rehabilitation framework to demonstrate the risk-averse optimization approach proposed in this study.

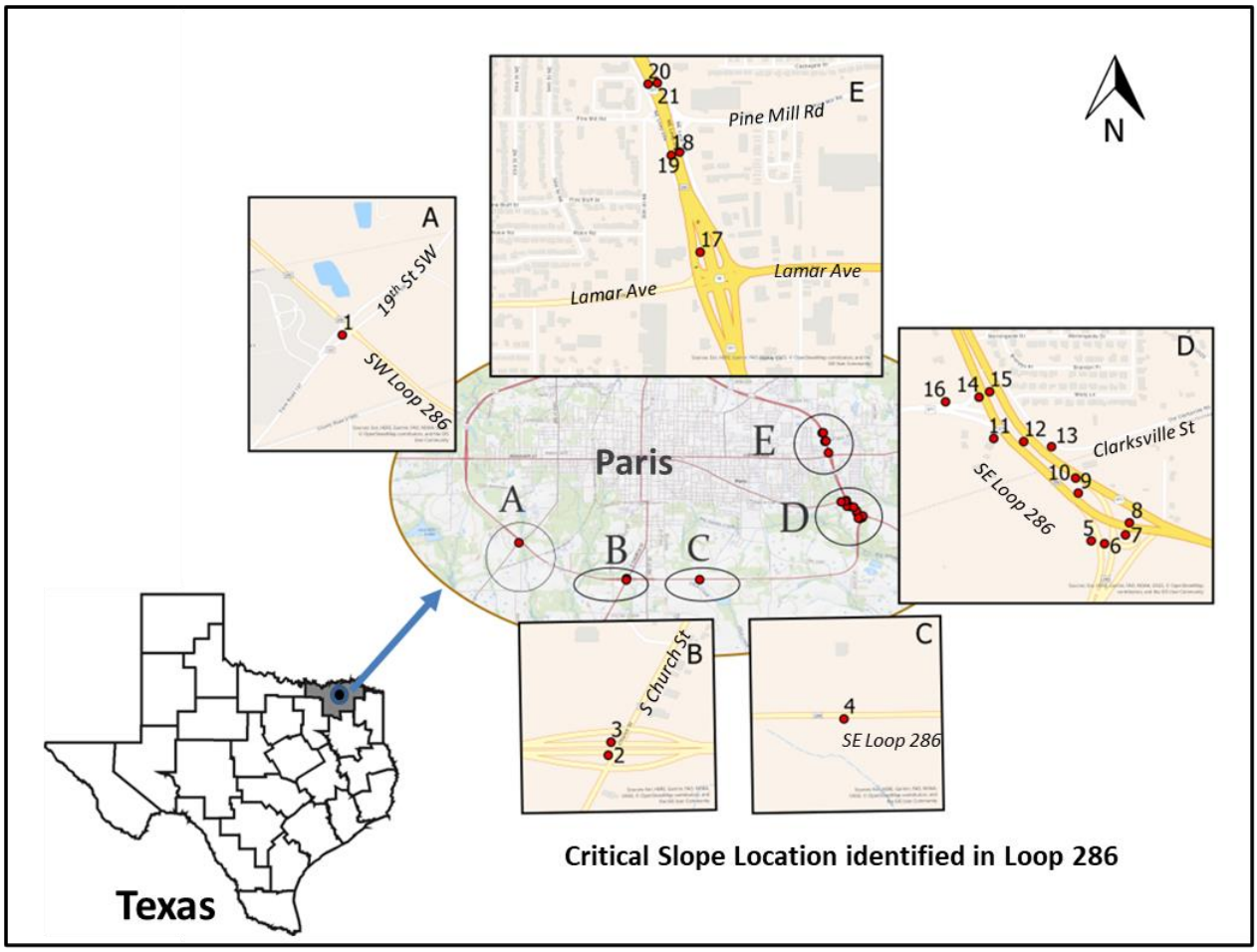


**Figure 5.5** Slopes with high failure susceptibility in Loop 286 of Paris district, Texas

For all the 21 slope segments identified to have high failure susceptibility, the slope rehabilitation cost was estimated using the rebuilding and compaction method (Shahandashti et al., 2022). For this study, the cost of restoring the slope after failure is assumed to be the same as the cost of proactively rehabilitating the slope segments. The cost of proactively rehabilitating the slope segments is shown in Table 5.1.

**Table 5.1** Cost for rehabilitation/restoration of different slope segments

| No. | Segment | Failure Probability ($P_f$) | Longitude | Latitude | Cost of Slope Rehabilitation (USD) |
|---|---|---|---|---|---|
| **1** | *S1* | 0.20 | -95.58627 | 33.640225 | 26890 |
| **2** | *S2* | 0.42 | -95.55988 | 33.631041 | 75574 |
| **3** | *S3* | 0.33 | -95.5598 | 33.631421 | 50542 |
| **4** | *S4* | 0.20 | -95.54185 | 33.631145 | 150104 |
| **5** | *S5* | 0.28 | -95.50286 | 33.646242 | 53022 |
| **6** | *S6* | 0.31 | -95.50248 | 33.646162 | 74904 |
| **7** | *S7* | 0.33 | -95.50187 | 33.646415 | 32054 |
| **8** | *S8* | 0.41 | -95.50176 | 33.646768 | 26132 |
| **9** | *S9* | 0.32 | -95.50324 | 33.647626 | 88389 |
| **10** | *S10* | 0.34 | -95.50331 | 33.648061 | 32889 |
| **11** | *S11* | 0.33 | -95.50568 | 33.649207 | 103890 |
| **12** | *S12* | 0.47 | -95.50482 | 33.649117 | 83582 |
| **13** | *S13* | 0.35 | -95.50401 | 33.648972 | 96023 |
| **14** | *S14* | 0.27 | -95.50611 | 33.650401 | 26142 |
| **15** | *S15* | 0.24 | -95.50581 | 33.650558 | 58700 |
| **16** | *S16* | 0.21 | -95.50708 | 33.65027 | 19023 |
| **17** | *S17* | 0.21 | -95.51022 | 33.662315 | 25721 |
| **18** | *S18* | 0.79 | -95.51106 | 33.665119 | 18953 |
| **19** | *S19* | 0.68 | -95.51082 | 33.665211 | 21151 |
| **20** | *S20* | 0.81 | -95.51173 | 33.667181 | 23787 |
| **21** | *S21* | 0.84 | -95.51146 | 33.667214 | 23517 |
| **Total Budget Required for Proactive Rehabilitation** | | | | | **1110989** |

The traffic count data in 98 different locations of the network was obtained from the traffic count database (TxDOT, 2021). The open-source simulation package SUMO (Simulation of Urban Mobility) was used to develop the traffic simulation in the network. The OpenStreetMap (OSM) was used to extract the map of the study area, and a network compatible for running traffic

simulation was obtained using the NETCONVERT tool in SUMO (DLR, 2021a). A NETEDIT tool in SUMO was used to manually modify the network (DLR, 2021b). The NETEDIT enables the addition of missing edges, links, connections, and traffic lights in the SUMO network. After the generation of the network, the 'routeSampler' tool was used to heuristically sample routes that matched the traffic count data obtained from the detectors at different locations of the network (DLR, 2021c).

After determining all critical slope segments and generation of network traffic, a convergence study was conducted to determine the average number of runs required for convergence of expected cost in each rehabilitation strategy. Figure 5.6 shows the average generalized cost for different Monte Carlo runs when no slopes in the network are rehabilitated. The convergence study considered no rehabilitation because the uncertainty is highest in the unrehabilitated network compared to a rehabilitated network.

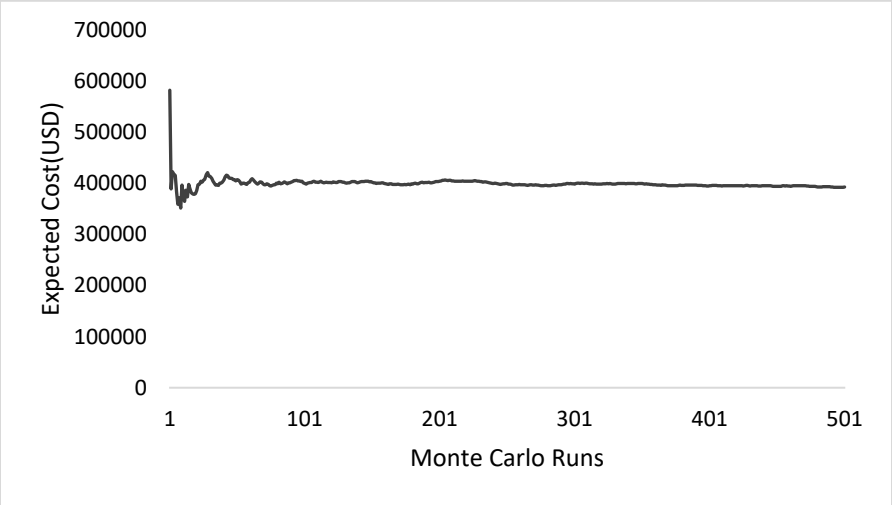


**Figure 5.6** Convergence study to determine Monte Carlo runs

After determining the required number of Monte Carlo runs from the convergence study, a risk-averse simulated annealing approach was used to determine the best slope rehabilitation policy

such that no rehabilitation strategy exceeds 25 percent of the total rehabilitation budget obtained in Table 1. Also, no rehabilitation strategy can have a conditional value at risk greater than 0.5 million USD. Parameters for risk-averse simulated annealing are shown in Table 5.2.

**Table 5.2** Parameters for risk-averse simulated annealing

| **Parameter** | **Value** |
|---|---|
| Initial Temperature | Expected cost when no slope is rehabilitated |
| Cooling factor | $1.5^{-1}$ |
| Final Temperature | Initial Temperature*$1.5^{-30}$ |
| Iteration per temperature | 10 |
| Monte Carlo runs for Convergence | 250 |
| Total iteration for Simulated Annealing | 300 |

The initial temperature in the first run of simulated annealing was set to the expected cost of slope failure considering no rehabilitation of roadside slopes (Figure 5.6). Ten iterations were conducted on each temperature. The cooling factor (Table 5.2) was used to lower the existing temperature after ten iterations of risk-averse simulated annealing. The expected cost and conditional value at risk obtained for different rehabilitation policies during the progression of risk-averse simulated annealing are shown in Figure 5.7. Five rehabilitation policies (RP1, RP2, RP3, RP4, and RP5) shown in Figure 5.7 represent the set of non-dominated solutions. A non-dominated solution set in a multi-objective optimization problem is the list of solutions in which one objective cannot be improved without compromising the other objective (Hwang and Masud, 2012). The five rehabilitation policies are shown in Figure 8 had either expected cost or conditional value at risk lower than the other policies. The rehabilitation policies represented by RP1, RP2, RP3, RP4, and RP5 are shown in Table 5.3. The rehabilitation policies RP1, RP2, RP3, RP4, and RP5

recommended the strategies for which the rehabilitation cost was 23.40, 24.24, 24.71, 23.26, and 23.86 percent of the rehabilitation budget obtained in Table 5.1. The non-dominated solutions obtained from the proposed risk-averse simulated annealing help transportation agencies select the optimum rehabilitation policies with different risk-aversion levels.

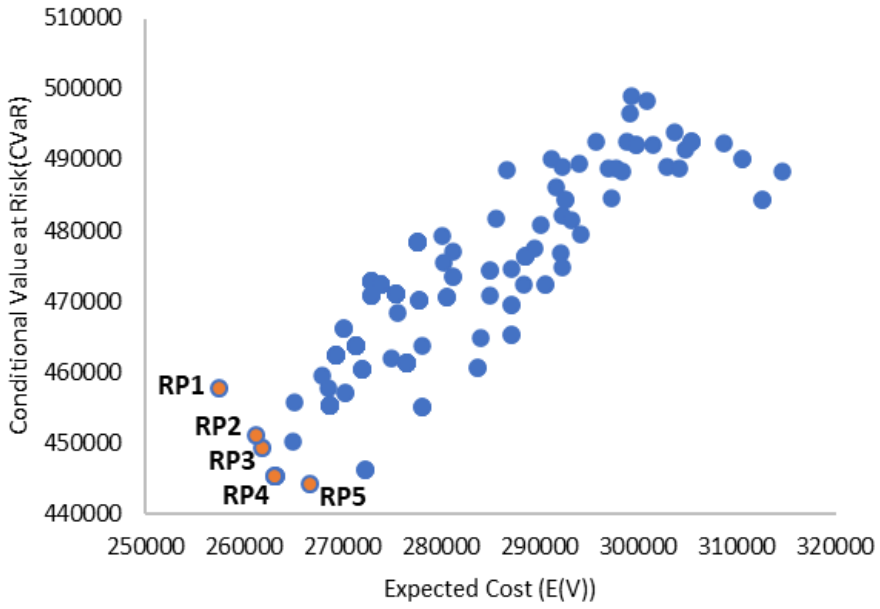


**Figure 5.7** Expected cost and Conditional Value at Risk for different rehabilitation policies obtained during the progression of simulated annealing

**Table 5.3** Slopes rehabilitated under rehabilitation policies RP1, RP2, RP3, RP4, and RP5

| S.N. | Segment | Rehabilitation Strategy | | | | |
|---|---|---|---|---|---|---|
| | | RP1 | RP2 | RP3 | RP4 | RP5 |
| **1** | *S1* | 0 | 0 | 0 | 0 | 0 |
| **2** | *S2* | 0 | 0 | 0 | 0 | 1 |
| **3** | *S3* | 0 | 0 | 0 | 0 | 0 |
| **4** | *S4* | 0 | 0 | 0 | 0 | 0 |
| **5** | *S5* | 0 | 0 | 0 | 1 | 0 |
| **6** | *S6* | 1 | 0 | 0 | 0 | 0 |
| **7** | *S7* | 0 | 0 | 1 | 1 | 0 |
| **8** | *S8* | 1 | 1 | 1 | 1 | 0 |
| **9** | *S9* | 0 | 0 | 0 | 0 | 0 |
| **10** | *S10* | 1 | 0 | 1 | 0 | 0 |
| **11** | *S11* | 0 | 0 | 0 | 0 | 0 |
| **12** | *S12* | 1 | 1 | 0 | 1 | 1 |
| **13** | *S13* | 0 | 1 | 1 | 0 | 0 |
| **14** | *S14* | 0 | 0 | 0 | 0 | 0 |
| **15** | *S15* | 0 | 0 | 0 | 0 | 1 |
| **16** | *S16* | 0 | 0 | 0 | 0 | 0 |
| **17** | *S17* | 0 | 0 | 0 | 0 | 0 |
| **18** | *S18* | 1 | 1 | 1 | 1 | 0 |
| **19** | *S19* | 0 | 1 | 1 | 1 | 0 |
| **20** | *S20* | 0 | 0 | 1 | 0 | 1 |
| **21** | *S21* | 1 | 1 | 1 | 1 | 1 |

Note: 1 represents rehabilitation and 0 represents no rehabilitation of the slope segment

## 5.3. VALIDATION

The proposed risk-averse optimization approach was compared with the genetic algorithm-based optimization approach to identify the critical combination of roadside slopes for proactive rehabilitation (Baral and Shahandashti, 2022a). This genetic algorithm-based approach for identifying the slope rehabilitation strategy was shown to outperform the existing index-based approach for prioritizing slope rehabilitation works (Baral and Shahandashti, 2022a). As the genetic algorithm-based optimization approach ignored the conditional value at risk associated

with rehabilitation strategy in the decision-making process, the importance of considering the risk-aversion in the optimization framework could be easily illustrated when the genetic algorithm-based approach was compared with the risk-averse simulated annealing approach proposed in this study. Initially, five random policies were generated such that no rehabilitation policy exceeded 25 percent of the total rehabilitation budget obtained in Table 5.1. The expected costs of the randomly generated five policies were determined and a two-point cross-over was performed on the rehabilitation policies with the least expected cost during each progression of genetic algorithms. The genetic algorithm was performed for 100 generations. The mutation was performed for 20 percent of the bits in the rehabilitation policy. The initial mutation rate was 90 percent and was gradually decreased by 5 percent in each generation of the genetic algorithm.

Figure 5.8 shows the expected cost and CVaR of rehabilitation policies obtained from the risk-averse simulated annealing and the genetic algorithm-based rehabilitation optimization approach that neglects the consideration of risk aversion in the optimization process. The genetic algorithm-based approach recommended the rehabilitation of slope segments S2, S3, S12, S18, S19, and S21. The genetic algorithm-based approach provides a single solution in the Pareto efficient frontier (Figure 5.8) limiting the choice of slope rehabilitation for the decision-makers. On the other hand, the proposed risk-averse simulated annealing approach provide decision-makers a range of solution in the risk-return space with different expected cost and CVaR. Compared to the CVaR of rehabilitation policy GA-RS obtained from the genetic algorithm-based approach (Figure 5.8), the CVaR of the rehabilitation strategy RP4 identified by the proposed risk-averse simulated annealing approach is lower by 2 percent. On the other hand, the expected cost of rehabilitation policy RP4 is only higher by 0.8 percent compared to the expected cost of rehabilitation policy GA-RS (Figure 5.8). Hence, the proposed risk-averse simulated annealing approach helps in the

selection of rehabilitation strategy of slope considering the suitable tradeoff between expected cost and CVaR.

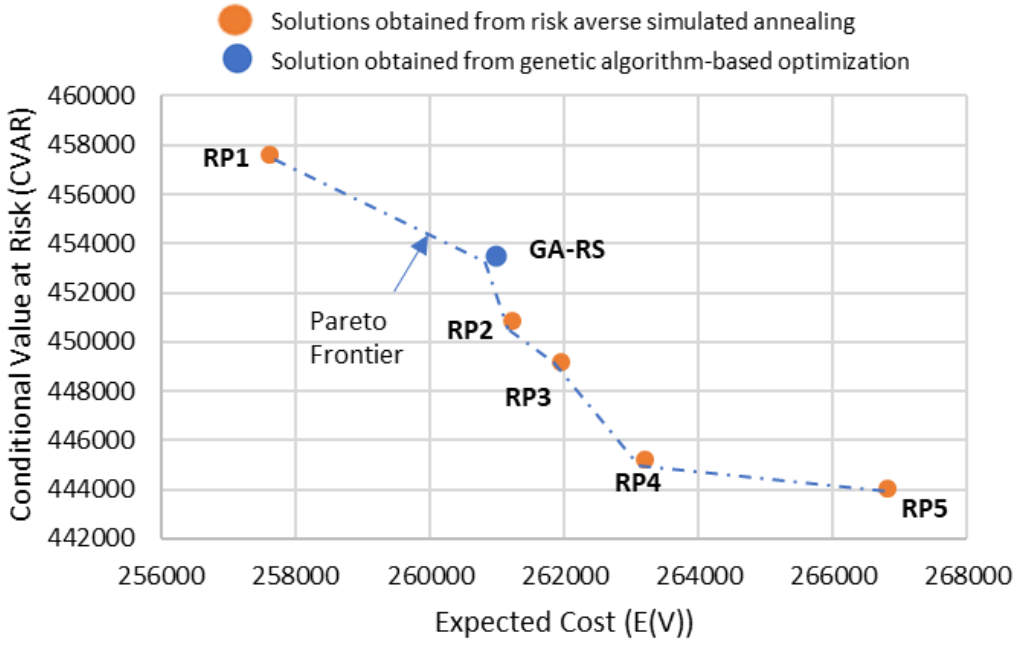


**Figure 5.8** Comparison of rehabilitation optimization results with and without the risk-averse condition

The approach to slope management in transportation agencies has so far been reactive. i.e., the slopes are only repaired after rainfall-induced failures disrupt the transportation network. This study provides transportation agencies with a tool to facilitate proactive decision-making. The risk-averse slope rehabilitation decision approach proposed in this study enables the identification of the most promising combination of slopes that should be proactively rehabilitated with a limited budget to minimize the impacts of rainfall-induced geohazard on highway networks. The optimization approach proposed in this study incorporates the expected cost (V) and Conditional Value at Risk (CVaR) associated with the rehabilitation policy to facilitate proactive rehabilitation decisions. At present the objective function is able to capture the impact of slope failure scenarios

on road users and agencies under different rehabilitation policies, but not over a planning time horizon or with consideration of longevity of repair methods adopted for proactive rehabilitation. The proposed risk-averse optimization approach can be further extended in future studies to consider the time horizon of maintenance planning and the longevity of the repair methods used in proactive rehabilitation.

# CHAPTER 6 CONCLUSION

The maintenance and management of roadside slopes is crucial for the smooth operation of the transportation system. The transportation agencies however are not able to proactively maintain or rehabilitate all the slopes due to competing maintenance needs between different transportation assets. Therefore, the transportation agencies must make a difficult decision to identify and rehabilitate the slope with a limited available budget. Current models to support the rehabilitation decision of roadside slopes do not consider budget constraints and risk associated with rehabilitation decisions in prioritizing slope rehabilitation works. Also, it is difficult to determine the condition (i.e., stability) of spatially distributed roadside slopes at a regional scale. Hence this study was conducted to attain three objectives: 1) to develop a data integration approach for performing slope failure susceptibility analysis to determine the usefulness of publicly available data sources for mapping rainfall-induced shallow slope failure susceptibilities in roadside slopes; (2) to integrate the slope failure susceptibility analysis with the metaheuristic optimization model to determine the most suitable combination of roadside slopes for proactive rehabilitation when agencies can only rehabilitate limited slopes due to budget constraint; (3) to incorporate the risk associated with the slope rehabilitation decisions into the optimization framework to facilitate the selection of rehabilitation strategies at appropriate risk-aversion levels.

A GIS-based data integration approach was developed to map the rainfall-induced shallow slope failure susceptibilities in clayey soils with high shrinkage and swelling potential. The publicly available data on slope stability variables, which have different levels of detail (granularity), representation (vector or raster data), and reference (coordinate) system, were made compatible with each other and stored in a geodatabase format. The dataset was then integrated with a combination of geotechnical and hydrological models considering the mobilization of fully

softened shear strength to determine the minimum duration of 10-year return period rainfall triggering slope instability in clayey slopes. The approach was implemented along 496 kilometers of highway corridors in the TxDOT Paris district. The geo-hazard potential of slopes along the highway corridors was classified based on the minimum duration of 10-year return period rainfall triggering shallow slope instability in roadside slopes. The result was delineated over the landscape cells in the study area with colors representing different susceptibility levels based on rainfall duration triggering slope instability. The slope failure susceptibility maps developed using the proposed approach were validated using a dataset of past slope failures. Nine out of ten recent slope failures recorded in the TxDOT Paris district occurred on the slopes that the proposed approach classified as highly critical regions, which require rainfall duration of fewer than 3 days of 10-year return period rainfall to trigger slope instability. The result demonstrated that the proposed GIS-based data integration approach could be an efficient tool to create shallow slope failure susceptibility maps through the use of publicly available data on slope stability variables. The proposed approach for developing slope susceptibility maps in clayey soil slopes can have a significant value in slope management of highway corridors for transportation agencies. The proposed data integration approach can also be useful in developing an early geo-hazard warning system based on rainfall forecasting.

In addition to the data integration approach, an approach to identify a proactive rehabilitation strategy for roadside slopes to minimize the impact of rainfall-induced slope failures on transportation networks was obtained by integrating the genetic algorithm with the generalized cost estimation model, which measures the combined user and agency cost associated with slope failure. The proposed approach helps identify the critical combination of slope segments to be proactively rehabilitated when the transportation agencies can only rehabilitate limited slope

segments due to constraints on the rehabilitation budget. The application of the proposed approach was demonstrated through a network in the highway network of North Texas, where rainfall-induced shallow slope failure frequently occurs in roadside slopes made of highly plastic clayey soils. The proposed approach was compared with the commonly used index-based method for identifying the critical slope segments for proactive rehabilitation. The results suggest that the proposed genetic algorithm-based approach is suitable for identifying the critical combination slope segments for proactive rehabilitation when the impact on network users and transportation agencies is to be minimized after the rainfall-induced slope failure. The genetic algorithm-based approach presented in this research highly benefits from publicly available data on slope stability variables. The developed genetic algorithm-based approach contributes to the existing body of knowledge a new and robust method for network-level distribution of limited resources to facilitate proactive slope rehabilitation decisions of roadside slopes.

Lastly, a risk-averse combinatorial optimization problem was devised to identify the critical combination of slopes that must be rehabilitated to minimize the impact of rainfall-induced slope failures on the highway networks. The combinatorial optimization problem was solved using a simulated annealing approach. The objective of the combinatorial optimization problem was to determine a rehabilitation policy that minimizes the user and agency costs during the extreme rainfall events triggering slope failure. The rehabilitation was constrained by the agency's limitation to rehabilitate only a limited length of slope segment due to budget constraints and with the risk aversion level such that the conditional value at risk does not exceed the tolerance cost. The application of the proposed risk-averse optimization approach was demonstrated using a highway network in the Paris district, Texas. The rehabilitation was constrained so that no policy can recommend rehabilitation exceeding 25 percent of the total budget required for proactive

maintenance. A set of non-dominated solutions (i.e., rehabilitation policies) on the Pareto front were obtained at the end of the simulated annealing process. The results were compared with the latest methodology in literature for determining the proactive rehabilitation strategy for roadside slopes. The comparison showed that the proposed risk-averse simulated annealing was able to identify the list of solutions with different risk-aversion levels, thereby diversifying the selection of rehabilitation strategies for the roadside slopes. The proposed risk-averse simulated annealing approach will help transportation agencies to identify the most suitable combination of slopes for rehabilitation within acceptable risk tolerance levels under a constrained rehabilitation budget.

The metaheuristic approaches developed in this research for proactive rehabilitation decision-making enable the network operators to prudently manage the geohazard risk associated with roadside slopes. The proposed approaches are demonstrated on the roadside slopes which are made up of clayey soil; these optimization approaches should be investigated on other soil types. It would further be helpful to incorporate the uncertainties associated with soils and traffic into the optimization framework as network uncertainties can have a significant impact on the post-disaster serviceability of spatially distributed infrastructures (Pudasaini and Shahandashti, 2021; Roy et al. 2021). The optimization approaches presented in this research have prohibitive runtimes due to repeated traffic simulation for assessing the cost of slope failures. Future work might explore the computationally efficient surrogate models (Pudasaini and Shahandashti, 2020), stochastic programming approaches (Boskabadi et al. 2020), and different topological connectivity metrics to support the proactive rehabilitation of roadside slopes along highway corridors.

# REFERENCES


Achour, Y., Boumezbeur, A., Hadji, R., Chouabbi, A., Cavaleiro, V., & Bendaoud, E. A. (2017). Landslide susceptibility mapping using analytic hierarchy process and information value methods along a highway road section in Constantine, Algeria. *Arabian Journal of Geosciences*, *10*(8), 1-16.

Adhikari, I., Baral, A., Zahed, E., Abediniangerabi, B., & Shahandashti, M. (2021). Early stage Multi-criteria Decision Support System for Recommending Slope Repair Methods. *Civil Engineering and Environmental Systems*, *38*(2), 127-144.

Anderson, S. A., & Rivers, B. S. (2013). Corridor management: A means to elevate understanding of geotechnical impacts on system performance. *Transportation research record*, *2349*(1), 9-15.

Baeza, C., & Corominas, J. (2001). Assessment of shallow landslide susceptibility by means of multivariate statistical techniques. Earth Surface Processes and Landforms: The Journal of the British Geomorphological Research Group, 26(12), 1251-1263.

Baral, A., & Shahandashti, S. M. (2022a). Identifying critical combination of roadside slopes susceptible to rainfall-induced failures. Natural Hazards. *Springer Nature*. 1-22.

Baral, A., & Shahandashti, S. M. (2022b). A Data Integration Approach for Assessment of Rainfall-Induced Slope Failure Susceptibility. In *Construction Research Congress 2022* (pp. 480-489).

Baral, A., & Shahandashti, M. (2022c). Risk-Averse Rehabilitation Decision Framework for Roadside Slopes Vulnerable to Rainfall-induced Geohazards. *Journal of Infrastructure Preservation and Resilience*.

Baral, A., Poumand, P., Adhikari, I., Abediniangerabi, B., & Shahandashti, M. (2021). GIS-Based Data Integration Approach for Rainfall-Induced Slope Failure Susceptibility Mapping in Clayey Soils. Natural Hazards Review, 22(3), 04021026.

Baum, R. L., Savage, W. Z., & Godt, J. W. (2002). TRIGRS—a Fortran program for transient rainfall infiltration and grid-based regional slope-stability analysis. US geological survey open-file report, 424, 38.

Baum, R. L., Savage, W. Z., & Godt, J. W. (2008). TRIGRS-A Fortran program for transient rainfall infiltration and grid-based regional slope-stability analysis, version 2.0 (No. 2008-1159). US Geological Survey.

Berti, M., & Simoni, A. (2010). Field evidence of pore pressure diffusion in clayey soils prone to landsliding. Journal of Geophysical Research: Earth Surface, 115(F3).

Beven, K. J., & Kirkby, M. J. (1979). A physically based, variable contributing area model of basin hydrology/Un modèle à base physique de zone d'appel variable de l'hydrologie du bassin versant. Hydrological Sciences Journal, 24(1), 43-69.

Bhattarai, P., Tiwari, B., Marui, H., & Aoyama, K. (2004). Quantitative slope stability mapping with ArcGIS: prioritize highway maintenance. In Proceedings of ESRI's 24th Annual International User's Conference, San Diego. ESRI.

Boskabadi, A., Rosenberger, J. M., & Shahandashti, M. (2020, January). A two-stage stochastic programming approach for enhancing seismic resilience of water pipe networks. In Proceedings of the 2020 IISE Annual Conference.

BTS (Bureau of Transportation Statistics) (2021). Average Cost of Owning and Operating an Automobile. Available at https://www.bts.dot.gov/content/mile-costs-owning-and-operating-automobile Accessed March 20 2022

Caine, N. (1980). The rainfall intensity-duration control of shallow landslides and debris flows. Geografiska annaler: series A, physical geography, 62(1-2), 23-27.

Carrara, A. (1983). Multivariate models for landslide hazard evaluation. Journal of the International Association for Mathematical Geology, 15(3), 403-426.

Carrara, A., Guzzetti, F., Cardinali, M., & Reichenbach, P. (1999). Use of GIS technology in the prediction and monitoring of landslide hazard. Natural hazards, 20(2-3), 117-135.

Cascetta, E. (2009). Transportation systems analysis: models and applications (Vol. 29). Springer Science & Business Media.

Castellanos, B. A., Brandon, T. L., & VandenBerge, D. R. (2016). Use of fully softened shear strength in slope stability analysis. Landslides, 13(4), 697-709.

Chau, K. T., Sze, Y. L., Fung, M. K., Wong, W. Y., Fong, E. L., & Chan, L. C. P. (2004). Landslide hazard analysis for Hong Kong using landslide inventory and GIS. Computers & Geosciences, 30(4), 429-443.

Chen, P. H., & Shahandashti, S. M. (2007, September). Simulated annealing algorithm for optimizing multi-project linear scheduling with multiple resource constraints. In Proceedings

of the 24th International Symposium on Automation and Robotics in Construction, ISARC 2007 (No. 2005, pp. 429-434).

Chen, P. H., & Shahandashti, S. M. (2009). Hybrid of genetic algorithm and simulated annealing for multiple project scheduling with multiple resource constraints. Automation in Construction, 18(4), 434-443.

Clerici, A., Perego, S., Tellini, C., & Vescovi, P. (2002). A procedure for landslide susceptibility zonation by the conditional analysis method. Geomorphology, 48(4), 349-364.

Crosta, G. B., & Frattini, P. (2001, October). Rainfall thresholds for triggering soil slips and debris flow. In Proceedings of the 2nd EGS Plinius Conference on Mediterranean Storms, edited by: Mugnai, A., Guzzetti, F., and Roth, G., Siena, Italy (pp. 463-487).

Das, B. M. (2010). Geotechnical engineering handbook. J. Ross Publishing.

Day, R. W., & Axten, G. W. (1989). Surficial stability of compacted clay slopes. Journal of Geotechnical Engineering, 115(4), 577-580.

Demšar, U., Špatenková, O., & Virrantaus, K. (2008). Identifying critical locations in a spatial network with graph theory. Transactions in GIS, 12(1), 61-82.

DLR German Aerospace Center (2021a). *netconvert - SUMO Documentation*. SUMO. https://sumo.dlr.de/docs/netconvert.html (Accessed 8 March 2022)

DLR. German Aerospace Center. (2021b). *netedit - SUMO Documentation*. SUMO. https://sumo.dlr.de/docs/netedit.html (Accessed 8 March 2022)

DLR. German Aerospace Center. (2021c). *routesamplerpy - SUMO Documentation*. SUMO. https://sumo.dlr.de/docs/Tools/Turns.html#routesamplerpy (Accessed 8 March 2022)

D'Odorico, P., Fagherazzi, S., & Rigon, R. (2005). Potential for landsliding: dependence on hyetograph characteristics. Journal of Geophysical Research: Earth Surface, 110(F1).

Duan, Y., & Lu, F. (2014). Robustness of city road networks at different granularities. Physica A: Statistical Mechanics and its Applications, 411, 21-34.

Fall, M., Azzam, R., & Noubactep, C. (2006). A multi-method approach to study the stability of natural slopes and landslide susceptibility mapping. Engineering Geology, 82(4), 241-263.

Gamez, J. A., & Stark, T. D. (2014). Fully softened shear strength at low stresses for levee and embankment design. Journal of Geotechnical and Geoenvironmental Engineering, 140(9), 06014010.

Geotechnical Control Office Engineering Development Department Hong Kong. (1984). Geotechnical manual for slopes. Geotechnical Control Office, Public Works Department.

Guzzetti, F., Carrara, A., Cardinali, M., & Reichenbach, P. (1999). Landslide hazard evaluation: a review of current techniques and their application in a multi-scale study, Central Italy. Geomorphology, 31(1-4), 181-216.

Guzzetti, F., Mondini, A. C., Cardinali, M., Fiorucci, F., Santangelo, M., & Chang, K. T. (2012). Landslide inventory maps: New tools for an old problem. Earth-Science Reviews, 112(1-2), 42-66.

Guzzetti, F., Peruccacci, S., Rossi, M., & Stark, C. P. (2008). The rainfall intensity–duration control of shallow landslides and debris flows: an update. Landslides, 5(1), 3-17.

He, Y., & Beighley, R. E. (2008). GIS-based regional landslide susceptibility mapping: a case study in southern California. Earth Surface Processes and Landforms, 33(3), 380-393.

Hidalgo, C. A., Vega, J. A., & Obando, M. P. (2018). Effect of the Rainfall Infiltration Processes on the Landslide Hazard Assessment of Unsaturated Soils in Tropical Mountainous Regions. Engineering and Mathematical Topics in Rainfall, 163.

Highland, L. (2004). Landslide types and processes (No. 2004-3072).

Holmstadt, J., Bradley, N., & Muehlbach, P. (2019). MnDOT Slope Vulnerability Assessments (No. MN/RC 2019-12).

Hossain, J. (2013). Geohazard potential of rainfall induced slope failure on expansive clay.

Huabin, W., Gangjun, L., Weiya, X., & Gonghui, W. (2005). GIS-based landslide hazard assessment: an overview. Progress in Physical Geography, 29(4), 548-567.

Iverson, R. M. (2000). Landslide triggering by rain infiltration. Water resources research, 36(7), 1897-1910.

Jafari, N., & Puppala, A. (2019). Prediction and Rehabilitation of Highway Embankment Slope Failures in Changing Climate.

Jaiswal, P., van Westen, C. J., & Jetten, V. (2010). Quantitative landslide hazard assessment along a transportation corridor in southern India. Engineering geology, 116(3-4), 236-250.

Janbaz, S., Shahandashti, M., & Najafi, M. (2017). Life cycle cost analysis of an underground freight transportation (UFT) system in Texas. In Pipelines 2017 (pp. 134-143).

Kayastha, P., Dhital, M. R., & De Smedt, F. (2013). Application of the analytical hierarchy process (AHP) for landslide susceptibility mapping: a case study from the Tinau watershed, west Nepal. Computers & Geosciences, 52, 398-408.

Kayyal, M. K., & Wright, S. G. (1991). Investigation of Long-Term Strength Properties of Paris and Beaumont Clays in Earth Embankments. Final Report (No. FHWA/TX-92+ 1195-2F).

Khademi, N., Balaei, B., Shahri, M., Mirzaei, M., Sarrafi, B., Zahabiun, M., & Mohaymany, A. S. (2015). Transportation network vulnerability analysis for the case of a catastrophic earthquake. International journal of disaster risk reduction, 12, 234-254.

Khan, M. S., Hossain, S., & Kibria, G. (2016). Slope stabilization using recycled plastic pins. Journal of Performance of Constructed Facilities, 30(3), 04015054.

Khan, M. S., Hossain, S., Ahmed, A., & Faysal, M. (2017). Investigation of a shallow slope failure on expansive clay in Texas. Engineering geology, 219, 118-129.

Kirkpatrick, S., Gelatt Jr, C. D., & Vecchi, M. P. (1983). Optimization by simulated annealing. science, 220(4598), 671-680.

Ko Ko, C., Flentje, P., & Chowdhury, R. (2004). Landslides qualitative hazard and risk assessment method and its reliability. *Bulletin of Engineering Geology and the Environment*, *63*(2), 149-165.

Lee, E. M. (2001). Geomorphological mapping. Geological Society, London, Engineering Geology Special Publications, 18(1), 53-56.

Lohnes, R. A., Kjartanson, B. H., & Barnes, A. (2001). Regional approach to landslide interpretation and repair (No. TR-430,).

Lopez, P. A., Behrisch, M., Bieker-Walz, L., Erdmann, J., Flötteröd, Y. P., Hilbrich, R., ... & WieBner, E. (2018, November). Microscopic traffic simulation using sumo. In 2018 21st International Conference on Intelligent Transportation Systems (ITSC) (pp. 2575-2582). IEEE.

Lords Hansard. 2010. Roads: Motorway lane closures. Lord Bassam of Brighton in answer to a question posed by Earl Attlee. 21 Nov 2007Q Column WA86. [online]

Ludeke, K., German, D., & Scott, J. (2009). Texas vegetation classification project: interpretive booklet for phase II. Texas Parks and Wildlife Department and Texas Natural Resources Information System, Austin, USA.

Matisziw, T. C, A. T Murray, T. H. Grubesic (2007). "Bounding Network Interdiction Vulnerability Through Cutset Identification." Critical Infrastructure, 243-256. Advances in Spatial Science, Springer.

Matisziw, T. C. (2007). "Evaluating Vulnerability and Risk in Interstate Highway Operation." Transportation Research Board (TRB) 86th Annual Meeting, Washington, DC.

Mattsson, L. G., & Jenelius, E. (2015). Vulnerability and resilience of transport systems–A discussion of recent research. Transportation Research Part A: Policy and Practice, 81, 16-34.

McMahan, C. A., Frye, R. G., & Brown, K. L. (1984). The vegetation types of Texas. Texas Parks and Wildlife Department, Austin, Texas, USA.

Mesri, G., & Shahien, M. (2003). Residual shear strength mobilized in first-time slope failures. Journal of geotechnical and geoenvironmental engineering, 129(1), 12-31.

Metropolis, N., Rosenbluth, A. W., Rosenbluth, M. N., Teller, A. H., & Teller, E. (1953). Equation of state calculations by fast computing machines. The journal of chemical physics, 21(6), 1087-1092.

Miller, P. E., Mills, J. P., Barr, S. L., & Birkinshaw, S. J. (2012). Geospatial Data Integration for Assessing Landslide Hazard on Engineered Slopes. International Archives of the Photogrammetry, Remote Sensing and Spatial Information Sciences, 39, B5.

Mohseni, O., Anderson, C., Strong, M., Conway, R., Hathaway, C., Grosser, A., & Mielke, A. (2018). Storm-Induced Slope Failure Susceptibility Mapping (No. MN/RC 2018-05). Minnesota. Dept. of Transportation.

Montgomery, D. R., & Dietrich, W. E. (1994). A physically based model for the topographic control on shallow landsliding. Water resources research, 30(4), 1153-1171.

Murray, A. T., & Grubesic, T. (Eds.). (2007). Critical infrastructure: Reliability and vulnerability. Springer Science & Business Media.

Myung, Y.S. and H.J. Kim (2004). "A Cutting Plane Algorithm for Computing K-Edge Survivability of a Network." European Journal of Operational Research 156(3), 579-589.

Nandi, A., & Shakoor, A. (2010). A GIS-based landslide susceptibility evaluation using bivariate and multivariate statistical analyses. Engineering Geology, 110(1-2), 11-20.

Nhu, V. H., Shirzadi, A., Shahabi, H., Singh, S. K., Al-Ansari, N., Clague, J. J., ... & Luu, C. (2020). Shallow Landslide Susceptibility Mapping: A Comparison between Logistic Model Tree, Logistic Regression, Naïve Bayes Tree, Artificial Neural Network, and Support Vector Machine Algorithms. International Journal of Environmental Research and Public Health, 17(8), 2749.

NOAA (National Oceanic and Atmospheric Administration). NWS/Office of Water Prediction, Hydrometeorological Design Studies Center (September 26, 2018). Precipitation Frequency for Texas, USA – NOAA Atlas 14 Volume 11, Retrieved on June 22, 2019, Available at: https://hdsc.nws.noaa.gov/hdsc/pfds/

O'loughlin, E. M. (1986). Prediction of surface saturation zones in natural catchments by topographic analysis. Water Resources Research, 22(5), 794-804.

Otto, J. C., & Smith, M. J. (2013). Geomorphological map-ping. In Chap. 2, Sec. 6. L. Clarke, y J. Nield (Eds.), Geomorphological Techniques (pp. 1–10). London: British Society for Geomorphology. ISSN: 2047-0371.

Pack, R. T., Tarboton, D. G., & Goodwin, C. N. (1998, September). The SINMAP approach to terrain stability mapping. In 8th congress of the international association of engineering geology, Vancouver, British Columbia, Canada (Vol. 21, p. 25).

Pellicani, R., Argentiero, I., & Spilotro, G. (2017). GIS-based predictive models for regional-scale landslide susceptibility assessment and risk mapping along road corridors. Geomatics, Natural Hazards and Risk, 8(2), 1012-1033.

Poorzahedy, H., & Bushehri, S. N. S. (2005). Network performance improvement under stochastic events with long-term effects. Transportation, 32(1), 65-85.

Pradhan, A., Akinci, B., & Haas, C. T. (2011). Formalisms for query capture and data source identification to support data fusion for construction productivity monitoring. Automation in Construction, 20(4), 389-398.

Pudasaini, B., & Shahandashti, M. (2020). Topological surrogates for computationally efficient seismic robustness optimization of water pipe networks. Computer-Aided Civil and Infrastructure Engineering, 35(10), 1101-1114.

Pudasaini, B., & Shahandashti, S. M. (2018). Identification of critical pipes for proactive resource-constrained seismic rehabilitation of water pipe networks. Journal of Infrastructure Systems, 24(4), 04018024.

Pudasaini, B., Shahandashti, S. M., & Razavi, M. (2017). Identifying critical links in water supply systems subject to various earthquakes to support inspection and renewal decision making. Computing in civil engineering, 2017, 231-238.

Pudasaini, B., & Shahandashti, M. (2021). Seismic Rehabilitation Optimization of Water Pipe Networks Considering Spatial Variabilities of Demand Criticalities and Seismic Ground Motion Intensities. Journal of Infrastructure Systems, 27(4), 04021028.

Raia, S., Alvioli, M., Rossi, M., Baum, R. L., Godt, J. W., & Guzzetti, F. (2014). Improving predictive power of physically based rainfall-induced shallow landslide models: a probabilistic approach. Geoscientific Model Development, 7(2), 495-514.

Ramanathan, R. S. (2012). Soil Slope Failure Investigation Management Systems (Doctoral dissertation).

Ramanathan, R., Aydilek, A. H., & Tanyu, B. F. (2015). Development of a GIS-based failure investigation system for highway soil slopes. Frontiers of Earth Science, 9(2), 165-178.

Ray, S. S. (2013). Cut Sets and Cut Vertices. In Graph Theory with Algorithms and its Applications (pp. 115-124). Springer, India.

Ressel, D. (1979). Soil survey of Lamar and Delta counties, Texas.

Rockafellar, R. T., & Uryasev, S. (2002). Conditional value-at-risk for general loss distributions. Journal of banking & finance, 26(7), 1443-1471.

Roy, A., Pudasaini, B., & Shahandashti, M. (2021). Seismic Vulnerability Assessment of Water Pipe Networks under Network Uncertainties. In Pipelines 2021 (pp. 171-179).

Saleh, A. A., & Wright, S. G. (1997). Shear strength correlations and remedial measure guidelines for long-term stability of slopes constructed of highly plastic clay soils (No. FHWA/TX-98/1435-2F).

Santacana, N., Baeza, B., Corominas, J., De Paz, A., & Marturiá, J. (2003). A GIS-based multivariate statistical analysis for shallow landslide susceptibility mapping in La Pobla de Lillet area (Eastern Pyrenees, Spain). Natural hazards, 30(3), 281-295.

Sarykalin, S., Serraino, G., & Uryasev, S. (2008). Value-at-risk vs. conditional value-at-risk in risk management and optimization. In State-of-the-art decision-making tools in the information-intensive age (pp. 270-294). Informs.

Seeley, M. W., & West, D. O. (1990). Approach to geologic hazard zoning for regional planning, Inyo National Forest, California and Nevada. Bulletin of the Association of Engineering Geologists, 27(1), 23-35.

Shahabi, H., Ahmad, B. B., & Khezri, S. (2013). Evaluation and comparison of bivariate and multivariate statistical methods for landslide susceptibility mapping (case study: Zab basin). Arabian journal of geosciences, 6(10), 3885-3907.

Shahandashti, M., Hossain, S., Baral, A., Adhikari, I., Pourmand, P., & Abediniangerabi, B. (2022). Slope repair and maintenance management system (No. FHWA/TX-20/5-6957-01-1). Texas Department of Transportation.

Shahandashti, M., Hossain, S., Khankarli, G., Zahedzahedani, S. E., Abediniangerabi, B., & Nabaei, M. (2019). Synthesis on Rapid Repair Methods for Embankment Slope Failure (No. FHWA/TX-18/0-6957-1).

Shahandashti, M., Hossain, S., Zamanian, M., & Akhtar, M. A. (2021). Advanced Geophysical Tools for Geotechnical Analysis.

Shahandashti, S. M., & Pudasaini, B. (2019). Proactive seismic rehabilitation decision-making for water pipe networks using simulated annealing. Natural Hazards Review, 20(2), 04019003.

Shahandashti, S. M., Razavi, S. N., Soibelman, L., Berges, M., Caldas, C. H., Brilakis, I., ... & Akinci, B. (2011). Data-fusion approaches and applications for construction engineering. Journal of construction engineering and management, 137(10), 863-869.

Shano, L., Raghuvanshi, T. K., & Meten, M. (2020). Landslide susceptibility evaluation and hazard zonation techniques–a review. Geoenvironmental Disasters, 7(1), 1-19.

Sharveen, S., Roy, A., & Shahandashti, M. Risk-Averse Proactive Seismic Rehabilitation Decision-Making for Water Distribution Systems. In Pipelines 2022 (pp. 81-90).

Singh, H., Huat, B. B., & Jamaludin, S. (2008). Slope assessment systems: A review and evaluation of current techniques used for cut slopes in the mountainous terrain of West Malaysia. Electronic Journal of Geotechnical Engineering, 13, 1-24.

Skempton, A. W. (1970). First-time slides in overconsolidated clays. Geotechnique, 20(3), 320-324.

Skempton, A. W. (1977). “Slope Stability of cuttings in brown London clay.” Proc., 9th Int. Conf. of Soil Mechanics and Foundations, Vol. 3, Springer, New York, 261–270.

Skempton, A. W., & Delory, I. A. (1957). “Stability of Natural slope in clayey soil.” 4th International Conference on Soil Mechanics and Foundation Engineering.

Soil Survey Staff, Natural Resources ConservationService, United States Department of Agriculture. Soil Survey Geographic (SSURGO) Database. Retrieved on June 22, 2019, Available online at: https://sdmdataaccess.sc.egov.usda.gov

Stark, T. D., & Eid, H. T. (1997). Slope stability analyses in stiff fissured clays. Journal of Geotechnical and Geoenvironmental Engineering, 123(4), 335-343.

Stark, T. D., & Hussain, M. (2013). Empirical correlations: drained shear strength for slope stability analyses. Journal of Geotechnical and Geoenvironmental Engineering, 139(6), 853-862.

Stark, T. D., Choi, H., & McCone, S. (2005). Drained shear strength parameters for analysis of landslides. Journal of Geotechnical and Geoenvironmental Engineering, 131(5), 575-588.

Strauch, R., Istanbulluoglu, E., & Riedel, J. (2019). A new approach to mapping landslide hazards: a probabilistic integration of empirical and physically based models in the North Cascades of Washington, USA. Natural Hazards & Earth System Sciences, 19(11).

Sullivan, J., Aultman-Hall, L., & Novak, D. (2009). A review of current practice in network disruption analysis and an assessment of the ability to account for isolating links in transportation networks. Transportation Letters, 1(4), 271-280.

Taneja, S., Akinci, B., Garrett, J. H., Soibelman, L., Ergen, E., Pradhan, A., ... & Anil, E. B. (2011). Sensing and field data capture for construction and facility operations. Journal of construction engineering and management, 137(10), 870-881.

Taylor, M. (2017). Vulnerability analysis for transportation networks. Elsevier.

Taylor, M. A., & D'este, G. M. (2003, October). Concepts of network vulnerability and applications to the identification of critical elements of transport infrastructure. Wellington, New Zealand: New Zealand Transport Research Forum.

Taylor, M. A., & D'Este, G. M. (2007). Transport network vulnerability: a method for diagnosis of critical locations in transport infrastructure systems. In Critical infrastructure (pp. 9-30). Springer, Berlin, Heidelberg.

Taylor, M. A., Sekhar, S. V., & D'Este, G. M. (2006). Application of accessibility based methods for vulnerability analysis of strategic road networks. Networks and Spatial Economics, 6(3-4), 267-291.

TNRIS (Texas Natural Resource Information Center). (2019) . Elevation-LiDAR. Retrieved on March 5, 2019. Available at: https://tnris.org/stratmap/elevation-lidar/

TxDOT, Statewide Connectivity Corridors (2018). Texas Department of Transportation. Retrieved on June 20, 2019, Available at: http://gis-txdot.opendata.arcgis.com

TxDOT.(2021). Traffic Count Database System (TCDS). Texas Department of Transportation. https://txdot.ms2soft.com/tcds/tsearch.asp?loc=Txdot&mod=TCDS

USACE (US Army Corps of Engineers). (2003). Engineering and design: slope stability, engineering manual EM 1110-2-1902.

Van Westen, C. J., Rengers, N., Terlien, M. T. J., & Soeters, R. (1997). Prediction of the occurrence of slope instability phenomenal through GIS-based hazard zonation. Geologische Rundschau, 86(2), 404-414.

Wachal, D. J., & Hudak, P. F. (2000). Mapping landslide susceptibility in Travis County, Texas, USA. GeoJournal, 51(3), 245-253.

Walkinshaw, J. (1992). Landslide correction costs on US state highway systems. Transportation Research Record, 36-36. https://www.americangeosciences.org/critical-issues/faq/how-much-do-landslides-cost-terms-monetary-losses

Whitworth, M., Anderson, I., & Hunter, G. (2011). Geomorphological assessment of complex landslide systems using field reconnaissance and terrestrial laser scanning. In Developments in Earth Surface Processes (Vol. 15, pp. 459-474). Elsevier.

Wilks, J. H. (2015). Transport infrastructure slope failures in a changing climate (Doctoral dissertation, Loughborough University).

Wilson, M. C. (2007). The impact of transportation disruptions on supply chain performance. Transportation Research Part E: Logistics and Transportation Review, 43(4), 295-320.

Winter, M. G. (2019). Landslide hazards and risks to road users, road infrastructure and socio-economic activity. Geotechnical Engineering, Foundation of the Future. Icelandic Geotechnical Society, Reykjavik, 196-228.

Wright, S. G., Zornberg, J. G., & Aguettant, J. E. (2007). The fully softened shear strength of high plasticity clays (No. FHWA/TX-07/0-5202-3).

Zahed, S. E., Shahandashti, S. M., & Najafi, M. (2018). Lifecycle benefit-cost analysis of underground freight transportation systems. Journal of Pipeline Systems Engineering and Practice, 9(2), 04018003.

Zahed, S. E., Shahooei, S., Farooghi, F., Shahandashti, M., & Ardekani, S. (2019). Life-cycle cost analysis of a short-haul underground freight transportation system for the DFW Airport. Built Environment Project and Asset Management, 9(3), 440-456.

Zamanian, M., Akhtar, A., Shahandashti, M., & Hossain S. (2022) Empirical Investigation of Spatial Association Between Electrical Resistivity Values and Geotechnical Properties of Clayey Soils.

Zamanian, M., & Shahandashti, M. Investigation of Relationship between Geotechnical Parameters and Electrical Resistivity of Sandy Soils. In Construction Research Congress 2022 (pp. 686-695).

Zhang, S., Zhao, L., Delgado-Tellez, R., & Bao, H. (2018). A physics-based probabilistic forecasting model for rainfall-induced shallow landslides at regional scale. Natural Hazards and Earth System Sciences, 18(3), 969-982.

Zimmermann, M., Bichsel, M., & Kienholz, H. (1986). Mountain hazards mapping in the Khumbu Himal, Nepal. Mountain Research and Development, 29-4